153p

FINAL REPORT

for

FEASIBILITY STUDY OF PASSIVELY ORIENTED LENTICULAR SATELLITES

(21 June 1963 to 30 Aug. 1963)

Contract No. NAS 5-2324

Prepared by

General Electric Company

Spacecraft Department

A Department of the Missile and Space Division

Valley Forge Space Technology Center

P.O. Box 8555 Philadelphia 1, Penna.

for

Goddard Space Flight Center

Greenbelt, Maryland

FINAL REPORT

for

FEASIBILITY STUDY OF PASSIVELY ORIENTED LENTICULAR SATELLITES

(21 June 1963 to 30 Aug. 1963)

Contract No. NAS 5-2324

Prepared by

General Electric Company

Spacecraft Department

A Department of the Missile and Space Division

Valley Forge Space Technology Center

P.O. Box 8555 Philadelphia 1, Penna.

for

Goddard Space Flight Center

Greenbelt, Maryland

TABLE OF CONTENTS

1.0 Introduction

2.0 Summary and Conclusions

3.0 Passive Attitude Control System Description

3.1 General

3.2 Gravity Gradient Rod Description

3.3 Description of Damper

4.0 Parametric Damping Studies

4.1 Characteristic Method of Solution

4.2 Significant Steady State Perturbations

4.3 System Parameter Tradeoffs

4.4 Selection of Optimum Parameters

5.0 Development of Three-Axis Digital Computer Program

5.1 Three Axis Digital Computer Program

5.1.1 General

5.1.2 Vehicle Description

5.1.3 Coordinate Systems and Transformations

5.1.4 Vehicle Attitude Dynamics

5.1.5 Digital Computer Program

5.2 Results of Preliminary Studies

6.0 Damper Design Analysis

6.1 Magnetic Material Selection

6.2 Weight Estimates

7.0 Sun Pressure Torques

7.1 Two Dimensional Skin

7.2 Three Dimensional Skin

8.0 Eddy Current Torques

8.1 Eddy Current Torque on a Wire Loop

8.3 Relative Magnitude of Eddy Current Torques

8.3.1 Torque on Wire Loop

8.3.2 Torque on a Thin Conducting Disc

8.4 Eddy Current Torques on Gravity Gradient Rods.

APPENDICES

I Planar Analysis

II Steady State Analysis

III Solar Torque on Radial Sides

LIST OF FIGURES

Figure 3-1	System Configuration
Figure 3-2	Anchored Viscous Damper
Figure 4-1	Natural Frequency Map
Figure 4-2	Steady State Errors Induced by Magnetic Field
Figure 4-3	Effect of Magnet Offset on Required Magnet Strength
Figure 4-4	Satellite Oscillation Amplitude Resulting from Orbit Eccentricity
Figure 4-5	Damper weight vs. Magnet Strength
Figure 4-6	Variation of Time Constant with Yaw Inertia Ratio, $M/I_B = 2$
Figure 4-7	Variation of Time Constant with Yaw Inertia Ratio, $M/I_B = 4$
Figure 4-8	Magnet Strength Requirements with Increased Damping
Figure 4-9	Variation of Time Constant with Damping Parameter for Optimum Magnet Strength
Figure 4-10	Relationship Between Time Constant and Steady State Error
Figure 4-11	Damper Weight vs. Time Constant
Figure 5-1	POLES Coordinate System
Figure 5-2	Inertial Reference Frame
Figure 5-3	Earth Reference Frame
Figure 5-4	Orbital Reference Frame
Figure 5-5	Orbital Angular Coordinates
Figure 5-6	Transformation $\left[E_b\right]$ from $\bar{r}$, $\bar{p}$, $\bar{q}$ to $\bar{x}_1$, $\bar{y}_1$, $\bar{z}_1$
Figure 5-7	Decay from 10 Degree Initial Angle
Figure 5-8	Steady State Oscillations
Figure 5-9	Transient Performance from Large Initial Angle
Figure 5-10	Effect of Solar Torque on Transient Decay

Figure 5-11 Solar Torque with Sun Normal to Orbit Plane
Figure 5-12 Solar Torque 45 Degrees to Orbit Plane
Figure 5-13 Solar Torque with 30 Degree Inclined Orbit
Figure 5-14 Solar Torque with 48 Degree Inclined Orbit
Figure 5-15 Solar Torque Normal to Eccentric Orbit
Figure 5-16 Effect on Transient Decay Time of Solar Torque and Orbit Eccentricity

Figure 7-1. Balloon Coordinate System with Sun in i, k Plane
Figure 7-2 Solar Torques on the Poles Satellite Vs Sun Angle $\rho_s = .65, \rho_d = .05, K_1 = 1.0$
Figure 7-3 Solar Torques on the Poles Satellite Vs Sun Angle $\rho_s = .65, \rho_d = .05, K_1 = .05$
Figure 7-4 Solar Torques on the Poles Satellite Vs Sun Angle $\rho_s = .65\ \rho_d = .05, K_1 = .018$

Figure 8-1 Description of Dipole Field
Figure 8-2 Loop in Orbit Around Magnetic Dipole
Figure 8-3 Eddy Currents in Thin Conducting Disc
Figure 8-4 Eddy Current Loops in a Wire Mesh
Figure 8-5 Maximum EMF Produced in a Circular Loop in Orbit Around the Earth
Figure 8-6 Average Eddy Current Torque on a Large, Circular Loop of 38 Gauge Wire in Orbit Around the Earth
Figure 8-7 Average Eddy Current Torque per Mil Thickness of a Large, Thin, Copper Disc in Orbit Around the Earth
Figure 8-8 Rod in Orbit Around a Magnetic Dipole
Figure 8-9 Eddy Currents in Gravity - Gradient Rod
Figure 8-10 Average Eddy Current Torque on Gravity - Gradient Rods

NOMENCLATURE*

Matrices

$[A]$	Matrix for conversion from inertial reference to orbital reference frame. Elements, a_{ij}.
$[B]$	Matrix for conversion from inertial reference to balloon body axis coordinate system. Elements, b_{ij}.
$[C]$	Matrix used to specify orientation of balloon magnet with respect to balloon body axes. Elements, c_{ij}.
$[D]$	Matrix used to convert components outputted from magnetic torque subroutine to magnetic components along orbital reference system. Elements, d_{ij}.
$[E]$	Matrix used to convert from orbital reference frame to body axes. Subscript b denotes balloon body axes while subscript m denotes magnet body axes. Elements, e_{ijb}, e_{ijm}.
$[F]$	Matrix to define solar vector components along inertial reference frame. Elements, f_{1j}.
$[H]$	Matrix for conversion from orbital reference frame to balloon magnet body axes. Elements, h_{ij}.

Coordinate Systems

$\bar{i}$, $\bar{j}$, $\bar{k}$	Reference frame for derivation of solar torque. The $\bar{i}$ axis is directed along the longitudinal axis of the balloon. The $\bar{j}$ axis is perpendicular to the solar vector and $\bar{k}$ forms a right-handed orthogonal system.
$\bar{l}$, $\bar{l}_n$, $\bar{w}$	Earth reference frame where $\bar{l}$ is directed from the geocenter to the point on the equator at the Greenwhich meridian; $\bar{l}_n$ is normal to l and in the equatorial plane and w points along the north pole.
$\bar{r}$, $\bar{p}$, $\bar{q}$	Orbital reference frame where $\bar{r}$ is directed from the geocenter along the local vertical; $\bar{p}$ is directed along the velocity vector and q is directed along the vehicle's orbital angular velocity vector in the right-handed screw sense.
$\bar{u}$, $\bar{v}$, $\bar{w}$	Inertial reference frame where $\bar{u}$ is directed from the heliocenter to the spring equinox position of the geocenter; $\bar{v}$ lies in the equatorial plane and is directed from the heliocenter to a point north of the summer solstice position of the geocenter. $\bar{w}$ is directed from the geocenter to the north pole.

* (FORTRAN language has been omitted unless it is used in other places than in section 5.1.5.1).

$\bar{x}_1, \bar{y}_1, \bar{z}_1$	Balloon yaw, pitch and roll body axes respectively.
$\bar{x}_2, \bar{y}_2, \bar{z}_2$	Balloon magnet body axes where $\bar{x}_2$ is the dipole axis; $\bar{y}_2$ and $\bar{z}_2$ are aligned along $\bar{y}_1$, $\bar{z}_1$ for $\beta = \gamma = 0$.
$\bar{x}_3, \bar{y}_3, \bar{z}_3$	Magnet body axes where $\bar{x}_3$ is the dipole axis; $\bar{y}_3$ and $\bar{z}_3$ are aligned along y_1, z_1 for zero balloon and magnet attitude angles.

English Symbols

a	Semi major axis of vehicle orbit.
a_o	Radius of loop or disc for eddy current analysis.
a_v	Width of wire.
A	Area of loop or disc.
APOG	Apogee of vehicle orbit.
A_m	Area of magnet.
b	Damping coefficient in ft# sec.
$\vec{B}$	Magnetic flux density.
B_R	Radial component outputted from magnetic torque subroutine.
B_θ	Magnetic component directed along the local meridian, positive in the direction of the velocity vector which is outputted from the magnetic torque subroutine.
B_ϕ	Magnetic component directed along the local latitude arc, positive in a westerly direction when the vehicle is moving south to north which is outputted from magnetic torque subroutine.
d_{al}	Density of aluminum.
d_{bi}	Density of bismuth
d_f	Density of fluid
D_L	Time in days from winter solstice to orbital injection.
dA	Incremental area.
e	Orbit eccentricity.
E	Eccentric anomaly, subscript o indicates value at orbit injection.
E/c	Ratio of the solar flux density to the velocity of light, also called P_o.

F	Force on the balloon due to solar torque. Subscript o denotes force on the inner surface of the mesh balloon due to the solar rays passing thru the top surface.
F_1 thru F_{13}	Intermediate parameters used to shorten solar torque equations.
G_{x1}, G_{y1}, G_{z1} / G_{x3}, G_{y3}, G_{z3}	Intermediate variables used to shorten Euler's dynamical equations.
GMTT	Instantaneous Greenwich Mean Time.
$\vec{h}$	Moment arm from arbitrary location of the center of rotation to each element dA of the surface which is used for the computation of solar torques. Superscript, prime, denotes corresponding moment arm for bottom spherical segment of lens.
h_o	Orbital angular momentum per unit mass.
$\vec{H}$	Magnetic field intensity.
H_r	Magnetic component along $\bar{r}$.
H_p	Magnetic component along $\bar{p}$.
H_q	Magnetic component along $\bar{q}$.
i_o	Current.
I	Moment of inertia in slug ft^2. Subscripts xx1,.....,yz_3 denote moments and cross products around subscripted balloon and magnet body axes.
I_B	Pitch and Roll Moment of inertia of vehicle.
I_B^o	Yaw moment of inertia of vehicle.
I_D	Damper moment of inertia.
k	Ratio of pole length to actual length.
K	Universal gravitational constant multiplied by the mass of earth.
K_1	Constant used to define ratio of closed area to open area of mesh material.
l_m	Length of magnet.
L	Length of gravity rod.
LAT	Latitude of projection of satellite on earth.

LONG	Longitude of projection of satellite on earth.
m	Magnet pole strength.
$\vec{M}$	Magnetic moment. Subscripts 2 and 3 denote magnetic moment of balloon and independent magnets respectively. Subscript e denotes magnetic dipole moment of earth. M sometimes appears as a magnitude of $\vec{M}$.
M	Mean anomaly, Subscript o denotes value at orbit injection.
$\bar{n}$	Unit vector normal to surface of balloon, positive toward center.
O	Center of curvature for top spherical segment of lens. Superscript, prime, denotes center for bottom spherical segment.
P_o	Solar radiation constant; see E/C.
r_d	Radius of damper sphere.
r_o	Radius of curvature of spherical segment of balloon.
r_s	Direction cosine between $\bar{r}$ and $\bar{s}$.
R	Distance from geocenter to vehicle, magnitude of $\bar{r}$, also called r.
R_c	Perpendicular distance of satellite from earth-sun line.
$\bar{s}$	Solar vector.
s_{x1}, s_{y1} , s_{z1}	Direction cosines between solar vector and balloon body axes.
t	Time.
t_o	Time at injection.
t_{out}	Elapsed time since injection for computer print out.
T	Torque. Subscripts d_1, s_1, m_1, t_1, g_1, m_3, d_3, x_1,....z_3, i, j, k or combinations of the preceding denote components due to a specified torque and along specified axes.
T_1 thru T_6	Amplitude of arbitrary torques.
v_o	Velocity.
W_t	Weight; subscript s denotes weight of inner sphere while subscript o denotes weight of outer sphere.

x_o	Offset measured along $\bar{i}$ axis from geometrical center of lens to arbitrary center of torque.
x_L	Distance from center of curvature of spherical segment to geometrical center of lens. Superscript, prime, denotes corresponding distance from center of curvature of bottom segment of lens.
y_L	Offset measured along $\bar{j}$ axis from geometrical center of lens to arbitrary center of torque.
y_{10}	Offset measured along the $\bar{y}_1$ axis from geometrical center of lens to arbitrary center of torque.
z_L	Offset measured along $\bar{k}$ axis from geometrical center of lens to arbitrary center of torque.
z_{10}	Offset measured along the $\bar{z}_1$ axis from geometrical center of lens to arbitrary center of torque.

Greek Letters

α	Angle between the $\bar{y}_1$ and $\bar{j}$ axes.
β	Rotation about $\bar{y}_2$ axis which represents one of the degrees of freedom used to specify the orientation of the balloon magnet with respect to the balloon body axes.
γ	Rotation about the z_1 axis which represents one of the degrees of freedom used to specify the orientation of the balloon magnet with respect to the balloon body axes.
Δ	Angle between satellite yaw axis and local vertical to earth.
δ	Gap distance between the inner and outer spheres of the magnet.
ϵ	Angle between ecliptic and equatorial planes.
$\mathcal{E}$	Electro motive force (emf).
η	Orbital central angle measured from right ascension. Subscript o denotes orbital angle at perigee measured from ascending node. Subscript 1 denotes orbital angle at injection measured from ascending node. Subscript 2 denotes vehicle orbital position at injection measured from perigee.
θ	Angle denoting position of sun in i, k plane measured from $\bar{i}$ axis.
θ_m	Angle between the magnetic axis and the local line of flux.
θ_p	Pitch attitude angle. Subscript b or m refers to balloon or magnet attitude angle respectively.
θ_r	Roll attitude angle. Subscript b or m refers to balloon or magnet attitude angle respectively.
θ_y	Yaw attitude angle. Subscript b or m refers to balloon or magnet attitude angle respectively.
λ	Integration variable for solar torque analysis which denotes an angle along a "longitude" line.
μ	Fluid viscosity.
μ_o	Constant equal to 4×10^{-7} Henry/meter.
ν	Orbit inclination.
ξ	Polar angle of satellite in polar orbit. $\bar{\xi}$ in a unit vector normal to $\bar{r}$ in direction of satellite velocity.

π	Constant, 3.1416.
ρ	Solar reflectivity parameter. Subscript s and d refer to specular and diffuse reflection coefficients of the surface material of the balloon.
σ	Orbital angular position of earth measured from winter solstice position.
σ_1	Projection of σ in equatorial plane.
σ_o	Resistance per unit length of wire.
τ	Orbital period. Also used to denote time constant in orbits.
τ_1	Distance from center of one wire to center of next wire.
τ_o	Thickness of the conducting disc.
τ_o'	Wall thickness of gravity rod.
τ_R	Regression period in days.
ϕ	Complement of lens half angle.
Φ	Magnetic flux.
ϕ_1 thru ϕ_6	Phase angles of miscellaneous torques.
ψ	Integration variable along a "latitude" line of the sphere. Subscript c denotes sun shade line on balloon.
Ω	Right ascension. Subscript 1 denotes Greenwich hour angle at injection. Subscript 3 represents projection of the orbit central angle measured from equatorial crossing on the equator.
ω_o	Orbital frequency.
ω_1, ω_2	Frequency of disturbance torques.
ω	Angular body rates where subscripts $x_1 \ldots\ldots z_3$ denote rates around respective balloon and magnet axes. Subscripts $b_{x3} \ldots\ldots b_{z3}$ denote balloon body rates resolved along magnet axes; subscripts $m_{x1} \ldots m_{z1}$ denote magnet body rates resolved along balloon axes.

1.0 INTRODUCTION

A preliminary study of the feasibility of passively orienting and damping the large lenticular satellite by the utilization of earth's gravity and magnetic fields has been completed as Phase I of Contract NAS 5-2324 with NASA/Goddard. This study, assigned the acronym POLES (Passively Oriented Lenticular Satellite), was accomplished during the scheduled period 21 June 1963 to 30 August 1963. This report documents the results of this contract phase, consistent with the final project report specifications of NASA document TID-S-100.

System performance analysis and damper design analysis and test will be carried out as follow-on to Contract NAS 5-2324, and the results will be reported on in monthly progress reports and in a final report to be submitted at the end of Phase II.

2.0 SUMMARY AND CONCLUSIONS

20009 A

The system investigated was a 267 foot diameter lens (200 foot radius of curvature) made of wire mesh material. Gravity gradient rods extending from top and bottom provide the required moments of inertia for accurate gravity gradient stabilization. The Magnetically Anchored Viscous Fluid Damper, conceived and developed by General Electric Company was taken as the passive damper model.

The major objective of the five tasks identified in the statement of work (Reference 1) was the development of analytical and machine program tools for subsequent system performance analysis.

A large angle, eight degree of freedom, digital computer program was developed to numerically integrate the differential equations of motion. Also, a characteristic root solution to the linearized planar motion equations was programmed for conducting parametric studies. Equations for the significant disturbance effects produced by solar pressure, eddy currents, and magnetic perturbations were derived and parametric studies and weight estimates were made to provide for system parameter tradeoffs.

A considerably more extensive performance study is required to verify the performance capabilities of the system for decay from large errors and the steady-state pointing accuracy when the satellite is subjected to eccentric orbits and various disturbance torques.

No attempt was made in this study to solve the problems associated with balloon inflation or of structural attachment of the gravity gradient rods and damper to the balloon skin. Purely from an attitude control standpoint, the passive stabilization of the lenticular balloon to an accuracy of $\pm$ 3 degrees does appear to be feasible. The total weight of the attitude control system including gravity gradient rods, their extension mechanisms and power supplies, and the passive damper would be approximately 90 to 150 pounds. Another

3.0 PASSIVE ATTITUDE CONTROL SYSTEM DESCRIPTION

3.1 GENERAL

The balloon was assumed to be made of two 84° segments of a 200 foot radius sphere joined together to form a lenticular shape, with principal moments of inertia of 178,000 and 90,000 slug ft.^{2}. The system configuration selected for stabilizing the lenticular balloon consisted of a pair of gravity gradient rods extended vertically (one up, one down) from the centers of the two spherical segments and a magnetically anchored viscous fluid damper which could be mounted either at the balloon skin line or on an internal support structure at the center of the balloon. (See Figure 3-1)

3.2 GRAVITY GRADIENT ROD DESCRIPTION

The gravity gradient rod is a tubular element formed out of beryllium copper, steel or a silver alloy strip metal heat-treated into a circular section in such a manner that the edges of the material overlap by approximately 180 degrees. The tubes under consideration for this application are about 1 inch in diameter with .005 inch thick wall. This provides an element with a bending strength almost equivalent to that of a seamless tube of the same diameter and thickness. The rods when retracted are stored in a strained, flattened condition by winding on a drum. As the flattened strip is extended it coils into a tubular shape as a result of pre-stressing. The elastic energy in the flattened strip and the energy generated by rolling the strip in the drum supplements the motor power in extending the rod. One-shot batteries would be carried to drive the extension motors.

The motor controls the rate of erection, insures ample erecting force, and allows retraction during ground testing. Spring retaining belts keep the strip wound tight on the drum in all extension positions. Other guidance devices ensure that the strip pays out and coils smoothly and is properly directed. These devices also support the extended rod. Light weight materials are used throughout the structure. The side plates are aluminum. Nylon, melamine and fiberglas are used for other parts. All ball bearings are of the double-shielded type, having low-vapor-pressure grease lubricants. A telemetry potentiometer is used to indicate the length of rod extended. Limit switches will cut off the power at full extension and retraction. Due to the irreversibility that results from the large reduction in the motor gear head, the rod is held at the position where the motor stops.

The system described above is known as the STEM (Self-storing Tubular Extendible Member) technique which has been under development by DeHavilland Aircraft of Canada, Limited for a number of years. Many configurations have been produced for use as antennae and successfully flight demonstrated on such programs as the Alouette S.27 Topside Sounder Satellite and the Mercury Capsule.

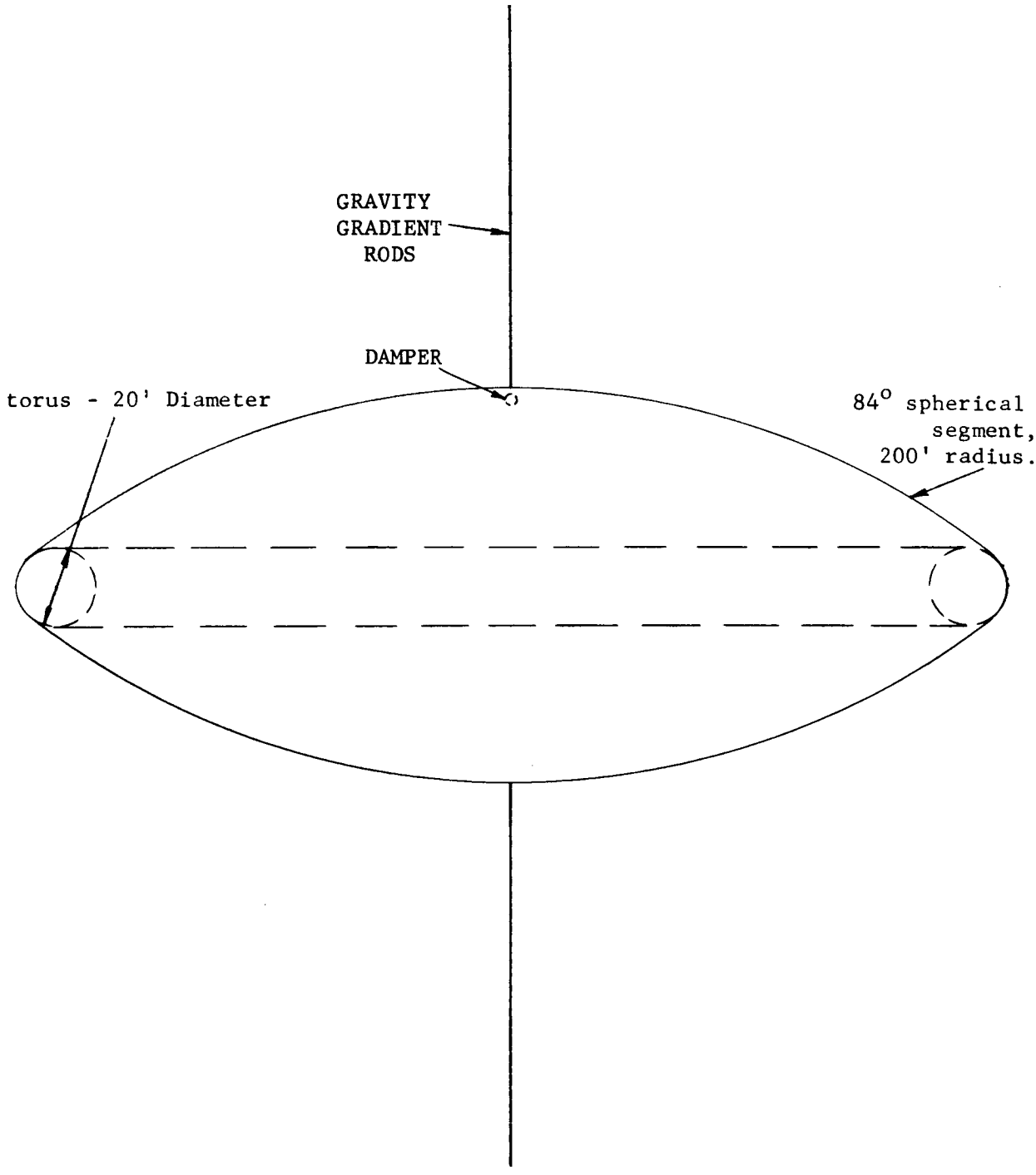

FIGURE 3-1 System Configuration

Beryllium copper tubes were used on the Alouette Program and steel tubes were extended on Mercury Capsules. For the lenticular balloon application, however, where very long rods are required for obtaining the high moments of inertia, a silver alloy rod currently under development by General Electric Company under contract to NASA-AMES is recommended because of its high thermal conductivity and solar reflectivity. Beryllium copper rods up to 850 feet in length have been built by DeHavilland to be used as antenna; however, thermal bending would produce a maximum tip deflection of this rod of approximately 330 feet. By using the silver alloy rod, the tip deflection of an 850 foot rod would be only about 50 feet. Placing a dead weight on the end of the rod can achieve the desired moments of inertia with shorter rods. The selection of the length to be used on the lenticular balloon would require an optimization study and trade off between system weight and thermal bending deflection.

3.3 DESCRIPTION OF DAMPER

The magnetically anchored viscous damper, see Figure 3-2, consists of three elements: (a) viscous damper, (b) magnetic anchor, and (c) magnetic suspension. The device is completely passive, requires no external sources of power for operation, has no rubbing parts and is ideally suited for long life reliable operation in a space environment. None of the elements incorporated represents an advance in the state of the art or represents basically new and untried concepts.

The viscous damper consists of two concentric spheres with a viscous fluid between them. When there is a difference in angular velocity, there will be a viscous shearing action which results in a dissipation of energy. In order to produce a difference in angular velocity of the spheres and to be assured that they do not eventually "lock-up" on each other, the inner sphere is fixed to the earth's field by the magnetic anchor. This is achieved by a bar magnet attached to the inner sphere, which acts essentially as a compass needle, always aligning itself parallel to the earth's magnetic field. The magnitude of torque exerted by the magnet is a function of its magnetic moment and the magnetic field intensity of the earth: $T = MH \sin \theta_m$ where

M is the magnetic dipole,

H is the earth's magnetic field intensity, and

θ_m is the angle between the magnetic axis and the local line of flux.

In order to assure the concentricity of the spheres and to prevent any possibility of rubbing under operating conditions, the spheres will be separated magnetically. This separation will be attained by a magnetic suspension in which a diamagnetic material is repelled by a magnetic field. The outer sphere will be made of a diamagnetic material, and the magnetic field will be produced by permanent magnets attached to the inner sphere.

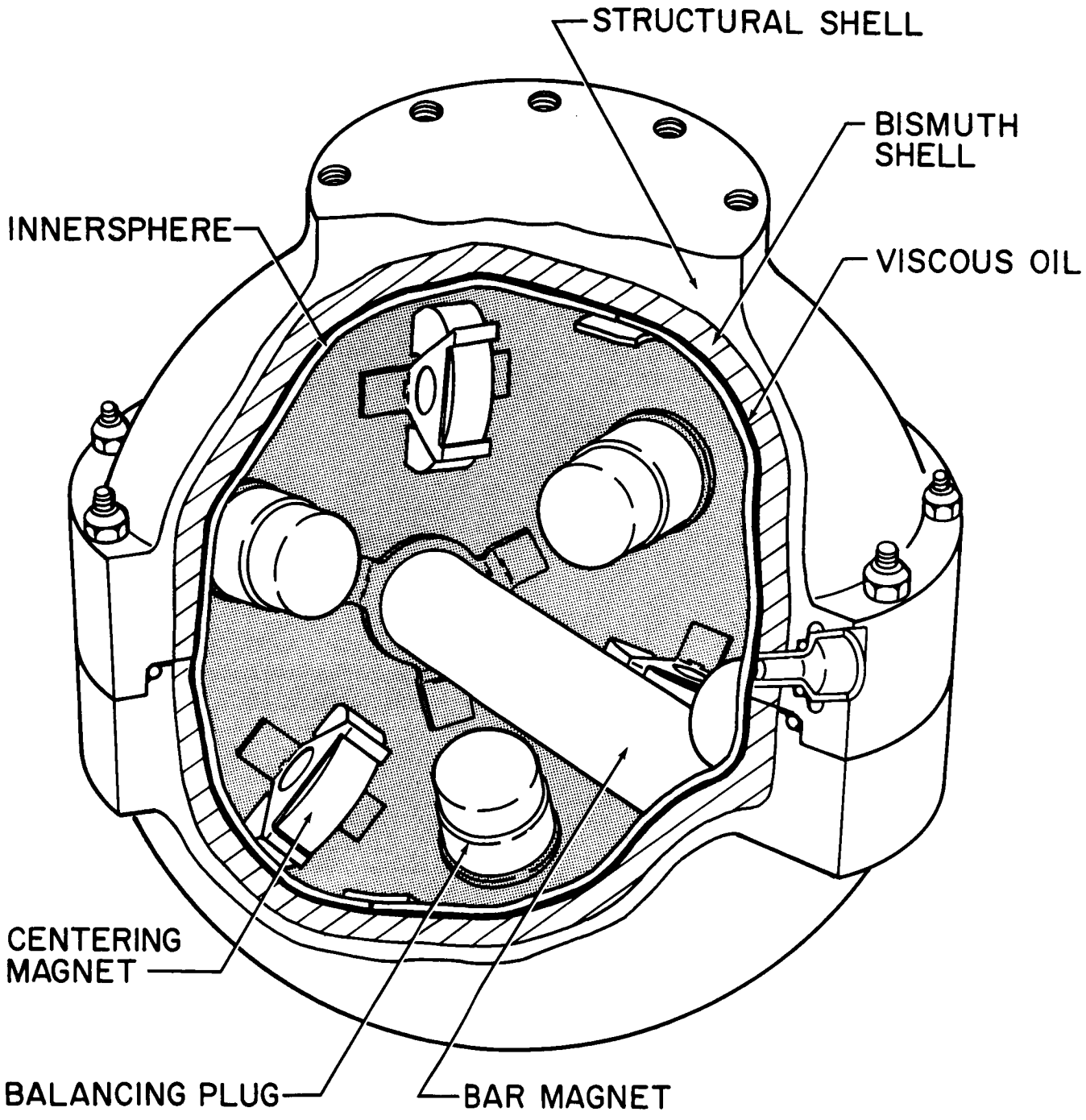

Figure 3-2. Viscous Fluid Damper

3.3.1 Viscous Damper

Damping will be obtained by the relative motion of two concentric spheres which are separated by a viscous fluid. The concept of utilizing the motion of concentric spheres to produce damping is not new in the state of the art. It results in a small, lightweight, and most important, a completely passive device.

For sphere of radius r_d, cm and angular velocity ω radians per second, it can be shown that the damping torque is

$$T = \frac{8}{3} \frac{\mu}{\delta} \pi r_d^4 \omega \text{ dyne cm.} \qquad (3.1)$$

where μ is the viscosity of fluid;

δ is the gap between the inner and outer spheres.

There are three general groups of fluids which can be considered for the damping media: hydrocarbons, silicones and fluorocarbons. The selection of fluid will depend upon its inherent physical and chemical properties together with the system requirements as to the allowable variation of damping as a function of temperature. The silicones are the least temperature sensitive and the fluorocarbons the most temperature sensitive. The specific gravity is another important physical criteria. Since it is anticipated that the inner sphere will be made buoyant, a more dense fluid could result in a smaller and lighter over-all component. If the high viscosity-temperature coefficient of the fluorocarbons can be tolerated by the system requirements, then its high specific gravity can prove to be a definite asset to the damper design.

Both the silicones and fluorocarbons show long term temperature stability, in the absence of oxygen, up to 575°F. They are not corrosive when in contact with the usual materials of construction. These fluids are in current use for aerospace application and are extensively used as damping media. The viscosity of the silicones and fluorocarbons will change slightly with time due to exposure to the radiation environment. However, the bismuth shell used for diamagnetic suspension also acts as an excellent radiation shield, holding the viscosity change to less than 3 per cent in three years.

3.3.2 Magnetic Anchor

The magnetic anchor serves to hold the inner sphere fixed while the outer sphere, which is attached to the spacecraft, rotates. The magnetic anchor locks the inner sphere to the earth's magnetic field by means of a longitudinally magnetized bar magnet attached to the inner sphere. This bar magnet act as a magnetic dipole which will be torqued by the earth's field. The use of a magnetic dipole to orient a satellite is not a new concept; it has been used successfully in Transit 1B and 2A, where an Alnico V bar magnet 4 inches long, and 1 inch in diameter was used.

4.0 PARAMETRIC DAMPING STUDIES

4.1 CHARACTERISTIC METHOD OF SOLUTION

Application of the root locus technique to the POLES satellite requires the derivation of the linearized equations of motion. The equations derived for the three axis computer program can not easily be linearized, and if linearized, would result in a set of equations which is unlikely to be amenable to optimization. It is simpler to make the appropriate assumptions prior to derivation. The analysis is given in Appendix I, but the assumptions made in the analysis will be discussed below.

The system being analysed consists of two bodies, each of which has three degrees of freedom (excluding orbital freedoms). Two three degree of freedom systems result in six second order dynamical differential equations. It is not practical to linearize all six equations, and only those degrees of freedom which are important should be linearized. The yaw position of the vehicle is irrelevant from the satellite mission standpoint, and roll motions appear on the yaw axis because of orbital rate, preventing accurate linearization. Therefore, the equations describing the motion in pitch have been linearized. However, pitch and roll motions are sufficiently similar that parameters optimum for pitch are nearly optimum for roll.

The analytical model of the earth's magnetic field assumed in the analysis is a simplified magnetic dipole. The simplified dipole permits the equations to be solved, but excludes many of the characteristics of the field. One such characteristic is the variation of the Earth's magnetic field due to the location of its equivalent dipole axis. The dipole magnet is not located on the Earth's spin axis, nor does it pass through the geographic center of the earth. As a consequence the magnetic field rotates every twenty four hours (with respect to inertial space), causing a change in the direction and magnitude of the field at any fixed point in space. A satellite in orbit will experience an additional field variation due to a change in field strength with magnetic latitude. If the orbit is in the plane of the magnetic equator, the field strength will be minimum and constant. For a polar orbit, however, the field strength will vary from a minimum at the equator to a maximum at the poles (equal to twice minimum). For orbital inclinations between zero degrees (equatorial) and ninety degrees (polar), the field strength will change from the minimum to a maximum dependent upon the orbital inclination.

A third characteristic of the magnetic field which must be simplified for analysis is the variation of the orientation of the lines of flux of the field. Consider the damper of the satellite in a polar orbit about a dipole magnet coincident with the spin axis of the earth. At the North Pole, the south seeking pole of the damper will be pointed toward the North Star (Polaris). At the South Pole, the south seeking pole of the damper will be pointed toward the North Star and toward the earth, which is exactly one inertial rotation. Hence, for every orbit, the damper makes two rotations, or its rotational rate is twice orbital. This is the average rate assumed in the analysis. It should be pointed out, however, that the actual rotational rate varies considerably throughout the orbit, since the magnet follows the magnetic lines of flux, not the local vertical. The rotational rate is largest at the magnetic equator and least at the poles. Since the damper is coupled to the vehicle by a viscous damper, the variation in damper rate appears as a disturbance torque on the vehicle.

Qualitative (as well as quantitative) analysis indicates that the disturbance torque is periodic with a period of approximately $2\pi/2\omega_o$, where ω_o is orbital rate. If the orbital inclination is not ninety degrees, the magnet rotates out of the roll-yaw plane, and its rate of rotation in pitch is altered. Hence for orbits other than polar, a planar analysis is not particularly meaningful.

As mentioned previously, the simplified dipole excludes many of the characteristics of the magnetic field from the analysis. However, the effect of these characteristics on the vehicle can be included. The planar analysis was restricted to polar orbits to avoid rotation of the damper magnet out of the roll-yaw plane, and the change of the magnetic field with latitude in this orbit is compensated for by using an average field strength for the orbit. (See equation I-12 in Appendix I). The effect of the non-uniform rotation of the flux lines is included by assuming a constant rate of twice orbital and employing a dynamic amplification factor. This factor will be discussed later in the section.

Additional limitations of a secondary nature noted in Appendix I are a circular orbit and equal pitch and roll inertias. These limitations do not significantly restrict the analysis.

With the above limitations and restrictions, the dynamical equations were derived and linearized about a final steady state position. The linearized equations were put in operator notation and a fourth order algebraic equation (quartic) was derived. By an appropriate change of time scale, the dynamical equations were non-dimensionalized, and the roots to the quartic, which was solved on a computer, are consequently non-dimensional. The roots to the quartic are either complex conjugates with negative real parts, or negative real roots. The imaginary part of the complex root is the ratio of the damped natural frequency to the orbital frequency, and the real part (and/or real root) is the ratio of the logarithmic decrement to orbital frequency. The logarithmic decrement is the exponent of the e term preceding the sine term in the closed form solution, and since exponential decay is desired, it should have a negative value. The reciprocal of the logarithmic decrement is the time constant in terms of orbital rate. Introducing a factor of 2π, the time constant can be put in terms of orbital period or simply orbits.

There are four roots to the quartic, two of which describe the damper mode and two of which describe the satellite mode. The differences in time constant and natural frequencies clearly indicate which numbers apply to the damper and which apply to the satellite.

The steady state conditions given by Equations I-32 and I-33 in Appendix I are average or static conditions used in the dynamic analysis. From the vehicle standpoint this angle is an error which cannot be compensated for because the yaw position of the balloon is not specified (i.e. there is no way of determining if the error is to the "right" or "left" of the yaw axis). In addition to this static error, there is a dynamic error caused by the variations in the magnetic field mentioned earlier in the report. The magnitude of the dynamic error is dependent upon the ratio of the forcing frequency to natural frequency. The forcing frequency is twice orbital, but the natural frequency of the satellite is dependent upon its yaw inertia ratio. Considering the maximum amplitude of the forcing function to be equal to that causing the error, the maximum anticipated error can be determined as a function of yaw inertia ratio. The analysis can be found in Appendix II.

A steady state error can also be determined for the magnet, but since the exact position of the magnet is of no concern, its error has been termed an offset and has not been limited to small angles. As will be indicated later, however, this offset does affect the performance of the damper. The analysis of the offset can be found in Appendix II.

4.2 SIGNIFICANT STEADY STATE PERTURBATIONS

The only steady state perturbation discussed in section 4.1 was that due to variations in the magnetic field. These were included in that section because of the close relationship between magnetically induced oscillations and the satellite damping time. Other steady state perturbations exist which are not associated with the magnetic field, the most significant of these being solar torques and orbit eccentricity. Of the two, orbit eccentricity appears to be the largest. The effect of these on the satellite performance and optimization will be discussed in sections 4.3 and 4.4.

4.3 SYSTEM PARAMETER TRADEOFFS

Computer solutions to the quartic indicated that the natural frequency of the satellite was unaltered by the presence of the damper. The natural frequency can therefore be computed from the linearized three axis equations for a single body under the influence of gravity gradient torques. Figure 4-1 is a plot of the natural frequencies for the three oscillatory modes as a function of the satellite inertia ratios. The right hand boundary of this frequency map represents the lenticular vehicle which has equal pitch and roll moments of inertia. The region of bi-stability is a region where the satellite has a stable position two 90° rotations away from the desired position. As a consequence this region will not be considered.

For all but the most lightly damped satellite, the damper was overdamped and had no natural frequency. Even where the natural frequency did exist, however, it was not plotted because it is not relevant to the vehicle behavior. In general its oscillation frequency is twenty to thirty times higher than that of the satellite.

The results of the steady state analysis are given in Figures 4-2 and 4-3. The steady state error shown in Figure 4-2 is a combination of static error and dynamic oscillations and should be a worst case. Preliminary three axis runs indicate that the linearized analysis is approximately correct. The optimum yaw inertia ratio to produce the least steady state error for a fixed damping coefficient is between .2 and .3. The value of the steady state error can be selected as an input, and the necessary damping determined. However, the damping also affects the decay time of the satellite and a tradeoff between decay time and steady state error is required. A complete tradeoff includes other steady state perturbations such as solar torques and orbit eccentricity. Orbit eccentricity appears to be the most significant factor (Figure 4-4) and may place a lower limit on accuracy capability. If so, there is no advantage to keeping the magnetically induced error small in comparison with the orbit eccentricity error. Selecting the allowable magnetically induced error to be of the same order of magnitude as the orbit eccentricity error permits reduction of the satellite time constant (Figure 4-10).

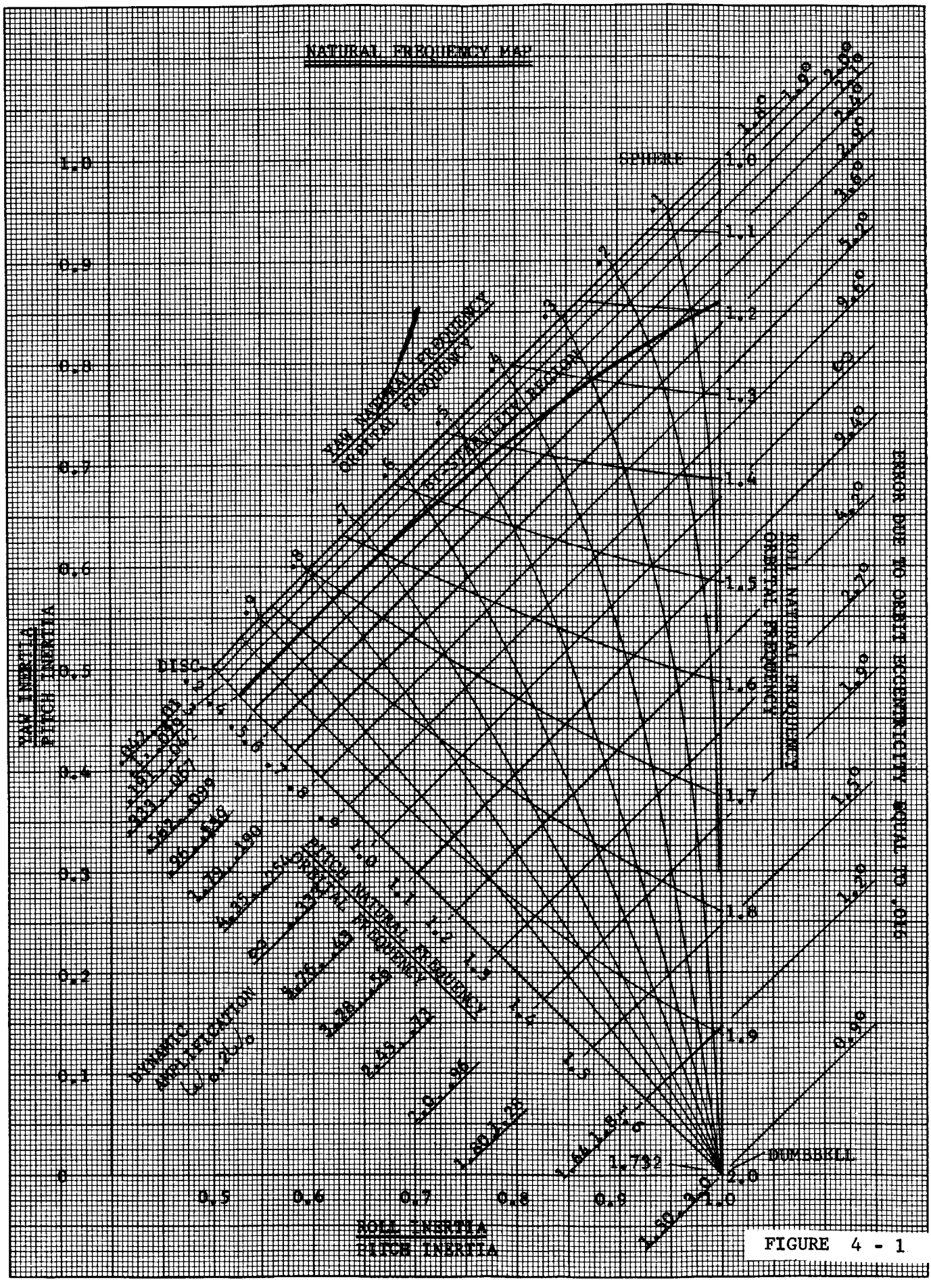

Figure 4-1. Natural Frequency Map

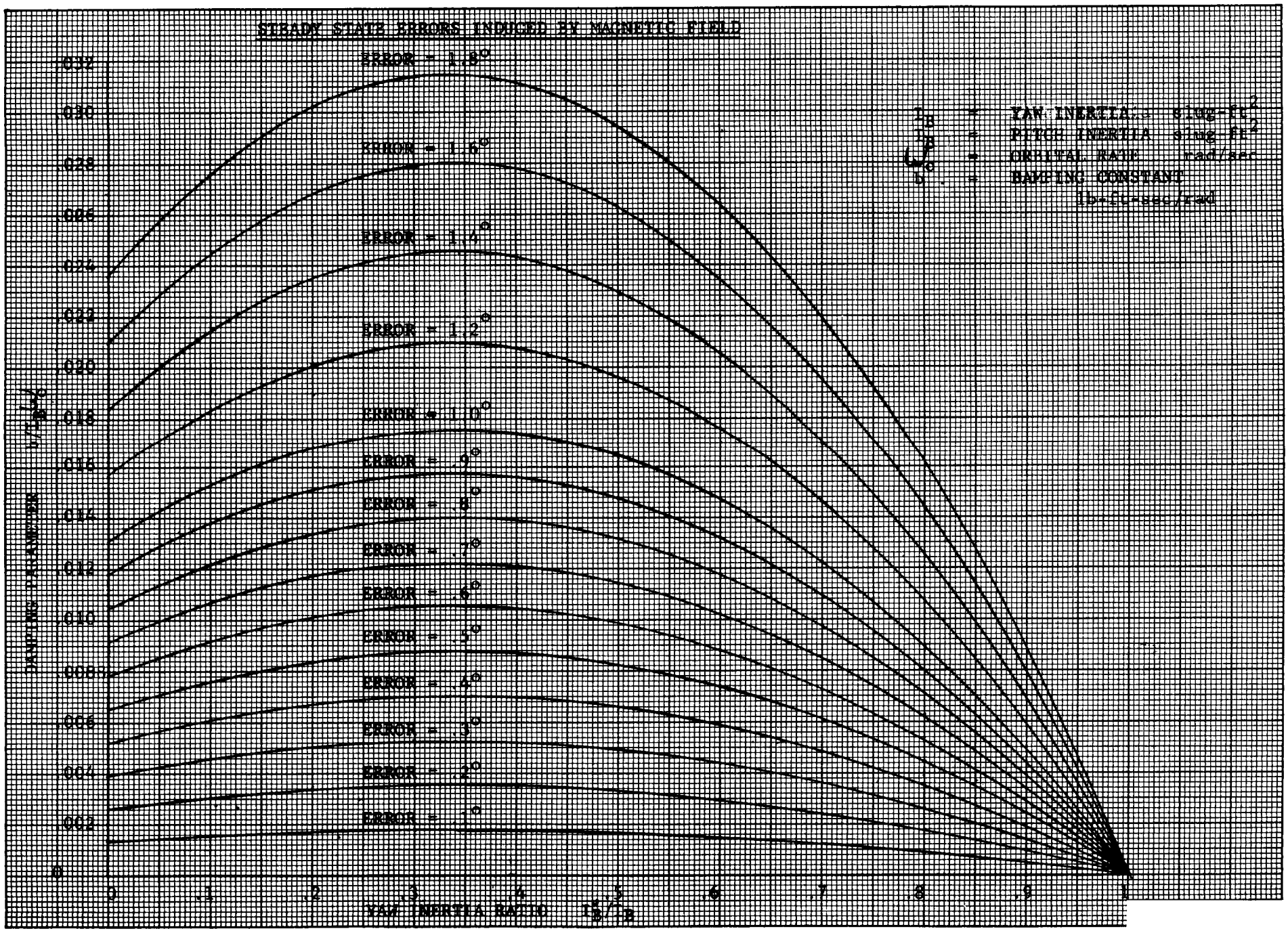

Figure 4-2. Steady State Errors Induced by Magnetic Field

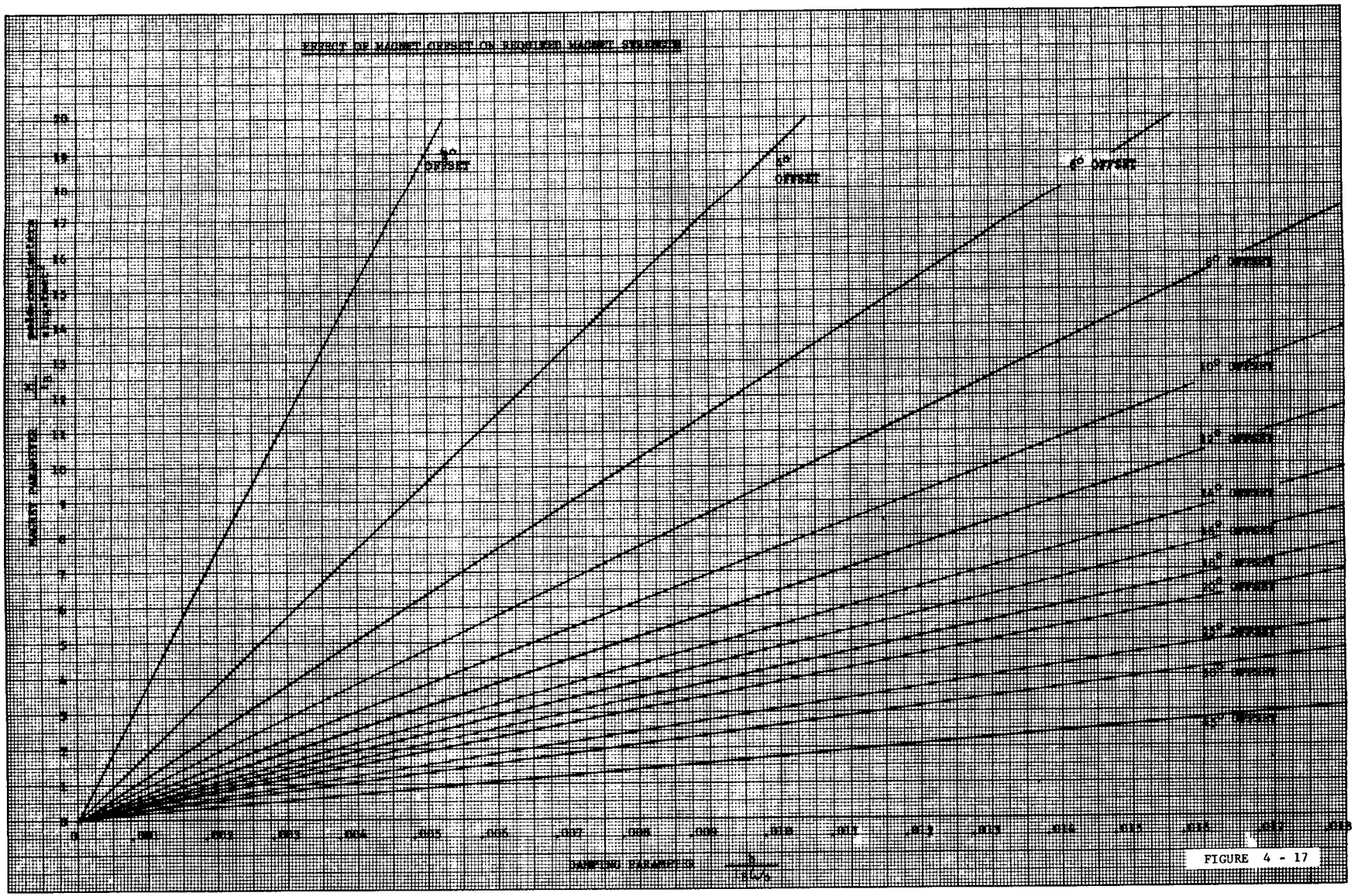

Figure 4-3. Effect of Magnet Offset on Required Magnet Strength

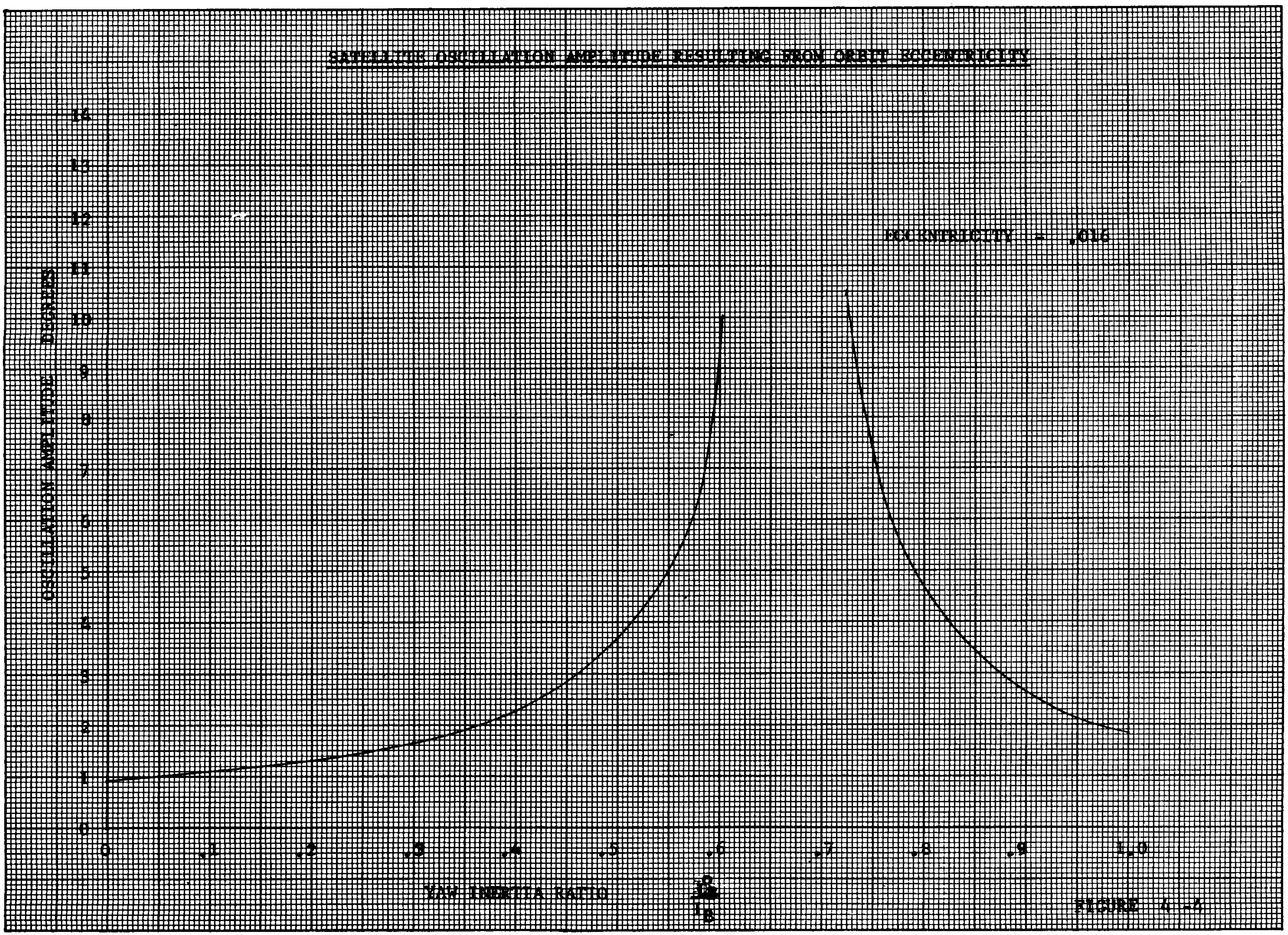
SATELLITE OSCILLATION AMPLITUDE RESULTING FROM ORBIT ECCENTRICITY
ECCENTRICITY = .016
OSCILLATION AMPLITUDE DEGREES
14
13
12
11
10
9
8
7
6
5
4
3
2
1
0
0
.1
.2
.3
.4
.5
.6
.7
.8
.9
1.0
YAW INERTIA RATIO
FIGURE 4-4

Figure 4-3 is the offset of the damper magnet from the magnetic field. The analysis which resulted in this plot is conservative, but the final system may be as conservative or as marginal as desired by the appropriate selection of offset. Preliminary three axis runs indicate offsets of twenty degrees or less all have identical damping characteristics. The "knee" of the curves in Figure 4-6 and 4-7 occurs at an offset of ninety degrees and cannot be used. The damper performance at intermediate values has not been determined, but offsets of forty-five degrees do not appear possible. A high offset allows a smaller magnet strength to be used, and since the magnet weight and damper weight both depend upon the magnet strength, high offsets result in lightweight dampers. Figure 4-5 is a preliminary weight estimate of the damper as a function of magnet strength. The maximum permissible offset will be determined by the three axis computer program. The damping parameter does not directly affect the damper weight, but a reduction of the damping parameter permits a similar reduction of magnet strength (Figure 4-3).

The real parts of the quartic roots which apply to the satellite were normalized to an orbit scale and plotted in Figures 4-6, 4-7, and 4-8. The introduction of the new time scale into the analysis (Appendix I) has permitted the use of non-dimensional parameters. Hence all the results are independent of orbit, including both the steady-state response and the transient response.

Of the four parameters $b/I_B\omega_o$, I_B/I_D, $I_B{}^o/I_B$, and M/I_B, only the damper inertia ratio, I_B/I_D, has been excluded from all the figures. It was found to be irrelevant. With the parameters of Figure 4-7 for example, changing the damper inertia ratio from 10^4 to 10^6, decreased the real root by .01 per cent. For all practical purposes, therefore, the damper inertia, for the range of satellite inertias under consideration, has no effect on performance and need not be considered, further.

Figure 4-6 shows the performance characteristics of a vehicle with a constant magnet parameter, M/I_B of two, and several yaw inertia ratios. For damping parameters less than 0.007, all the inertia ratios examined have the same time constant. For damping levels greater than .02 a larger magnet parameter is required for stability. Figure 4-7 is the same set of curves with a magnet parameter of four. The result of magnet parameter increase is to shift the "knee" of the curves into the region of higher damping parameter. Thus, all the yaw inertia ratios have identical time constants below a damping parameter value of .015 for $M/I_B = 4$ compared to the value of .007 for $M/I_B = 2$.

Figure 4-8 is a composite of Figures 4-6 and 4-8 considering only one yaw inertia ratio. A magnet parameter of eight was also included. This figure indicates that if the magnet parameter is increased as the damping parameter is increased, the curve reduces to a straight line (on logarithmic graph paper) which is the envelope of all the magnet parameter curves. The envelope is plotted in Figure 4-9.

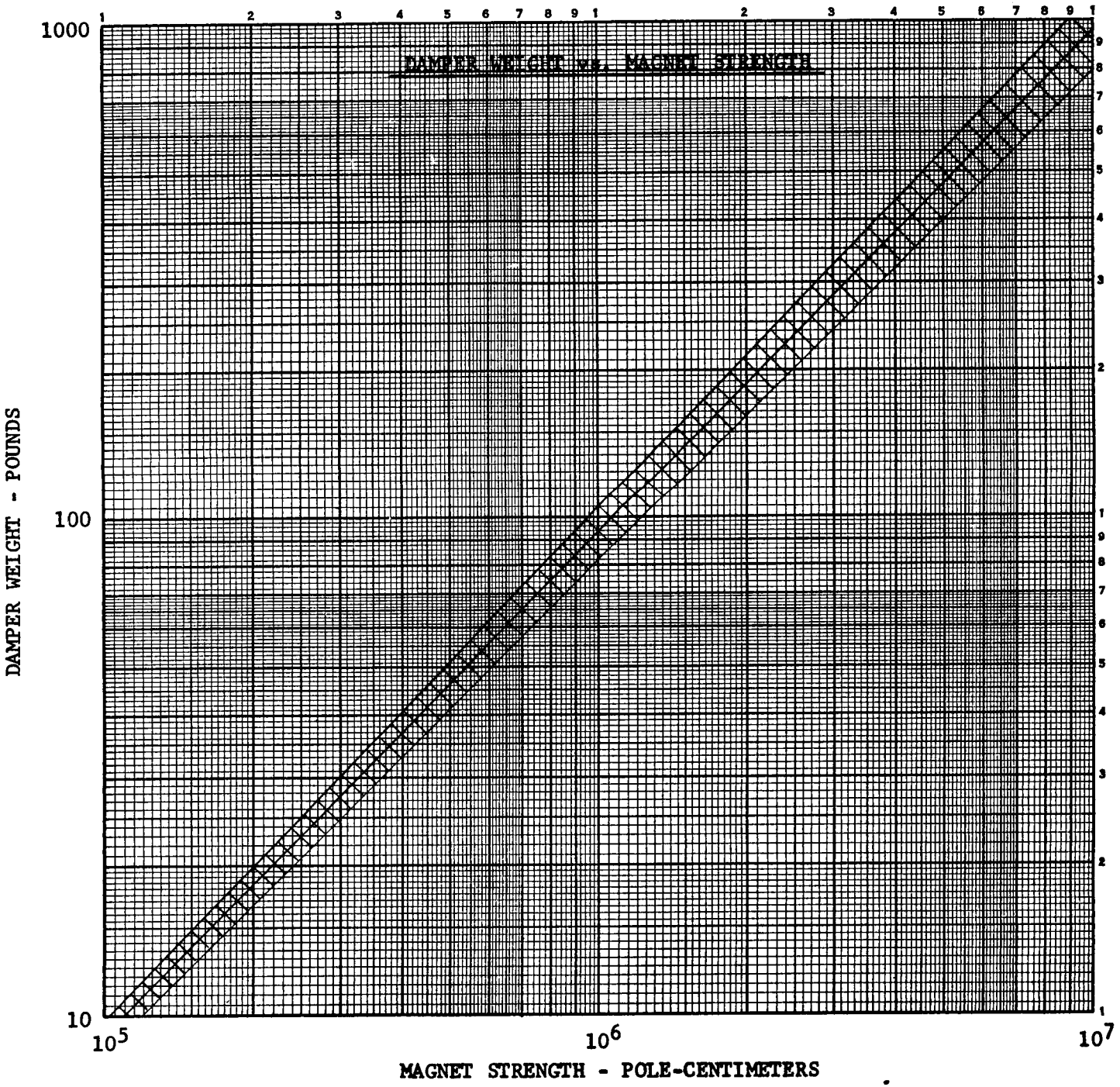
DAMPER WEIGHT vs. MAGNET STRENGTH
DAMPER WEIGHT - POUNDS
1000
100
10
10^5
10^6
10^7
MAGNET STRENGTH - POLE-CENTIMETERS

FIGURE 4-5

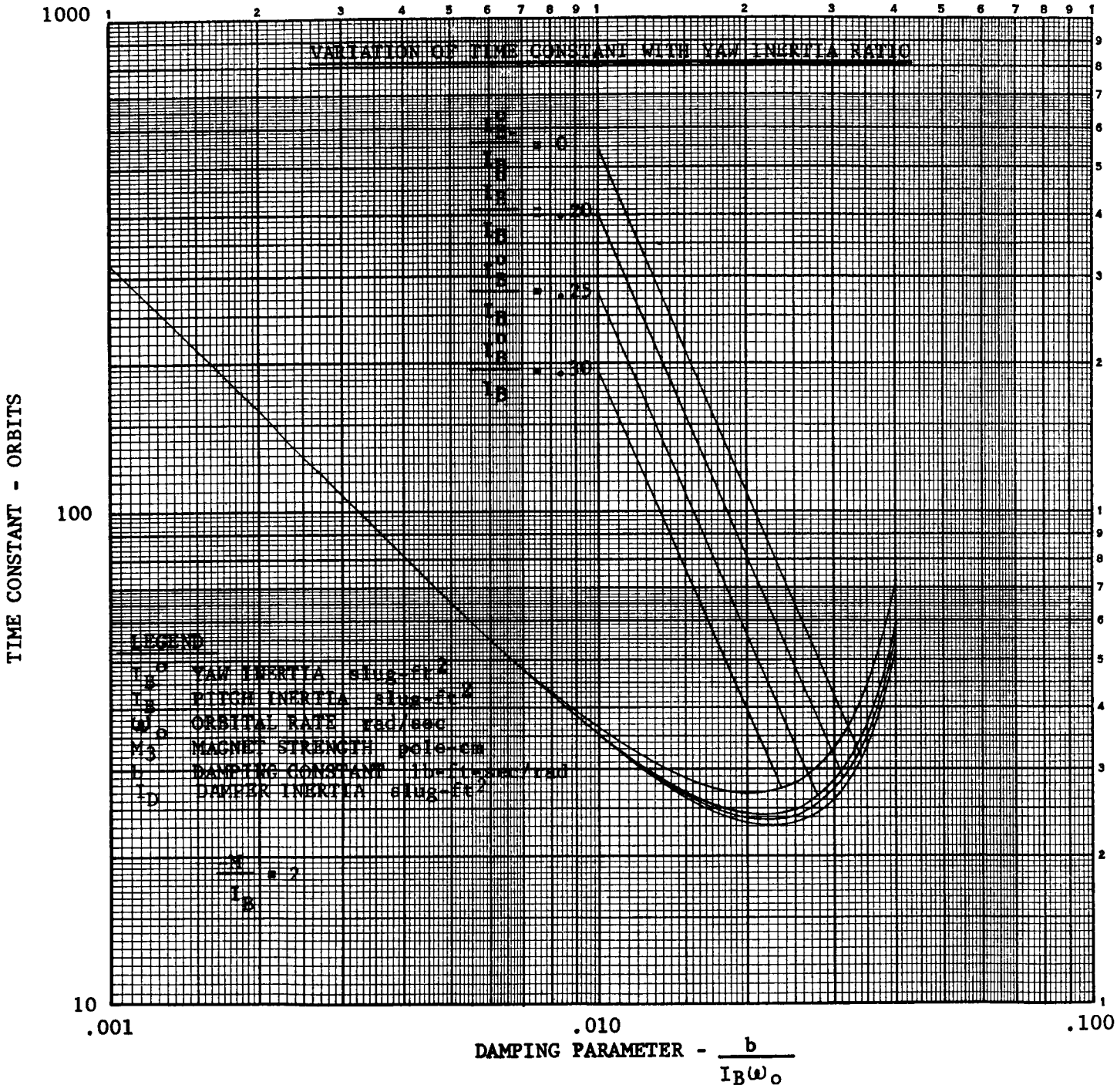

Figure 4-6. Variation of Time Constant with Yaw Inertia Ratio

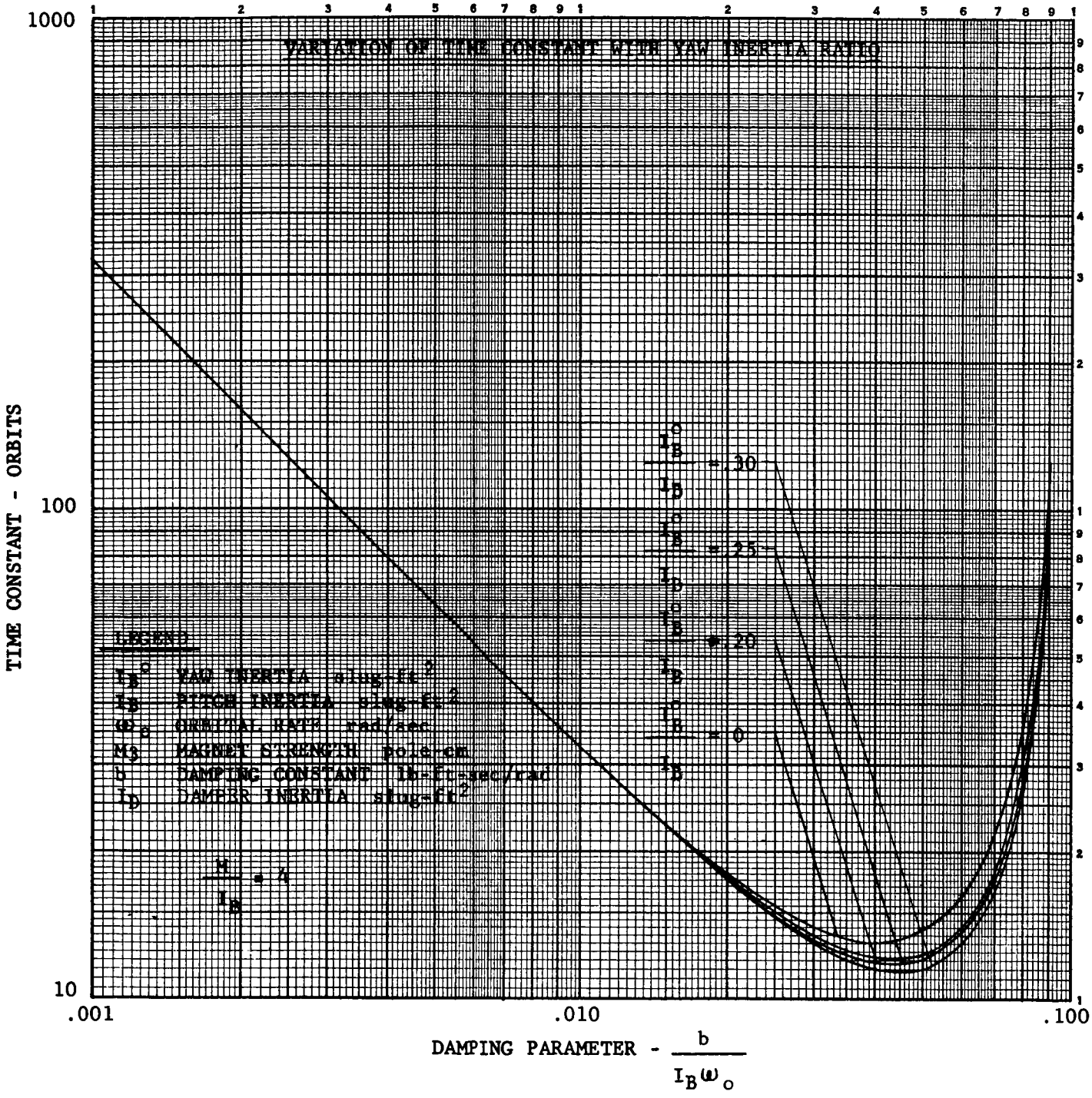

Figure 4-7. Variation of Time Constant with Yaw Inertia Ratio

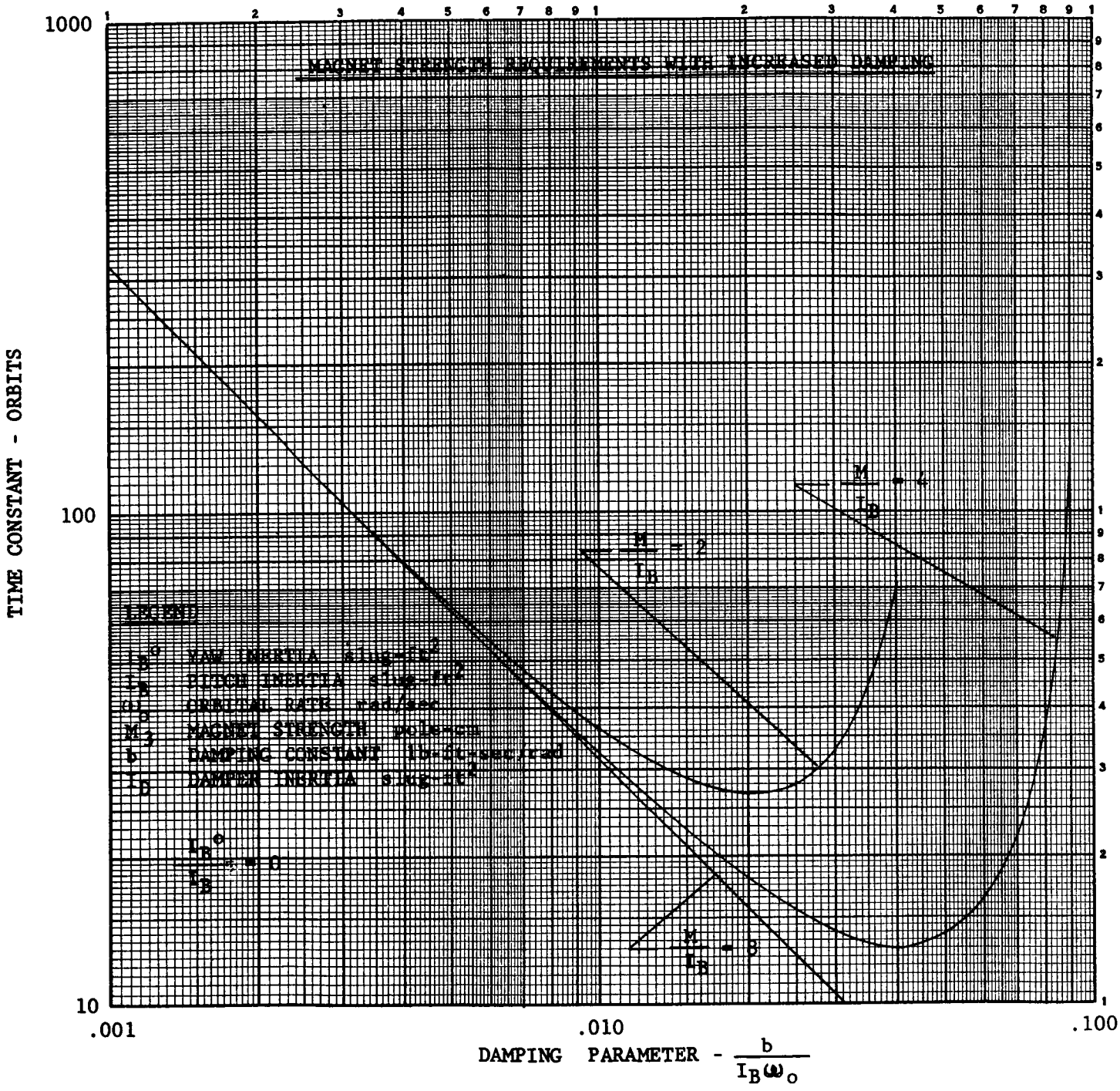

Figure 4-8. Magnet Strength Requirements with Increased Damping

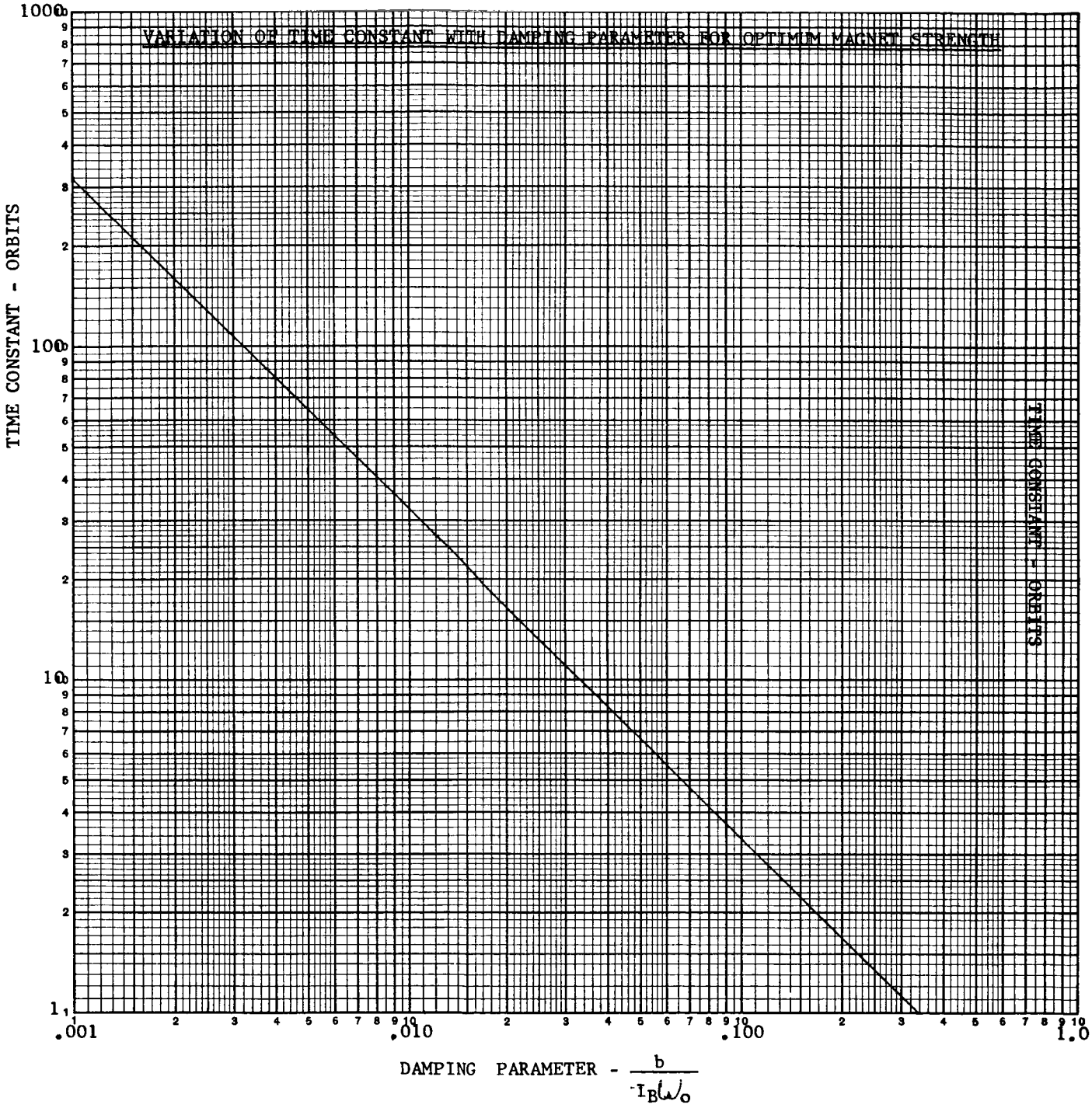

Figure 4-9. Variation of Time Constant with Damping Parameter for Optimum Magnet Strength

The reduction of the quartic solutions to the curve of Figure 4-9 indicates that the only parameter of significance is the damping parameter, providing the magnet parameter is selected adequate to the task. Figure 4-8 indicates that extremely strong magnet would perform satisfactorily, but a weight penalty would be incurred as discussed previously. Selecting the magnet parameter from Figure 4-3, consistent with a reasonable offset, will provide adequate damping and prevent the damper weight from becoming excessive. Optimization of the magnet offset should provide the least damper weight for any selected damping parameter.

Since steady state damper induced error and the decay time constant both depend solely upon the damping parameter, a cross plot of these parameters is possible. Figure 4-10 is this cross plot, employing lines of constant yaw inertia ratio. These lines appear because the steady state error is dependent upon the yaw inertia ratio, whereas the time constant is not. The lines represent more than one inertia ratio, because the steady state errors "double back" on themselves (Figure 4-2), and attempting to plot all the lines would cloud the graph. Hence, lines representing two inertias were employed.

4.4 SELECTION OF OPTIMUM PARAMETERS

Optimization of the POLES satellite requires that weight as well as performance be optimized. Considering Figure 4-2, a yaw inertia ratio of .25 has a minimum magnetically induced error, and can be tentatively accepted as optimum. At the anticipated eccentricity of .016, the steady state error would be approximately 1.5 degrees (Figure 4-4). Selecting a magnetically induced error of one degree (which is the same order of magnitude as the orbit eccentricity error) yields a damping parameter of .0171 and a time constant of twenty orbits (Figures 4-2 and 4-9). From the performance standpoint this is adequate. However, with a twenty degree offset, the necessary damping parameter requires a magnet parameter of 6.6. The pitch moment of inertia of the POLES satellite if 712,000 slug-ft^2. This inertia necessitates a magnet strength of 4,700,000 pole-cm. The weight of the damper required for this task (from Figure 4-5) is 540 lb. The satellite has a nominal weight (excluding damper) when fully deployed of approximately 500 lb. If the damping level is reduced, the damper weight is reduced and the time constant is increased. Figure 4-11 is a curve of damper weight versus time constant and indicates a sharp decline in damper weight with increasing time constant. The optimum point should be near the "knee" of the curve and a time constant of forty orbits and a damper weight of 170 pounds has been selected. The weight is still somewhat larger than desired, but has been tentatively selected as an operating point. For this operating point, the damping constant is 3.59 lb-ft-sec/rad, and the magnet strength is 2,700,000 pole-cm.

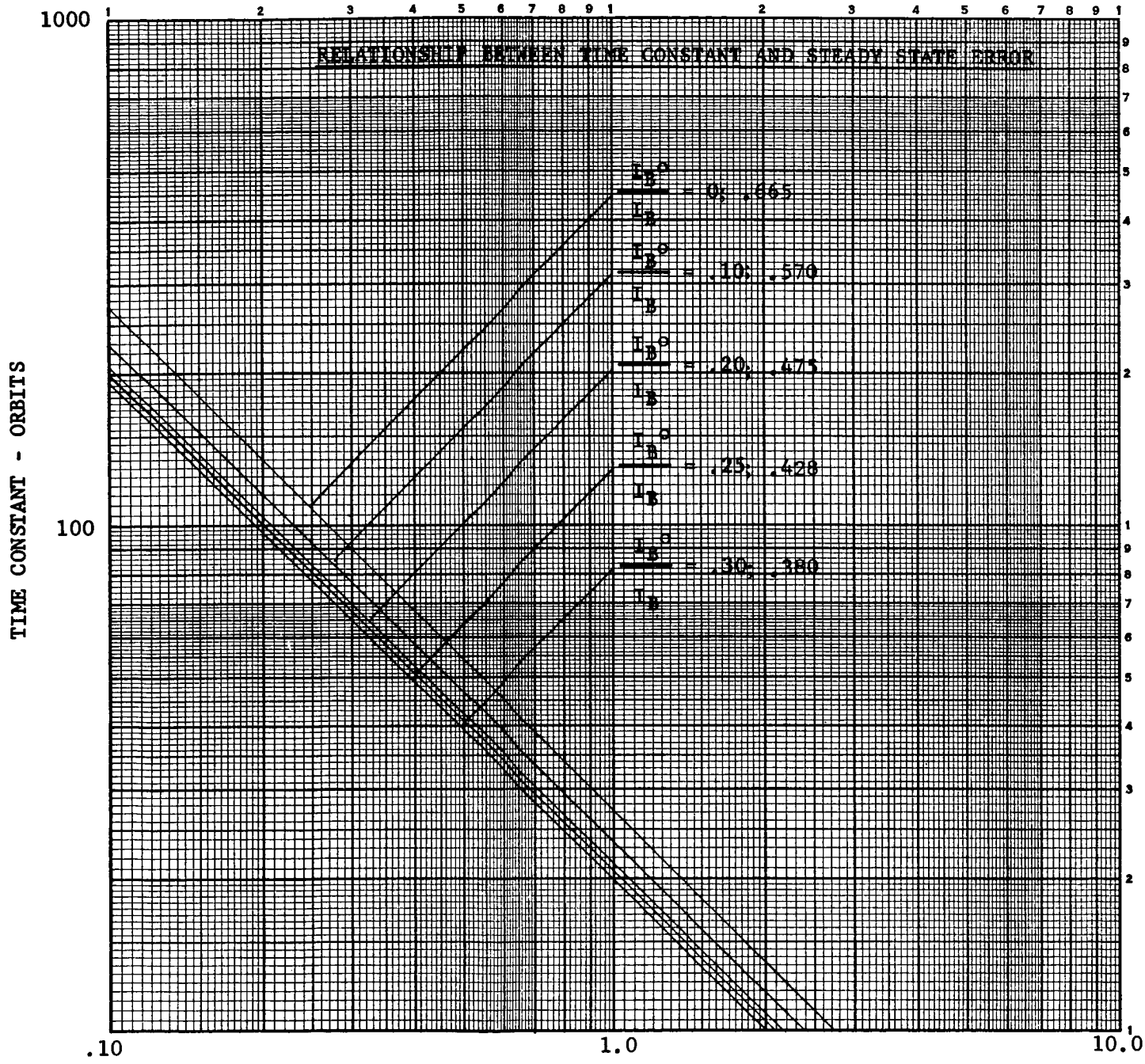

Figure 4-10. Relationship Between Time Constant and Steady State Error

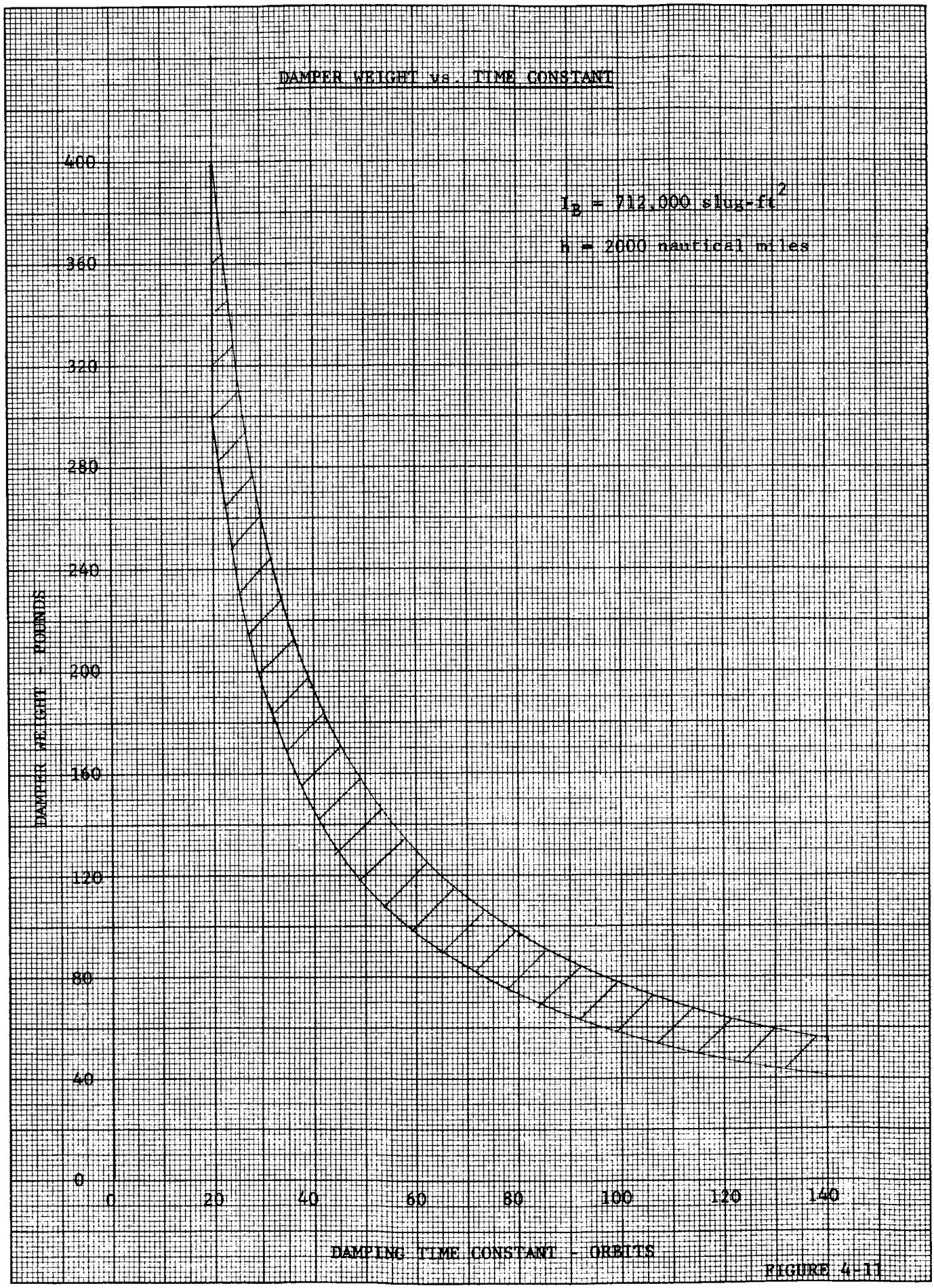
DAMPER WEIGHT vs. TIME CONSTANT
I_B = 712,000 slug-ft^2
h = 2000 nautical miles
DAMPER WEIGHT - POUNDS
400
360
320
280
240
200
160
120
80
40
0
0
20
40
60
80
100
120
140
DAMPING TIME CONSTANT - ORBITS

FIGURE 4-11

5.0 DEVELOPMENT OF THREE-AXIS DIGITAL COMPUTER PROGRAM

This section contains the complete description and equations for the computer program. Some results of preliminary studies are also included.

5.1 THREE-AXIS DIGITAL COMPUTER PROGRAM

5.1.1 General

This report includes the attitude dynamical equations of a satellite, consisting of two independent rigid bodies which are coupled through damping, and describes an IBM 7090 computer program which solves these equations by numerical integration. The use of the computer is mandatory because of the magnitude of the problem and because of the nonlinearities due to cross-coupling effects and to the relations between the external torques and the vehicle attitude and angular rates. The program is a tool for studying the attitude behavior of the vehicle under a variety of initial conditions and vehicle parameter values. Thus it is suitable for feasibility studies and approximate parameter optimization.

The heart of the analysis is the set of Euler's dynamical equations. These are written for torques, angular velocities, and angular accelerations about geometric axes. Hence, the terms involving products of inertia are retained. For the main body, the geometric axes used are parallel to those of symmetry, but translated so that the origin is at the center of mass of the main body.

The center of mass of the main body is assumed to follow a circular or elliptical orbit about the geocenter in a plane whose orientation is fixed in inertial space. The coupling effects between the vehicle's attitude motion and the vehicle's orbital motion are neglected. An approximation to orbital regression is included.

The external torques on the main body are those due to gravity gradient, solar radiation pressure, miscellaneous disturbances, magnetic damping and magnetic torque due to the net dipole of satellite in the earth's field. The external torques on the magnet are those due to its orientation in the earth's field and damping from the vehicle. The program has sufficient flexibility for the incorporation of torques due to other effects such as solar torques on the gravity rods, thermal bending on the rods and eddy currents caused by the earth's magnetic field.

The solar torque subroutine, which is included, defines solar torques on a lens shaped satellite composed of two dimensional mesh material. Equations are now available for the three dimensional mesh material. This change will pose no problem to the program since the net result will merely be the substitution of one subroutine for another.

The effects of the earth's shadow are also accounted for. Whenever the vehicle is in the earth's shadow, all solar torques are zero. In the derivation of all solar torques and of all shadow effects, it is assumed that all of the sun's rays in the vicinity of the earth or of the satellite are parallel, and that the intensity of the radiation is constant.

The effects of other celestial bodies, magnetic storms, internal moving parts, particle impacts, earth's albedo, etc. are neglected.

The angular accelerations about the body geometric axes are obtained as the solution of Euler's dynamical equations. These angular accelerations are numerically integrated to obtain the angular rates about the body axes. The required Euler angular rates are calculated from the body axis rates. The necessary equations are obtained by differentiating the equations describing the appropriate Euler transformation and solving for the rates. These rates are also integrated numerically to obtain the Euler angles. The angles used are those involved in the transformation from the orbital reference frame to the main vehicle reference frame, and in the transformation from the latter frame to the auxiliary vehicle reference frame.

The numerical integration method used provides for a variable integration interval, controlled by the computer in accordance with the computed numerical integration errors and a set of specified tolerable errors. This provides a consistent balance between accuracy and economy.

The maximum degree of flexibility in the whole program is achieved by the use of flexible subroutines for initialization, orbital parameters and variables, time derivatives to be integrated, numerical integration, external torques, and output. The output may be plotted by an X-Y plotter.

5.1.2 Vehicle Description

The vehicle has been described in section 3.0 to be basically composed of a lens shaped mesh balloon, two gravity gradient rods and a magnetically anchored damper system. It is intended here to define the coordinate axis system which was used in this program to define the POLES satellite. Figure 5-1 shows the satellite in a typical orbital attitude. The following axis definition assumes zero vehicle attitude angles. The axis from the local vertical to earth, positive away from earth, is the vehicle yaw axis which is called $\bar{x}_1$. The vehicle roll axis is directed along the velocity vector and is defined as $\bar{y}_1$. $\bar{z}_1$, the vehicle pitch axis, is directed along the vehicle's orbital angular velocity vector; it is approximately out of the plane of the paper in Figure 5-1. To simulate any net dipole of the satellite, provision has been made in the program for a magnet which is rigidly attached to the vehicle with its dipole at some fixed orientation with respect to the balloon body axis. This magnet dipole axis has been defined as $\bar{x}_2$. The $\bar{y}_2$ and $\bar{z}_2$ axes are normal to $\bar{x}_2$ and aligned along $\bar{y}_1$ and $\bar{z}_1$ if $\bar{x}_2$ is also aligned along $\bar{x}_1$.

The free floating magnet is defined by axes, x_3, y_3 and z_3. These axes are defined in the same sense as the x_1, y_1, z_1 system. The magnet dipole axis is $\bar{x}_3$.

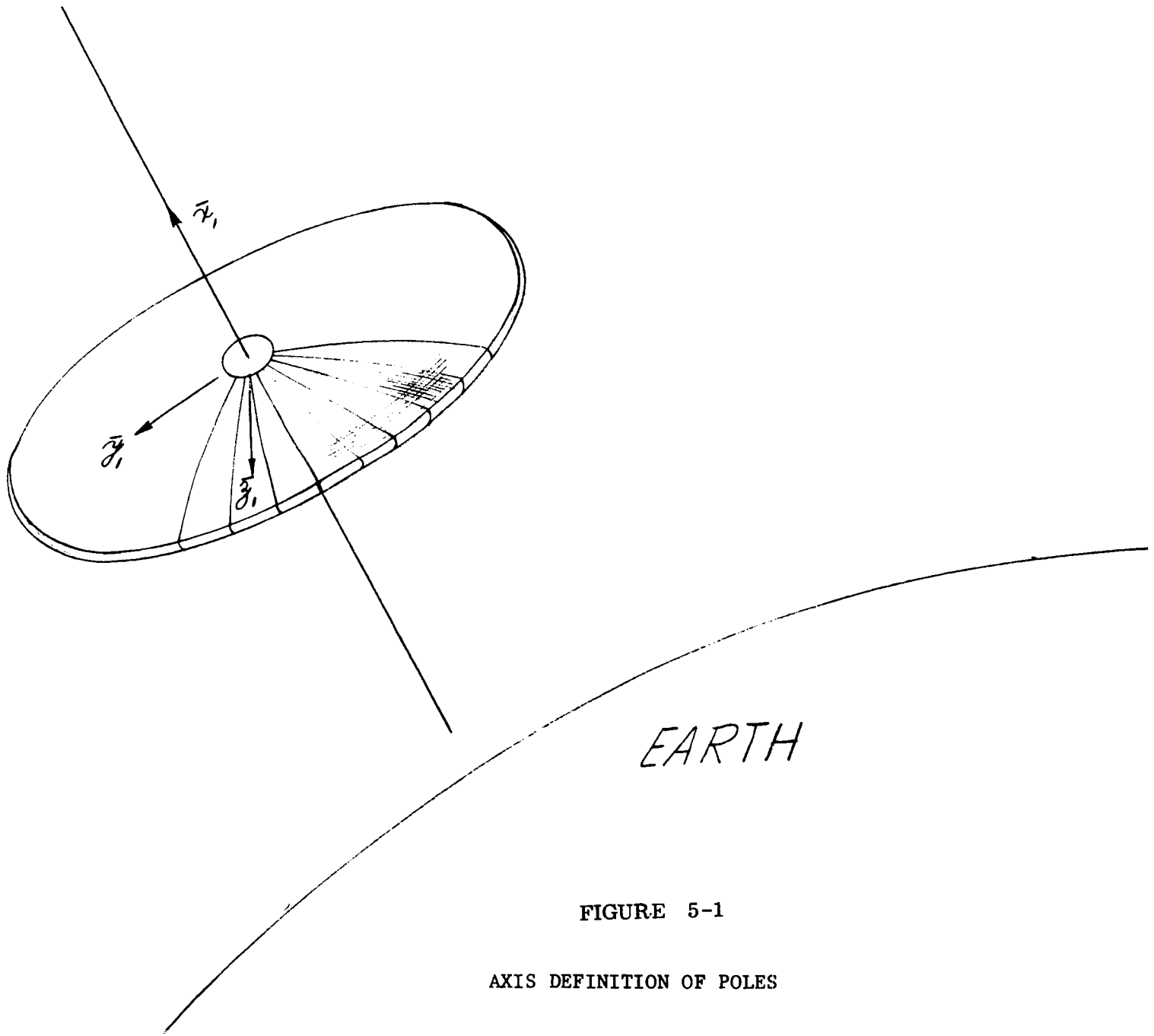

FIGURE 5-1

AXIS DEFINITION OF POLES

5.1.3 Coordinate Systems and Transformations

Several reference frames are required for the analysis. Each of these is described in terms of a right-handed orthonormal triad of vectors.

The first is the inertial reference frame, described by the triad uvw, and illustrated in Figure 5-2. $\bar{u}$ is directed from the helio center to the spring equinox position of the geocenter. $\bar{v}$ lies in the equatorial plane and is directed from the heliocenter to a point north of the summer solstice position of the geocenter. $\bar{w}$ is directed from the geocenter to the north pole.

The angle between the ecliptic and equatorial planes is $\epsilon = 23.45$ degrees. The orbital angular position of the earth, measured from the winter solstice position, is designated σ. The unit vector $\bar{s}$, directed from the heliocenter to the geocenter, is expressible in terms of a row-matrix $[F]$.

$$\bar{s} = [F] \begin{bmatrix} u \\ v \\ w \end{bmatrix} \tag{5.1}$$

The elements of the matrix $[F]$ are

$$\begin{aligned} f_{11} &= \sin \sigma \\ f_{12} &= -\cos \epsilon \cos \sigma \\ f_{13} &= \sin \epsilon \cos \sigma . \end{aligned} \tag{5.2}$$

The second reference frame is fixed in and rotates with the earth. This frame is described by the right-handed orthonormal triad, 1, 1_n, and w and is illustrated in Figure 5-3. $\bar{1}$ is directed from the geocenter to the point on the equator at the Greenwich meridian. The Greenwich hour angle, measured from u, is Ω_1, and

$$\bar{1} = \bar{u} \cos \Omega_1 + \bar{v} \sin \Omega_1 . \tag{5.3}$$

An expression for Ω_1, in terms of time of year, Greenwich Mean Time at injection and instantaneous orbital time will be discussed in Section 5.1.5.5.

The third reference frame is the orbital frame, described by the right-handed orthonormal triad rpq, and illustrated in Figure 5-4; $\bar{r}$ is the unit vector directed from the geocenter to the satellite position. $\bar{q}$ is the unit vector directed along the vehicle's orbital angular velocity vector in the right-handed screw sense. $\bar{p}$ is a unit vector in the orbital plane and is directed along the velocity vector if the orbit is circular. $\bar{r}$, $\bar{p}$, and $\bar{q}$ may be expressed in terms of $\bar{u}$, $\bar{v}$, and $\bar{w}$ by means of a matrix $[A]$,

$$\begin{bmatrix} r \\ p \\ q \end{bmatrix} = [A] \begin{bmatrix} u \\ v \\ w \end{bmatrix} \tag{5.4}$$

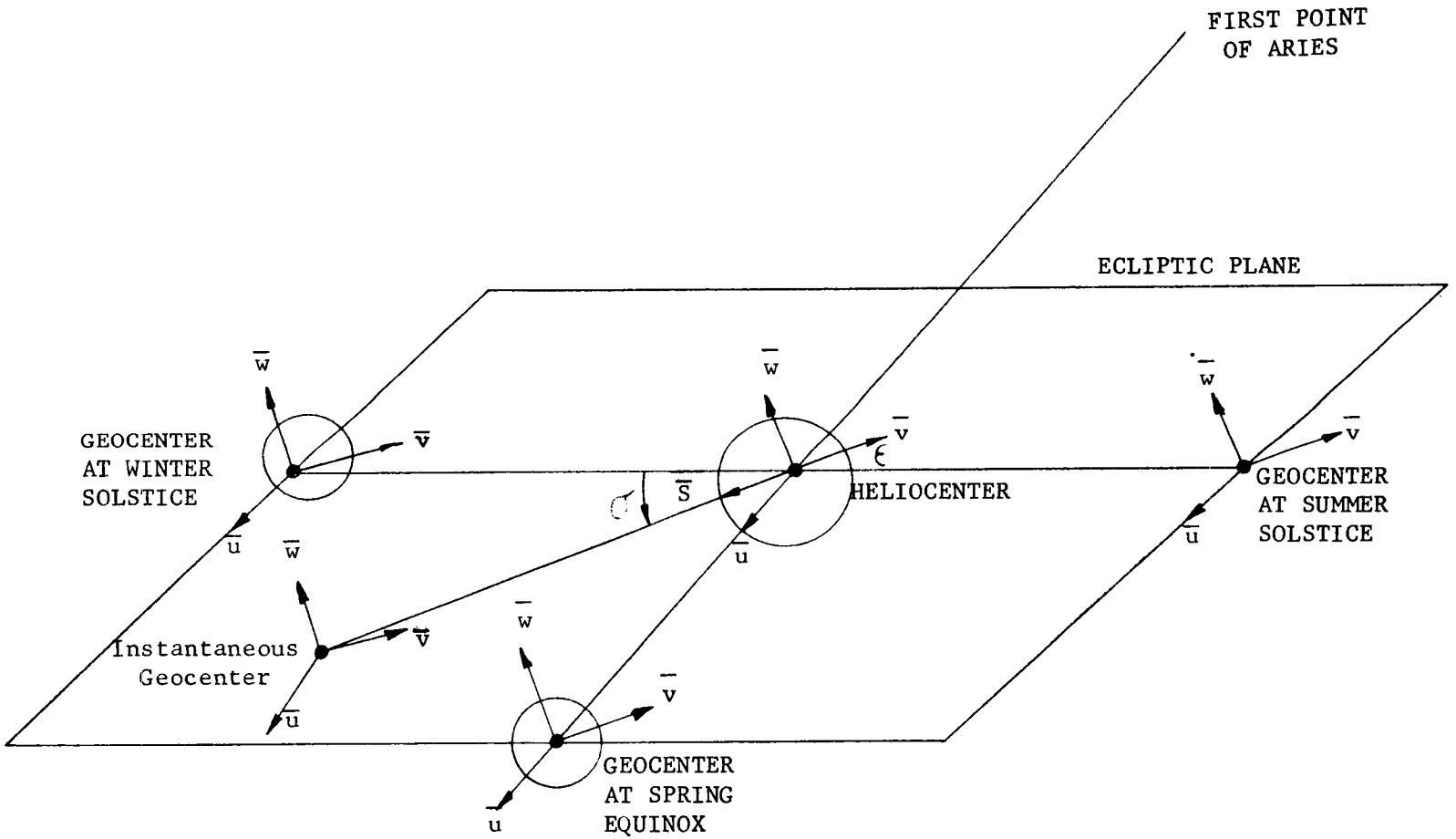

Figure 5-2 Inertial Reference Frame

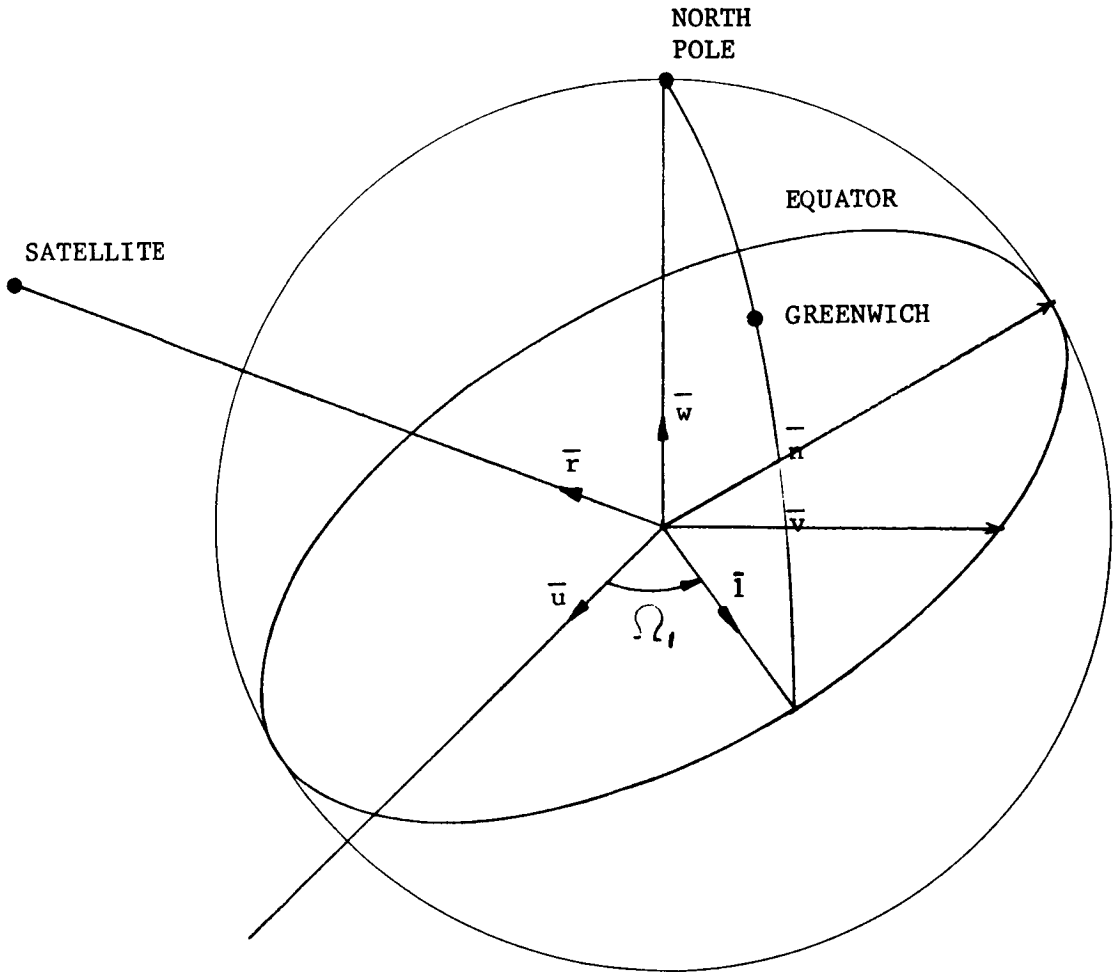

Figure 5-3 Earth Reference Frame

The elements of the matrix $[A]$ are

$$
\begin{aligned}
a_{11} &= \cos\Omega\cos\eta - \sin\Omega\cos\nu\sin\eta \\
a_{12} &= \sin\Omega\cos\eta + \cos\Omega\cos\nu\sin\eta \\
a_{13} &= \sin\nu\sin\eta \\
a_{21} &= -\sin\Omega\cos\eta\cos\nu - \cos\Omega\sin\eta \\
a_{22} &= \cos\Omega\cos\eta\cos\nu - \sin\Omega\sin\eta \\
a_{23} &= \sin\nu\cos\eta \\
a_{31} &= \sin\Omega\sin\nu \\
a_{32} &= -\cos\Omega\sin\nu \\
a_{33} &= \cos\nu.
\end{aligned}
\tag{5.5}
$$

As illustrated in Figure 5-5 Ω is the right ascension of the ascending node, ν is the orbital inclination, and η is the orbital angular position measured from the ascending node. The transformation from the inertial frame to the orbital frame corresponds to three rotations, each in a right-handed screw sense: (1) Ω about the $\bar{w}$ axis, (2) ν about the line of nodes (positive from the geocenter to the ascending node), and (3) η about the $\bar{q}$ axis. When Ω, ν, and η are all zero, $\bar{r}$ is along $\bar{u}$, $\bar{p}$ is along $\bar{v}$, and $\bar{q}$ is along $\bar{w}$.

The subroutines used for computing the orbital parameters and the orbital position η are described in Section 5.1.5.

The fourth reference frame is fixed in the main body of the vehicle (balloon). This frame is described by the right-handed orthonormal triad x_1 y_1 z_1. The designation of these main vehicle geometric axes has been described in Section 5.1.2 and illustrated in Figure 5-1.

The balloon coordinates x_1, y_1, z_1 and the magnet coordinates x_3, y_3, z_3 are related to the orbital coordinates by the Euler angle transformations $[E_b]$ and $[E_m]$ respectively:

$$
\begin{bmatrix} x_1 \\ y_1 \\ z_1 \end{bmatrix} = [E_b] \begin{bmatrix} r \\ p \\ q \end{bmatrix} \tag{5.6}
$$

$$
\begin{bmatrix} x_3 \\ y_3 \\ z_3 \end{bmatrix} = [E_m] \begin{bmatrix} r \\ p \\ q \end{bmatrix} \tag{5.7}
$$

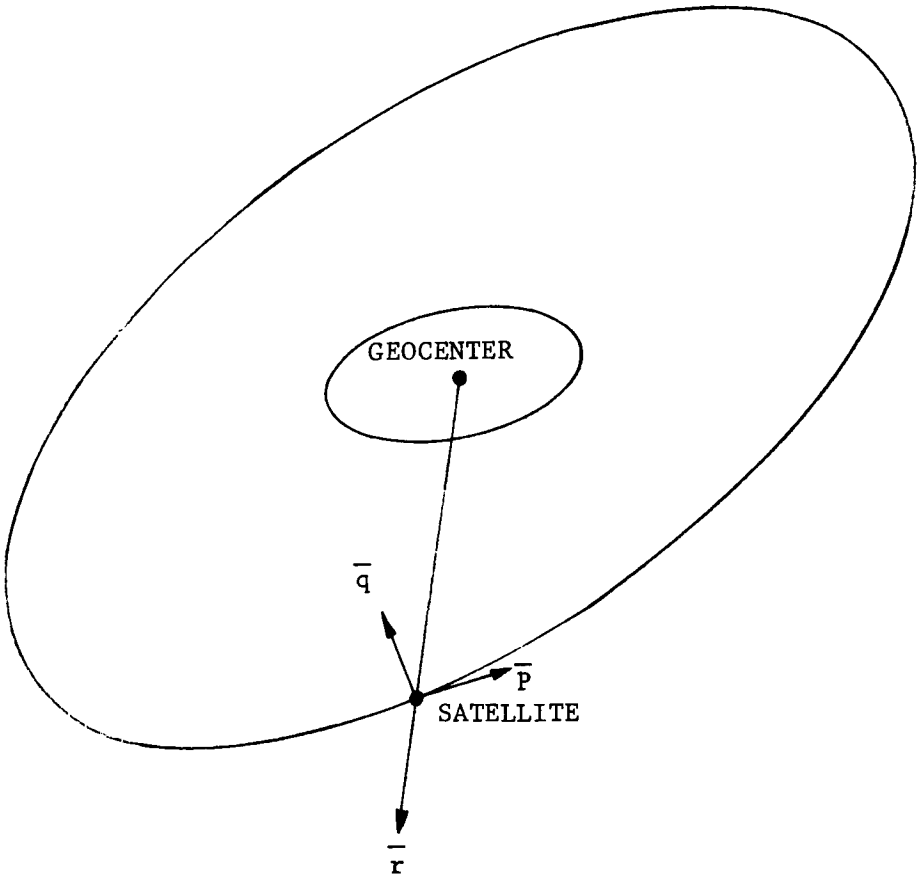

Figure 5-4 Orbital Reference Frame

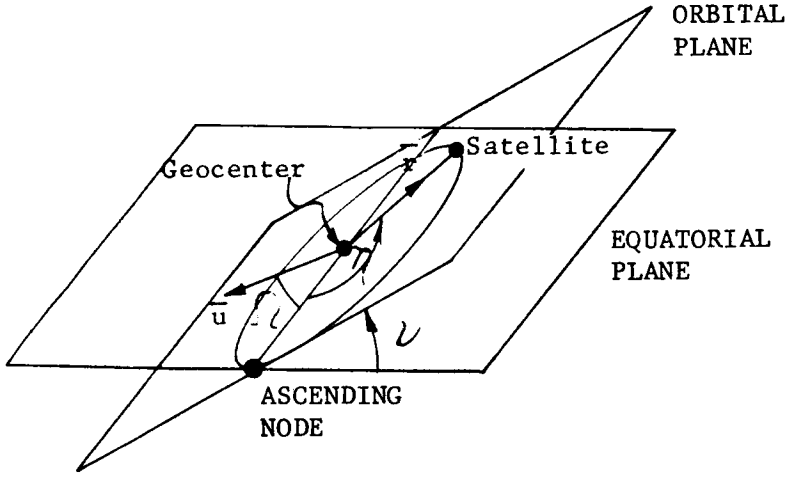

Figure 5-5 Orbital Angular Coordinates

The elements of the $[E]$ matrix are:

$$
\begin{aligned}
e_{11} &= \cos\theta_p \cos\theta_r \\
e_{12} &= \sin\theta_p \cos\theta_r \\
e_{13} &= -\sin\theta_r \\
e_{21} &= \cos\theta_p \sin\theta_r \sin\theta_y - \sin\theta_p \cos\theta_y \\
e_{22} &= \cos\theta_p \cos\theta_y + \sin\theta_p \sin\theta_r \sin\theta_y \\
e_{23} &= \cos\theta_r \sin\theta_y \\
e_{31} &= \sin\theta_p \sin\theta_y + \cos\theta_p \sin\theta_r \cos\theta_y \\
e_{32} &= \sin\theta_p \sin\theta_r \cos\theta_y - \cos\theta_p \sin\theta_y \\
e_{33} &= \cos\theta_r \cos\theta_y
\end{aligned}
\tag{5.8}
$$

Note, the subscripts b or m must be attached to the above matrix elements and Euler angles to denote whether the parameters denote the relation of the balloon or magnet to the orbit coordinates. Figure 5-6 illustrates the $[E_b]$ transformation from orbital coordinates to the balloon body axes. A similiar figure could be used to illustrate the transformation from orbital coordinates to the magnet coordinates, x_3 , y_3 , z_3 .

In Section 5.1.2 it is seen that $\overline{x}_3$ represents the dipole axes of the magnet while $\overline{y}_3$ and $\overline{z}_3$ are aligned along the roll and pitch axes of the balloon for zero attitude angles.

The transformation matrix $[E_b]$ corresponds to three right-handed rotations; (1) θ_{pb} about the $\overline{q}$ axis, (2) θ_{rb} about the intermediate $\overline{y}_1$ axis and (3) θ_{yb} about the $\overline{x}_1$ axis. When θ_{pb}, θ_{rb}, and θ_{yb} are all zero, $\overline{x}_1$ lies along $\overline{r}$, $\overline{y}_1$ lies along $\overline{p}$ and $\overline{z}_1$ lies along $\overline{q}$. When θ_{pb}, θ_{rb} and θ_{yb} are all small, they may be considered pitch, roll and yaw attitude errors respectively. Similiar remarks hold for the transformation $[E_m]$.

Besides the magnet which is floating free with respect to the balloon, another magnet must be simulated. This magnet is rigidly attached to the balloon although its axes are not necessarily aligned with the balloon axis. For purposes of identification, this magnet will be spoken of as the"balloon magnet" while the independent magnet will not be specially identified. Two degrees of freedom will be sufficient to relate the new magnet axes, x_2, y_2, z_2 to the balloon axes, x_1, y_1, z_1.

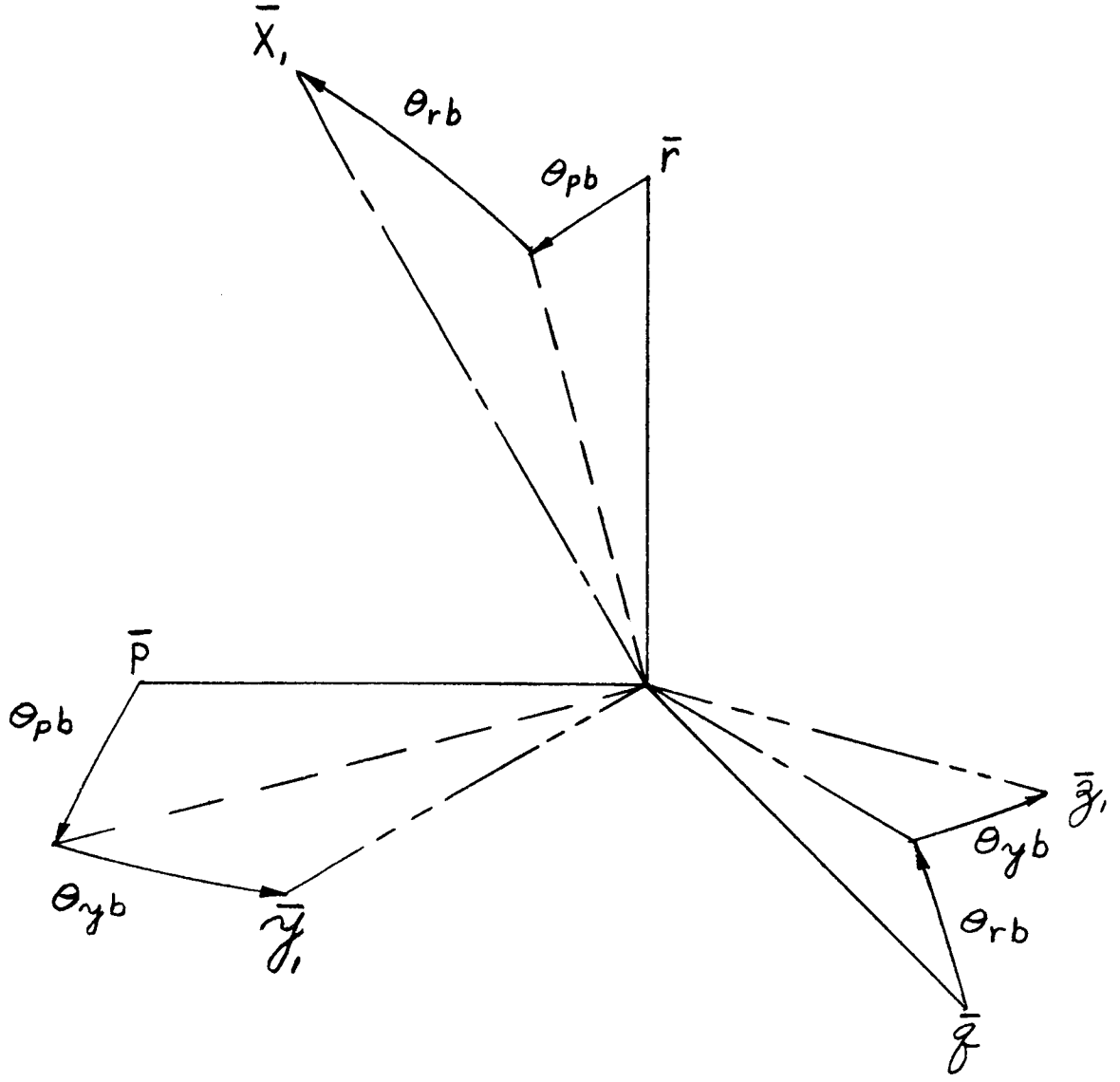

Figure 5-6 Transformation $[E_b]$ from $\bar{r}$, $\bar{p}$, $\bar{q}$ to $\bar{x}_1, \bar{y}_1, \bar{z}_1$.

Therefore,

$$\begin{bmatrix} x_2 \\ y_2 \\ z_2 \end{bmatrix} = [C] \begin{bmatrix} x_1 \\ y_1 \\ z_1 \end{bmatrix} \tag{5.9}$$

where $\overline{x}_2$ is the dipole axis and

$$\begin{aligned} c_{11} &= \cos\gamma \cos\beta \\ c_{12} &= \sin\gamma \cos\beta \\ c_{13} &= -\sin\beta \\ c_{21} &= -\sin\gamma \\ c_{22} &= \cos\gamma \\ c_{23} &= 0 \\ c_{31} &= \cos\gamma \sin\beta \\ c_{32} &= \sin\gamma \sin\beta \\ c_{33} &= \cos\beta \end{aligned} \tag{5.10}$$

γ is a rotation about the $\overline{z}_1$ axis while β is a rotation about the $\overline{y}_2$ axis. These angles will be constant for a given configuration.

It can be seen that the balloon magnet can be related to orbit coordinates by $[H]$:

$$\begin{bmatrix} x_2 \\ y_2 \\ z_2 \end{bmatrix} = [H] \begin{bmatrix} r \\ p \\ q \end{bmatrix} \tag{5.11}$$

where $$[H] = [C]\ [E_b] \tag{5.12}$$

The position of the sun with respect to the balloon axes is necessary for the computation of the solar torques on the balloon. This can be represented as the dot product of the body axes and the sun vector expressed in the earth-centered inertial coordinate system, u, v, w. The balloon axes may be related to the orbital coordinates by the matrix $[B]$:

$$\begin{bmatrix} x_1 \\ y_1 \\ z_1 \end{bmatrix} = [B] \begin{bmatrix} u \\ v \\ w \end{bmatrix} \tag{5.13}$$

where $[B] = [E_b] [A]$ (5.14)

Therefore, from equations (5.1) and (5.13)

$$s_{x1} = s \cdot x_1 = f_{11}b_{11} + f_{12}b_{12} + f_{13}b_{13}$$
$$s_{y1} = s \cdot y_1 = f_{11}b_{21} + f_{12}b_{22} + f_{13}b_{23} \quad (5.15)$$
$$s_{z1} = s \cdot z_1 = f_{11}b_{31} + f_{12}b_{32} + f_{13}b_{33}$$

The magnetic field is computed by a subroutine programmed by Dr. R. T. Frost. The inputs to this subroutine are altitude in kilometers, longitude and latitude. The output represents the magnetic torque and the components along earth referenced coordinates. These components are

B_R, radial component, positive inward

B_θ, directed along the local meridian, positive in the direction of the velocity vector

B_ϕ, directed along the local latitude arc, positive in a westerly direction when the vehicle is moving south to north.

These magnetic components must be resolved along the orbital coordinates. Thus

$$\begin{bmatrix} H_r \\ H_p \\ H_q \end{bmatrix} = [D] \begin{bmatrix} -B_R \\ B_\theta \\ B_\phi \end{bmatrix} \quad (5.16)$$

where H_r, H_p, H_q are the components along the r, p, q axes respectively. Since $H_r = -B_R$, the $[D]$ transformation is a rotation about H_r. It can be shown that the matrix elements of $[D]$ are:

$$d_{11} = 1$$
$$d_{12} = 0$$
$$d_{13} = 0$$
$$d_{21} = 0$$
$$d_{22} = \sin\nu \cos\Omega_3$$
$$d_{23} = -\cos\nu / \cos \text{LAT}$$
$$d_{31} = 0$$
$$d_{32} = \cos\nu / \cos \text{LAT} \quad (5.17)$$
$$d_{33} = \sin\nu \cos\Omega_3$$

To define the damper torques which the magnet exerts on the balloon and which the balloon exerts on the magnet, it will be necessary to define the balloon body rates in terms of the magnet body rates and vice versa. The rates around the magnet axes can be resolved along the balloon body axes by the following transformation:

$$\begin{bmatrix} \omega_{mx1} \\ \omega_{my1} \\ \omega_{mz1} \end{bmatrix} = \left[E_b\right]\left[E_m^{-1}\right]\begin{bmatrix} \omega_{x3} \\ \omega_{y3} \\ \omega_{z3} \end{bmatrix} \tag{5.18}$$

The rates around the balloon body axes can be resolved along the magnet axes by the following transformation:

$$\begin{bmatrix} \omega_{bx3} \\ \omega_{by3} \\ \omega_{bz3} \end{bmatrix} = \left[E_m\right]\left[E_b^{-1}\right]\begin{bmatrix} \omega_{x1} \\ \omega_{y1} \\ \omega_{z1} \end{bmatrix} \tag{5.19}$$

5.1.4 Vechicle Attitude Dynamics

The attitude dynamics for the two body simulation are expressed in Euler's dynamical equations. The interaction of the two bodies is expressed through the magnetic damper torque.

The dynamic equations for the balloon contain terms for changing moments of inertia. These are included so that the satellite may be studied during rod extension. Provisions have been made in the program so that a subroutine to define the time varying moments of inertia can be included for each vehicle configuration.

The dynamic equations for the balloon are as follows:

$$\begin{aligned} T_{x1} &= \dot{I}_{xx1}\,\omega_{x1} - \dot{I}_{xy1}\,\omega_{y1} - \dot{I}_{xz1}\,\omega_{z1} + I_{xx1}\,\dot{\omega}_{x1} - I_{xy1}\,\dot{\omega}_{y1} \\ &\quad - I_{xz1}\,\dot{\omega}_{z1} + \omega_{y1}\,G_{z1} - \omega_{z1}\,G_{y1} \\ T_{y1} &= \dot{I}_{yy1}\,\omega_{y1} - \dot{I}_{xy1}\,\omega_{x1} - \dot{I}_{yz1}\,\omega_{z1} + I_{yy1}\,\dot{\omega}_{y1} - I_{xy1}\,\dot{\omega}_{x1} \\ &\quad - I_{yz1}\,\dot{\omega}_{z1} + \omega_{z1}\,G_{x1} - \omega_{x1}\,G_{z1} \\ T_{z1} &= \dot{I}_{zz1}\,\omega_{z1} - \dot{I}_{xz1}\,\omega_{x1} - \dot{I}_{yz1}\,\omega_{y1} + I_{zz1}\,\dot{\omega}_{z1} - I_{xz1}\,\dot{\omega}_{x1} \\ &\quad - I_{yz1}\,\dot{\omega}_{y1} + \omega_{x1}\,G_{y1} - \omega_{y1}\,G_{x1} \end{aligned} \tag{5.20}$$

where

$$\begin{aligned} G_{x1} &= I_{xx1}\,\omega_{x1} - I_{xy1}\,\omega_{y1} - I_{xz1}\,\omega_{z1} \\ G_{y1} &= -I_{xy1}\,\omega_{x1} + I_{yy1}\,\omega_{y1} - I_{yz1}\,\omega_{z1} \\ G_{z1} &= -I_{xz1}\,\omega_{x1} - I_{yz1}\,\omega_{y1} + I_{zz1}\,\omega_{z1} \end{aligned} \tag{5.21}$$

The equations of motion for the magnet are the same as those listed above for the balloon except that the subscript must be changed from (1) to (3). Also the moments of inertia will not change with time.

Therefore,

$$T_{x3} = I_{xx3}\dot{\omega}_{x3} - I_{xy3}\dot{\omega}_{y3} - I_{xz3}\dot{\omega}_{z3} + \omega_{y3}G_{z3} - \omega_{z3}G_{y3}$$
$$T_{y3} = I_{yy3}\dot{\omega}_{y3} - I_{xy3}\dot{\omega}_{x3} - I_{yz3}\dot{\omega}_{z3} + \omega_{z3}G_{x3} - \omega_{x3}G_{z3}$$
$$T_{z3} = I_{zz3}\dot{\omega}_{z3} - I_{xz3}\dot{\omega}_{x3} - I_{yz3}\dot{\omega}_{y3} + \omega_{x3}G_{y3} - \omega_{y3}G_{x3} \qquad (5.22)$$

where

$$G_{x3} = I_{xx3}\omega_{x3} - I_{xy3}\omega_{y3} - I_{xz3}\omega_{z3}$$
$$G_{y3} = -I_{xy3}\omega_{x3} + I_{yy3}\omega_{y3} - I_{yz3}\omega_{z3}$$
$$G_{z3} = -I_{xz3}\omega_{x3} - I_{yz3}\omega_{y3} + I_{zz3}\omega_{z3} \qquad (5.23)$$

The T's represent generalized torques. The balloon will have five torques acting on it:

T_{g1} gravity restoring torque

T_{d1} damper torque

T_{s1} solar torque

T_{m1} torque on rigidly attached magnet, must be resolved along x_1, y_1, z_1 axes

T_{t1} disturbance torque on balloon

The magnet will have two torques acting on it:

T_{m3} magnetic restoring torque

T_{d3} damper torque

Thus $T_1 = T_{g1} + T_{d1} + T_{s1} + T_{m1} + T_{t1}$

$T_3 = T_{m3} + T_{d3}$ (5.24)

T_1 and T_3 may be broken into their components:

T_{x1}, T_{y1}, T_{z1}, T_{x3}, T_{y3}, T_{z3}

5.1.4.1 Gravity Restoring Torques on Balloon

The non-uniformity of the earth's gravitational field results in a field gradient. In this analysis the earth is assumed to be perfectly spherical, so the gravitational field varies inversely as the square of the geocentric distance. Thus, when a satellite is in orbit, the force per unit mass is greater in the region occupied by that portion of the satellite closer to the earth, and it is less in the region occupied by that portion of the satellite farther from the earth. If the satellite has three unequal moments of inertia about its principal axes, the only position of stable equilibrium is that in which the axis of least moment of inertia points along the local vertical, and in which the axis of greatest moment of inertia is perpendicular to the orbital plane. In any other position the satellite will experience torques which tend to turn it into the position of stable equilibrium.

Equations are given for the gravity gradient torques acting on the balloon, about axes parallel to the geometric axes but which pass through the center of mass. The moments of inertia of the balloon (including gravity rods) about center of mass are I_{xx1}, I_{yy1}, I_{zz1}. The corresponding products of inertia are I_{xy1}, I_{xz1}, and I_{yz1}. During rod extension these moments of inertia will change with time. The respective components of the gravity torque are:

$$T_{gx1} = \frac{3K}{R^3}\left[e_{21b}e_{31b}(I_{zz1}-I_{yy1})+I_{yz1}(e_{31b}^2-e_{21b}^2)+e_{11b}e_{31b}I_{xy1}-e_{11b}e_{21b}I_{xz1}\right]$$

$$T_{gy1} = \frac{3K}{R^3}\left[e_{11b}e_{31b}(I_{xx1}-I_{zz1})+I_{xz1}(e_{11b}^2-e_{31b}^2)+e_{11b}e_{21b}I_{yz1}-e_{21b}e_{31b}I_{xy1}\right] \quad (5.25)$$

$$T_{gz1} = \frac{3K}{R^3}\left[e_{11b}e_{21b}(I_{yy1}-I_{xx1})+I_{xy1}(e_{21b}^2-e_{11b}^2)+e_{21b}e_{31b}I_{xz1}-e_{11b}e_{31b}I_{yz1}\right]$$

K is the universal gravitational constant multiplied by the mass of the earth,

R is the geocentric distance calculated by the orbit subroutine.

The e_{i1b} are the direction cosines of the local vertical unit vector $\bar{r}$ with respect to the balloon axes.

5.1.4.2 Damper Torque on Balloon

Damping will be obtained by the relative motion of two concentric spheres which are separated by a viscous fluid. When there is a difference in angular velocity, there will be a viscous shearing action exerted on the fluid which results in a dissipation of energy. In order to produce a difference in angular velocity of the spheres and to be assured that they do not eventually "lock up" on each other, the inner sphere is fixed to the earth's field by the magnetic anchor. The torque which is transmitted to the balloon thru the viscous coupling is a function of the damping coefficient, b, and the relative angular velocities of the two spheres. The following equations define the damping torque on the balloon:

$$T_{dx1} = -b(\omega_{x1} - \omega_{mx1})$$

$$T_{dy1} = -b(\omega_{y1} - \omega_{my1}) \qquad (5.26)$$

$$T_{dz1} = -b(\omega_{z1} - \omega_{mz1})$$

ω_{mx1}, ω_{my1}, ω_{mz1}, are the components of the magnet body rates resolved along the balloon body axes. This resolution is defined by equation (5.18).

5.1.4.3 Solar Torques on Balloon

Solar torques arise from solar radiation pressure on the surfaces of a body. This pressure is the result of bombardment of the surfaces by photons. The pressure is exerted on both absorbing and reflecting surfaces. This program has the capability of computing solar torques on both a solid and mesh lens shaped balloon. The equations for the mesh balloon are a first approximation and do not consider the thickness of the wires which make up the mesh satellite. However, the solar torque resulting on the bottom surface as a result of the sun's rays passing through open spaces on the top part of the lens is considered. It is felt that the present definition of the mesh balloon is a good approximation. The equations to define the torques on the i, j, k axes of a lens shaped balloon are given in Section 7.1. These equations consider the sun to be always in the i, k plane which will not necessarily be so. Therefore, a transformation is necessary to convert the torque components T_i, T_j and T_k into components about the body axes. The following equations express this transformation:

$$T_{sx1} = T_i$$

$$-T_{sy1} = \frac{s_{z1}}{\sin\theta} T_j + \frac{s_{y1}}{\sin\theta} T_k \qquad (5.27)$$

$$-T_{sz1} = \frac{-s_{y1}}{\sin\theta} T_j + \frac{s_{z1}}{\sin\theta} T_k$$

$$\text{where } \sin\theta = \sqrt{s_{y1}^2 + s_{z1}^2}. \qquad (5.28)$$

when $\theta = 0$, $T_{sy1} = T_{sz1} = 0$.

The offsets y_L, z_L must also be expressed in terms of offsets, y_{10}, z_{10} along the body axes. This transformation is

$$z_L = -(y_{10}s_{y1} + z_{10}\, s_{z1})/\sin\theta \qquad (5.29)$$

$$y_L = -(y_{10}s_{z1} - z_{10}\, s_{y1})/\sin\theta$$

5.1.4.4 Effect of Earth's Shadow

If the vehicle is in the earth's shadow, all of the solar torques are zero. For simplicity, all of the sun's rays are considered parallel, and the earth's shadow is thus a cylinder. The shadow criterion is based on the relation between two unit vectors, $\bar{s}$ in the direction of the sun's rays and $\bar{r}$ in the direction of the local

vertical, positive upward. The component of $\bar{r}$ in the direction of $\bar{s}$ is:

$$r_s = \bar{r} \cdot \bar{s} = a_{11}f_{11} + a_{12}f_{12} + a_{13}f_{13}. \tag{5.30}$$

If r_s is zero or negative, the vehicle is in the half of the orbit toward the sun and can not be in shadow. If r_s is positive, the vehicle is in the half of the orbit away from the sun, and its being in the earth's shadow depends upon its perpendicular distance R_c from the earth-sun line.

$$R_c = R\sqrt{1 - r_s^2} \tag{5.31}$$

If R_c is equal to or less than the earth's radius, .20902956 x 10^8 feet, then the vehicle is in the earth's shadow. If R_c is greater than the earth's radius, the vehicle is not in the earth's shadow.

5.1.4.5 Magnetic Torque on Balloon Magnet

The balloon magnet will exert a magnetic restoring torque on the balloon which is dependent on the magnet orientation in the balloon and the satellite's position with respect to the earth's magnetic field. The magnetic restoring torque can be written:

$$T_{m2} = M_2 \ (\bar{x}_2 \times \bar{H}) \tag{5.32}$$

where $\bar{x}_2$ and $\bar{H}$ are vectors whose components are expressed in the r, p, q orbital coordinate system; M_2 is the magnetic moment of the dipole expressed in appropriate units. $\bar{x}_2$ is the dipole axis of the magnet which is rigidly attached to the balloon. This axis expressed in orbital coordinates is

$$\bar{x}_2 = h_{11}\bar{r} + h_{12}\bar{p} + h_{13}\bar{q} \tag{5.33}$$

where h_{1j} are the direction cosines of the dipole axis with respect to the r, p, q axes. $\bar{H}$ is the earth's magnetic field intensity which is outputted from Dr. Frost's subroutine to define the earth's magnetic field. Equation (5.16) defines the components of the magnetic field in the orbital coordinate system. Therefore, equation (5.32) may be written:

$$T_{m2} = M_2 \begin{bmatrix} \bar{r} & \bar{p} & \bar{q} \\ h_{11} & h_{12} & h_{13} \\ H_r & H_p & Hq \end{bmatrix} \tag{5.34}$$

or

$$\begin{aligned} T_{mr2} &= M_2 \ (h_{12}H_q - h_{13}H_p) \\ T_{mp2} &= M_2 \ (h_{13}H_r - h_{11}H_q) \\ T_{mq2} &= M_2 \ (h_{11}H_p - h_{12}H_r) \end{aligned} \tag{5.35}$$

and

$$\begin{bmatrix} T_{mx1} \\ T_{my1} \\ T_{mz1} \end{bmatrix} = \left[E_b \right] \begin{bmatrix} T_{mr2} \\ T_{mp2} \\ T_{mq2} \end{bmatrix} \tag{5.36}$$

5.1.4.6 Miscellaneous Disturbance Torques on Balloon

For increased flexibility it is desired to have provision for periodic and secular disturbance torques on the main body. The general expressions for the body-axis components of these torques are:

$$\begin{aligned} T_{tx1} &= T_1 + T_2 \sin(\omega_1 t + \phi_1) + T_3 \sin(\omega_2 t + \phi_2) \\ T_{ty1} &= T_4 + T_5 \sin(\omega_1 t + \phi_3) + T_6 \sin(\omega_2 t + \phi_4) \\ T_{tz1} &= T_7 + T_8 \sin(\omega_1 t + \phi_5) + T_9 \sin(\omega_2 t + \phi_6) \end{aligned} \tag{5.37}$$

The T_i are torque amplitudes. The angular frequencies ω_1 and ω_2 may correspond to the orbital rate or one of its harmonics or any other angular rates desired. The phase angles ϕ_i provide increased flexibility.

The indicator 0 or 1 is used in the input data. If the indicator is 0, all of the miscellaneous torques are zero and the T_i, ω_i and ϕ_i are not listed in the input.

5.1.4.7 Magnetic Restoring Torque on Magnet

The independent magnet will also experience a restoring torque since the dipole axis will tend to line up with its axis parallel to the magnetic field. This torque can be written:

$$T_{m3} = M_3 (\bar{x}_3 \times \bar{H}) \tag{5.38}$$

where M_3 is the magnetic moment of the dipole expressed in appropriate units. $\bar{x}_3$ is the dipole axis expressed in orbital coordinates; thus,

$$\bar{x}_3 = e_{11m}\bar{r} + e_{12m}\bar{p} + e_{13m}\bar{q} \tag{5.39}$$

where e_{1jm} are the direction cosines between the dipole axis and the orbital axes r, p, q. $\bar{H}$ is the magnetic field intensity which is defined by equation (5.16).

Therefore,

$$T_{m3} = M_3 \begin{bmatrix} \bar{r} & \bar{p} & \bar{q} \\ e_{11m} & e_{12m} & e_{13m} \\ H_r & H_p & H_q \end{bmatrix} \tag{5.40}$$

or

$$T_{mr3} = M_3 \ (e_{12m}H_q - e_{13m} H_p)$$
$$T_{mp3} = M_3 \ (e_{13m}H_r - e_{11m} H_q) \qquad (5.41)$$
$$T_{mq3} = M_3 \ (e_{11m}H_p - e_{12m} H_r)$$

and

$$\begin{bmatrix} T_{mx3} \\ T_{my3} \\ T_{mz3} \end{bmatrix} = \begin{bmatrix} E_m \end{bmatrix} \begin{bmatrix} T_{mr3} \\ T_{mp3} \\ T_{mq3} \end{bmatrix} \qquad (5.42)$$

5.1.4.8 Damper Torque on Magnet

The damper torque on the magnet will be similar to that on the balloon. Except that in this case, the torque is transmitted from the balloon through the viscous coupling to the magnet. The damping torque on the magnet will be a function of the damping coefficient, b, and the difference in angular velocities between the magnet body axes and the components of the balloon angular velocity which are experienced along the magnet body axes. This transformation is defined in equation (5.19). Thus, the damper torque on the magnet may be written:

$$T_{dx3} = -b \ (\omega_{x3} - \omega_{bx3})$$
$$T_{dy3} = -b \ (\omega_{y3} - \omega_{by3}) \qquad (5.43)$$
$$T_{dz3} = -b \ (\omega_{z3} - \omega_{bz3})$$

5.1.4.9 Euler Rates

The dynamic equations needed to complete this simulation are the Euler angle rate as a function of body rates:

$$\dot{\theta}_{pb} = -\dot{\eta} + \frac{1}{\cos \theta_{rb}} \ (\omega_{y1} \sin \theta_{yb} + \omega_{z1} \cos \theta_{yb})$$
$$\dot{\theta}_{rb} = \omega_{y_1} \cos\theta_{yb} - \omega_{z1} \sin \theta_{yb}$$
$$\dot{\theta}_{yb} = \omega_{x1} + (\dot{\theta}_{pb} + \dot{\eta}) \sin \theta_{rb} \qquad (5.44)$$
$$\dot{\theta}_{pm} = -\dot{\eta} + \frac{1}{\cos \theta_{rm}} \ (\omega_{y3} \sin \theta_{ym} + \omega_{z3} \cos \theta_{ym})$$
$$\dot{\theta}_{rm} = \omega_{y3} \cos \theta_{ym} - \omega_{z3} \sin \theta_{ym}$$
$$\dot{\theta}_{ym} = \omega_{x3} + (\dot{\theta}_{pm} + \dot{\eta}) \sin \theta_{rm} \qquad (5.45)$$

Each of these angular rates is numerically integrated by the IBM 7090 computer to obtain the corresponding Euler angle.

5.1.5 Digital Computer Program

The program for the IBM 7090 computer is a compilation of subroutines. Each of these subroutines, as well as the input data, is described below.

5.1.5.1 Input Data

The input data are listed in Table 5.1. The units and a brief definition for the parameters are included. A few brief remarks on some of the angles are in order. The time of injection D_L is positive if measured after a winter solstice and negative if measured before the solstice. Greenwich mean time is zero at midnight. The orbital inclination ν is always positive. The orbital angular position η_2 is measured from perigee in the direction of travel. η_1, the orbital position at injection, is measured from the ascending node.

Table 5.1 Input Table

Universal Constants		
Symbol	Units	Description
ϵ (EPS)	DEGREES	Angle between ecliptic and equatorial planes
K (FKK)	$FEET^3/SECOND^2$	Gravitational constant multiplied by earth mass
E/C (EC)	$POUNDS/FOOT^2$	Solar pressure constant
Orbital Parameters		
DL	DAYS	Time from winter solstice to orbital injection
APOG	FEET	Geocentric distance at apogee
PERI	FEET	Geocentric distance at perigee
GMT	HOURS	Greenwich mean time at injection
ν (FNU)	DEGREES	Inclination of orbital plane, with respect to equatorial plane
η_2(ETA2)	DEGREES	Vehicle orbital position angle at injection measured from perigee
η_1(ETA1)	DEGREES	Vehicle orbital position angle at injection measured from the ascending node
Ω	DEGREES	Right ascension
R_e	FEET	Radius of earth
τ_R	DAYS	Regression Period

Table 5.1 Continued

Symbol	Units	Description
Initial Conditions		
θ_{pbo}	DEGREES	Initial value of θ_{pb}
θ_{rbo}	"	" θ_{rb}
θ_{ybo}	"	" θ_{yb}
θ_{pmo}	"	" θ_{pm}
θ_{rmo}	"	" θ_{rm}
θ_{ymo}	"	" θ_{ym}
ω_{x10}	DEGREES/SECONDS	Initial value of ω_{x1}
ω_{y10}	"	" ω_{y1}
ω_{z10}	"	" ω_{z1}
ω_{x30}	"	" ω_{x3}
ω_{y30}	"	" ω_{y3}
ω_{z30}	"	" ω_{z3}
Vehicle Characteristics		
β	DEGREES	Angle to define position of rigid magnet
γ	DEGREES	Angle to define position of rigid magnet
δ	DEGREES	Complement of lens half angle
r_o	FEET	Radius of sphere of which the lens is a segment
K_1	—	Constant to define ratio of "open area" in mesh skin
ρ_s		Specular reflection coefficient for lens
ρ_d		Diffuse reflection coefficient for lens
b	#FT.SEC.	Damping Coefficient
M_2	.73593E-7 POLE CM.	Magnetic moment of balloon magnet dipole
M_3	.73593E-7 POLE CM.	Magnetic moment of independent magnet dipole
I_{xx1o}, I_{yy1o}, I_{zz1o}, I_{xy1o}, I_{xz1o}, I_{yz1o}	SLUG-FT^2	Initial moments of inertia of balloon
$\dot{I}_{xx1o}$, $\dot{I}_{yy1o}$, $\dot{I}_{zz1o}$, $\dot{I}_{xy1o}$, $\dot{I}_{xz1o}$, $\dot{I}_{yz1o}$	SLUG-FT^2/SEC	Initial rate of the balloon moments of inertia
I_{xx3}, I_{yy3}, I_{zz3}, I_{xy3}, I_{xz3}, I_{yz3}	SLUG-FT^2	Moments of inertia of independent magnet

Table 5.1 Continued

Symbol	Units	Description
x_L	FEET	Offset of balloon c.g. from "circular" center of top lens
x'_L	FEET	Offset of balloon c.g. from "circular" center of bottom lens
y_{10}	FEET	Offset of balloon c.g. along y_1 from geometric center of balloon
z_{10}	FEET	Offset of balloon c.g. along z_1 from geometric center of balloon
Numerical Integration Parameters and Other Indicators		
Sets 6, 7, 8 in Table 5.2		
Miscellaneous Torque Constants		
T_1, T_2, T_3, T_4, T_5, T_6 T_7, T_8, T_9	POUND-FEET	Coefficients of miscellaneous disturbance torques
ω_1, ω_2 (Omega 1, Omega 2)	DEGREES/SECOND	Angular frequencies of miscellaneous disturbance torques
ϕ_1, ϕ_2, ϕ_3 ϕ_4, ϕ_5, ϕ_6 (Phi 1, etc.)	DEGREES	Phase angles of miscellaneous torques

Following is a description and input format (table 5.2) to this FORTRAN program with variable field input. Each set begins on a new card with a field specification in column 1, each field is separated by commas. Each data card requires an asterisk at or before column 72; this does not include the title card.

Table 5.2 Input Format

SET	FIELD	SPECIFICATION
1		F & G tables (standard)
*2	F	EPS, FKK, EC
3	F	DL, APOG, PERI, GMT, FNU, ETA2, ETA1, OMEGA, TAUR
4	F	THPB, THRB, THYB, THPM, THRM, THYM, ω_{X1}, ω_{Y1}, ω_{Z1}, ω_{X3}, ω_{Y3}, ω_{Z3}
5	F	BETA, GAM, PHI, RHOS, RHOD, R, FKK1, RE ,
		BB, FIXX1, FIYY1, FIZZ1, FIXY1, FIXZ1, FIYZ1, FIXX1D, FIYY1D,
		FIZZ1D, FIXY1D, FIXZ1D, FIYZ1D, FIXX3, FIYY3, FIZZ3, FIXY3,
		FIXZ3, FIYZ3, XL, XPL, Y10, Z10, FM2, FM3

Table 5.2 Continued

SET	FIELD	SPECIFICATION
6	F	GDSTPS, DT, TSTOP, DTPRNT
	X	INTRVL, MISC
7	X	NERR
NERR $\geq$ 0		
8A	F	ERMN1, ERMX1, ERMN2, ERMX2, ERMN3, ERMX3, ERMN4, ERMX4, ERMN5, ERMX5
NERR $<$ 0		
8B	F	EMAX(1), EMIN(1), EMAX(2), EMIN(2)...EMAX(12), EMIN(12)
MISC (SET 6) $\neq$ 0		
9	F	T1, T2, T3, T4, T5, T6, T7, T8, T9, ω_1, ω_2, PH1, PH2, PH3, PH4, PH5, PH6

If MISC = 0, no SET 9 is required. Any number of complete groups of SET 2-9 may be run at one time.

An Adams-Moulton method of numerical integration with Runge Kutta starter is used. SET 6, 7 and 8 are integration controls. These controls provide for application of error criteria to determine whether the integration interval is satisfactory. The criteria are applied separately to each integrated variable, as described below. If the integration interval is satisfactory with respect to all variables, the program proceeds with the integration. After the number of consecutive satisfactory integration intervals reaches the number GDSTPS specified in the input the program tentatively doubles the integration interval. If the larger interval is satisfactory, the program proceeds with the integration. If at any time the integration interval is found to be unsatisfactory with respect to one or more variables, the program will halve the integration interval until it is found to be satisfactory with respect to all variables. DT is the initial step size in seconds. TSTOP is the number of seconds real time for the run. DTPRNT is the real time print interval. INTRVL is 0 for constant DT and 1 for a variable step size. MISC is 0 for no miscellaneous disturbance torques and 1 for non-zero miscellaneous torques. NERR is the type of error criteria desired.

In set 8 the ERMN's refer to a minimum absolute error. If all the estimated errors are less than the ERMN the step size is doubled. The ERMX's refer to the maximum allowable error. If any single error is larger than the appropriate ERMX the step size is halved.

In set 8A:

ERMN1, ERMX1 refer to θ_{pb}, θ_{rb}, θ_{yb}, θ_{pm}, θ_{rm}, θ_{ym}

ERMN2, ERMX2 refer to ω_{x1}, ω_{y1}

ERMN3, ERMX3 refer to ω_{z1}

ERMN4, ERMX4 refer to ω_{x3}, ω_{y3}

ERMN5, ERMX5 refer to ω_{z3}

In Set 8B, the error criteria refer to the integration variables in the following order: θ_{pb}, θ_{rb}, θ_{yb}, θ_{pm}, θ_{rm}, θ_{ym}, $\omega_{x1}, \omega_{y1}, \omega_{z1}, \omega_{x3}, \omega_{y3}, \omega_{z3}$.

5.1.5.2 Subroutine for Changing Moments of Inertia

Provision has been made in the program for changing moments and products of inertia for the balloon during rod extension, balloon ablation, or any other time during which the moments of inertia are changing. The inputs to this program are the initial moments and products of inertia as well as the initial rates of these same parameters. Since the time history of these moments and products of inertia will depend on the vehicle configuration, this subroutine is not in the program. At present the program treats the initial moments and products of inertia as constants for the entire duration of the run. Note, no provision has been made for time varying moments and products of inertia for the magnet.

5.1.5.3 Initialization Subroutine for Orbital Parameters

This subroutine computes additional orbital parameters from those listed in the input and from the constants K and ϵ . The semimajor axis a and the eccentricity e are computed from the apogee and the perigee,

$$a = \tfrac{1}{2} (APOG + PERI) \text{ (feet)}, \tag{5.46}$$

$$e = \frac{APOG - PERI}{APOG + PERI} \tag{5.47}$$

The angular momentum per unit mass is:

$$h_o = \sqrt{Ka\ (1 - e^2)}\ (\text{feet}^2/\text{second}). \tag{5.48}$$

The orbital period is

$$\tau = 2\pi a\sqrt{\frac{a}{K}}\ \text{(seconds)}. \tag{5.49}$$

The orbital angle at perigee, measured from the ascending node, is:

$$\eta_0 = \eta_1 - \eta_2\ \text{(radians)}. \tag{5.50}$$

The eccentric anomaly at injection, E_o, is found from:

$$\cos E_o = \frac{e + \cos \eta_2}{1 + e \cos \eta_2} \tag{5.51}$$

The quadrant of E_o can be determined from Table 5.3, using the value of η_2.

The mean anomaly at injection time is

$$M_o = E_o - e \sin E_o \text{ (radians)}. \tag{5.52}$$

The time at injection is

$$t_o = \frac{M_o T}{2\pi} \quad \text{(seconds)}. \tag{5.53}$$

Table 5.3 Relation Between E_o and η_2

η_2 (Radians)	E_o (Radians)
0	0
$\frac{\pi}{2}$	$\cos^{-1}(e)$
$\cos^{-1}(-e)$	$\frac{\pi}{2}$
$\cos^{-1}(-e)$	$\frac{3\pi}{2}$
$\frac{3\pi}{2}$	$\cos^{-1}(e)$
2π	2π

5.1.5.4 Earth's Orbital Position

This subroutine must be computed initially and thereafter when the Greenwich Mean Time is zero. At this time, D_L will be incremented by one day. The decision to increment D_L will come from the subroutine for the computation of latitude and longitude.

The earth's orbit is considered to be circular, and therefore, its orbital position σ is a linear function of time

$$\sigma = \frac{2\pi D_L}{365.24} - \frac{2\pi D_L}{T_R} \quad \text{(radians)} \tag{5.54}$$

where T_R is the regression period in days. If $T_R > 1000$ then $\sigma = \frac{2\pi D_L}{365.24}$.

Both σ and D_L are measured from the winter solstice, are positive after the solstice and are negative before the solstice.

σ_1 is the projection into the equatorial plane of the earth's orbital position angle

$$\sin \sigma_1 = \frac{\sin \sigma}{\sqrt{\cos^2 \epsilon \cos^2 \sigma + \sin^2 \sigma}}$$
$$\cos \sigma_1 = \frac{\cos \sigma \cos \epsilon}{\sqrt{\cos^2 \epsilon \cos^2 \sigma + \sin^2 \sigma}} \qquad (5.55)$$

5.1.5.5 Subroutine for Computation of Latitude and Longitude

This subroutine which is necessary to provide input to the magnetic field subroutine, must be calculated for each time step. The latitude which is a function of inclination and orbital angle can be written:

$$\text{LAT} = \sin^{-1} \left[\sin \eta \quad \sin \nu \right] \qquad (5.56)$$

LAT can vary between $\pm 90^\circ$ and the sign will be determined by the sign of the argument.

The angle which the Greenwich Meridian makes with the $\bar{u}$ axis is a function of the time of year, Greenwich Mean Time at injection and orbital time.

Therefore,

$$\Omega_1 = \sigma_1 - \pi/2 + \pi/12 \text{ GMTT} \qquad (5.57)$$

where $$\text{GMTT} = \text{GMT} + \frac{t - t_o}{3600} . \qquad (5.58)$$

σ_1 is the projection of the earth's orbital position into the equatorial plane, GMT is the Greenwich Mean Time at injection and t_o is the time measured from perigee at injection in seconds. When GMTT reaches 24 hours, D_L should be incremented by one day and GMTT set equal to zero. Thereafter, D_L should be incremented every twenty four hours and GMTT reduced to zero.

The longitude of the satellite at any point may be written:

$$\text{LONG} = \Omega - \Omega_1 + \Omega_3 \qquad (5.59)$$

where Ω_3 is the projection of the orbit central angle measured from the equatorial crossing onto the equator. It is calculated from the following equations:

$$\sin \Omega_3 = \frac{\tan \text{LAT}}{\tan \nu}$$
$$\cos \Omega_3 = \frac{\cos \eta}{\cos \text{LAT}} \qquad (5.60)$$

5.1.5.6 Orbital Subroutine

This subroutine is known as ELLIP. It receives the inputs from the initialization subroutine listed in Table 5.4.

Table 5.4 Inputs to ELLIP

SYMBOL	UNITS	DESCRIPTION
Ω (OMEG)	Radians	Right ascension of the ascending node.
a (SMA)	Feet	Semimajor axis of orbit.
ϵ (BCC)	———	Eccentricity of orbit.
h_o (ALTB)	$Feet^2/Second$	Orbital angular momentum per unit mass.
τ (TAU)	Seconds	Orbital period.
η_o (ETAO)	Radians	Orbital angular position at perigee, measured from ascending node.

If the eccentricity e is zero, the program computes the circular orbital parameters only once.

$$\dot{R} = 0, \tag{5.61}$$

$$R = a \quad \text{(feet)} \tag{5.62}$$

and

$$\dot{\eta} = \frac{h_o}{R^2} \quad \text{(radians/second)}. \tag{5.63}$$

For each time interval of integration, the program computes the mean anomaly,

$$M = \frac{2\pi t}{\tau} \text{ (radians)}, \tag{5.64}$$

the eccentric anomaly,

$$E = M \quad \text{(radians)}, \tag{5.65}$$

the orbital angle measured from perigee,

$$\eta - \eta_o = E \text{ (radians)}, \tag{5.66}$$

and the orbital angle measured from the ascending node,

$$\eta = (\eta - \eta_o) + \eta_o \text{ (radians)}. \tag{5.67}$$

If the eccentricity is not zero, the variables pertaining to the elliptical orbit are calculated at each integration interval. The mean anomaly is calculated from equation (5.64) and then reduced by multiples of 2π, as required. The eccentric anomaly E is calculated from Kepler's equation,

$$E - e \sin E = M \text{ (radians)}. \tag{5.68}$$

As an aid to solving this transcendental equation, the program computes a table of values of M for values of E at one-degree intervals. To solve equation (5.68) the program enters the table with the value of M and interpolates to obtain E. The quadrant of E may be found from Table 5.5, using the value of M. The geocentric distance is:

$$R = a\,(1 - e \cos E) \quad \text{(feet)} \tag{5.69}$$

The orbital angle $(\eta - \eta_o)$ measured from perigee is calculated from:

$$\cos(\eta - \eta_o) = \frac{\cos E - e}{1 - e \cos E} \tag{5.70}$$

The quadrant of $(\eta - \eta_o)$ is found from Table 5.5, using the value of E. The orbital angular position is found from equation (5.67). The radial velocity is:

$$\dot{R} = \frac{e\, h_o \sin(\eta - \eta_o)}{a(1 - e^2)} = \frac{e\, h_o \sin E}{a\sqrt{1 - e^2}(1 - e \cos E)} \text{(feet/second)} \tag{5.71}$$

The orbital angular rate is found from equation (5.63).

Table 5.5 Relations Between M, R, E, and $(\eta - \eta_o)$

M (Radians)	$\frac{R}{a}$	E (Radians)	$(\eta - \eta_o)$ (Radians)
0	1 - e	0	0
$\cos^{-1}e - e\sqrt{1 - e^2}$	$1 - e^2$	$\cos^{-1}e$	$\frac{\pi}{2}$
$\frac{\pi}{2} - e$	1	$\frac{\pi}{2}$	$\cos^{-1}(-e)$
π	1 + e	π	π
$\frac{3\pi}{2} + e$	1	$\frac{3\pi}{2}$	$\cos^{-1}(-e)$
$\cos^{-1}e - e\sqrt{1 - e^2}$	$1 - e^2$	$\cos^{-1}e$	$\frac{3\pi}{2}$
2π	1 - e	2π	2π

5.1.5.7 Derivative Subroutine

This subroutine, which is titled DERIV, calculates the coordinate transformations and the twelve time derivatives. These derivatives include the angular accelerations about the body geometric axes and the Euler angular rates.

5.1.5.8 External Torque Subroutine

A subroutine is used for each kind torque acting on each of the bodies. For example, there are five torque subroutines for the balloon: gravity gradient torques, damper torques, solar radiation pressure torques, magnetic torques and miscellaneous disturbance torques. Only two of these are applicable for the magnet: magnetic and damper torques. The total torque components (torques resolved along body geometric axes) are the algebraic sums of the various individual torque components for the balloon:

$$\begin{aligned} T_{x1} &= T_{gx1} + T_{dx1} + T_{sx1} + T_{mx1} + T_{tx1} \\ T_{y1} &= T_{gy1} + T_{dy1} + T_{sy1} + T_{my1} + T_{ty1} \\ T_{z1} &= T_{gz1} + T_{dz1} + T_{sz1} + T_{mz1} + T_{tz1} \end{aligned} \tag{5.72}$$

For the magnet:

$$\begin{aligned} T_{x3} &= T_{mx3} + T_{dx3} \\ T_{y3} &= T_{my3} + T_{dy3} \\ T_{z3} &= T_{mz3} + T_{dz3} \end{aligned} \tag{5.73}$$

Other torque subroutines can be easily added to the program,

5.1.5.9 Output Subroutine and Plotting Option

Most of the required output is available from the computations performed by the various subroutines. Additional required output data are described next.

The elapsed time t_{out} since injection is printed-out to the nearest tenth of an hour.

$$t_{out} = \frac{t - t_o}{3,600} \tag{5.74}$$

The angle Δ between the satellite yaw axis and the local vertical to earth may be calculated:

$$\Delta = \cos^{-1} (\cos \theta_{pb} \cos \theta_{rb}) \tag{5.75}$$

The angle θ between the sun's rays and the longitudinal axis of the balloon lies between zero and 180 degrees and is computed from

$$\theta = \cos^{-1} (s_{x1}) \tag{5.76}$$

The angle α between the y_1 axis of the balloon and the normal (j axis) to the plane containing the sun is

$$\alpha = \cos^{-1}\left[\frac{-s_{z1}}{\sqrt{s_{z1}^2+s_{y1}^2}}\right] = \sin^{-1}\left[\frac{-s_{y1}}{\sqrt{s_{z1}^2+ s_{y1}^2}}\right] \tag{5.77}$$

Two pages are available. On page 1, t_{out}, θ_{pb}, θ_{rb}, θ_{yb}, θ_{pm}, θ_{rm}, θ_{ym}, $(\omega_{x1},-\omega_{mx1})$,$(\omega_{y1}-\omega_{my1})$,$(\omega_{z1}-\omega_{mz1})$ and Δ. Page 2 is stored on B6 and printed on request. It contains: t_{out}, B, H_r, H_p, H_q, θ, α , T_{sx1}, T_{sy1}, T_{sz1}, LAT and LONG. A binary tape A5 is written for plotting which contains all the information on pages 1 and 2 with the exception of latitude and longitude.

When the elapsed time $(t - t_o)$ in seconds exceeds the value TSTOP specified in the input, the computation stops. The machine operator may also be instructed to stop the run after a certain amount of computer running time.

The print-out interval DTPRNT is also specified in the input. The print-out will seldom occur at exact multiples of the specified interval but will occur at the end of the next integration interval. This slight defect occurs because the specified print-out interval is usually not a multiple of the integration intervals on account of the variable integration intervals.

5.2 RESULTS OF PRELIMINARY STUDIES

The optimum parameters selected for poles (Section 4.) result in a time constant of forty orbits, and a steady state magnetically induced error of one-half degree. To determine the validity of the planar analysis, the optimum parameters were put into the three axis computer program and the performance checked. Figure 5-7 is the graph of the computer results with the optimum parameters. The initial error in pitch is ten degrees and with a time constant of forty orbits, the error after 112 hours should be 3.7 degrees. The actual error is approximately 4.1 degrees indicating a time constant of 45 orbits. The discrepancy between the predicted value and the actual value is primarily due to the damper induced disturbance at the small angles. This is evident in Figure 5-7 by the presence of small fluctuations on the decay curve. The nature of the fluctuations is illustrated in Figure 5-8. This is a steady state run, with all the fluctuations the result of damper induced disturbances. The estimated steady state error was one-half degree and the system remains within that angle for the majority of its life. The occasional six tenths of a degree is caused by the beating of satellite natural frequency and the magnetic disturbance. This effect decays and is disappearing by the end of the run. A twenty four hour cycle is noticeable on roll and yaw due to the rotation of the earth. The magnetic influence on roll is, however, small.

The optimization analysis was a linearized analysis, and decay from large initial angles had to be checked using the three axis computer program. Figure 5-9 is such a run with initial angles of 45 degrees. The decay time for pitch is 32.5 orbits, as is the decay time for roll. This value is considerably less than the predicted and is due primarily to the non-linear behavior of the satellite at large angles. Note that yaw, with an initial angle of zero, makes eight complete revolutions before the end of the run.

To determine the effect of solar pressure upon the satellite, an orbit was selected with the sun in the orbit plane and the vehicle was given on initial error. This computer run is shown on Figure 5-10 and comparison with Figure 5-7 indicates little difference.

Figures 5-11 and 5-12 show the steady state response to solar torques with the sun normal to the orbit plane and 45 degrees to the orbit plane, respectively. When the sun is normal to the plane, there are no solar torques on pitch, and since the vehicle is symmetrical with no center of mass offset, the solar torques on roll are small. The oscillations in roll are primarily the result of damper induced disturbances. With the sun at 45 degrees (Figure 5-12), the satellite is in the earth's shadow for a short period of time, which causes a periodic disturbance on the satellite. The greatest effect is in roll, where the steady state error increased from .25 degrees (Figure 5-11) to .6 degrees. The amplitude of oscillation of pitch did not increase, but the characteristics of the oscillations have changed.

Figures 5-13 and 5-14 illustrate the steady state behavior of the vehicle for for a 30 degree and 48 degree inclined orbit, respectively. (Please note the change in pitch and roll scales in Figure 5-14). The sun would be 45 degrees to the orbit plane if the orbit were polar. For both inclinations the oscillation amplitude in roll has increased beyond those for the polar orbit at the same sun angle. The oscillations in pitch have, however, decreased.

The effect of orbit eccentricity also had to be checked and Figure 5-15 shows the vehicle steady state performance in an eccentric orbit. The sun is normal to the orbit plane. After one time constant the satellite oscillates at orbital frequency (as anticipated) with an oscillation amplitude of 2.1 degrees. The error due to eccentricity alone (Figure 4-4) is 1.5 degrees. The damper induced error is .5 degrees. The effect of solar torque is therefore, small, as indicated previously.

Figure 5-16 illustrates the effect of solar torque and eccentricity upon transient decay time. When compared with Figure 5-9 there is little difference. After 240 hours the vehicle is oscillating at orbital frequency with a five degree amplitude. The motion is still decaying.

The results of these preliminary three axis runs indicate that the performance of the system is as anticipated. The computer program that is required for large angle three axis motion studies is operational, providing the capability for more detail include: orientation during rod extension and balloon deployment; error decay from large error with disturbance torques imposed; and steady state oscillations produced by the combined effects of thermal bending of the rods, orbit eccentricity, earth's magnetic field and solar pressure.

DECAY FROM 10 DEGREE INITIAL ANGLE

PITCH INERTIA	712,000 slug-ft^2
ROLL INERTIA	712,000 slug-ft^2
YAW INERTIA	178,000 slug-ft^2
MAGNET STRENGTH	2,200,000 pole-cm
DAMPING CONSTANT	3.59 lb-ft-sec/rad
ORBIT ALTITUDE	2000 n. miles
ORBIT PERIOD	2.8 hours
ORBITAL INCLINATION	90 deg.
RIGHT ASCENSION	90 deg.
INITIAL TIME FROM WINTER SOLSTICE	91.31 days

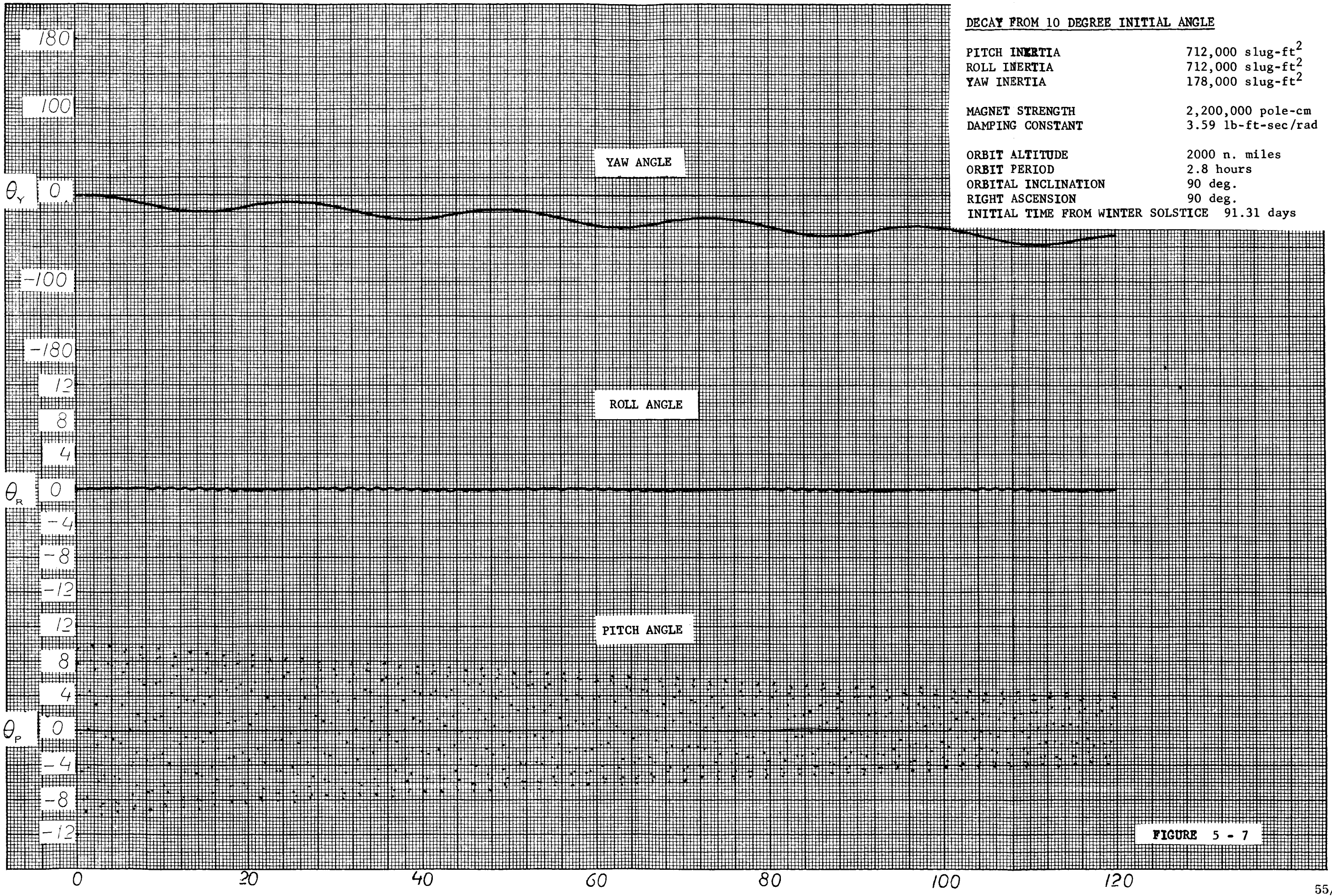

FIGURE 5 - 7

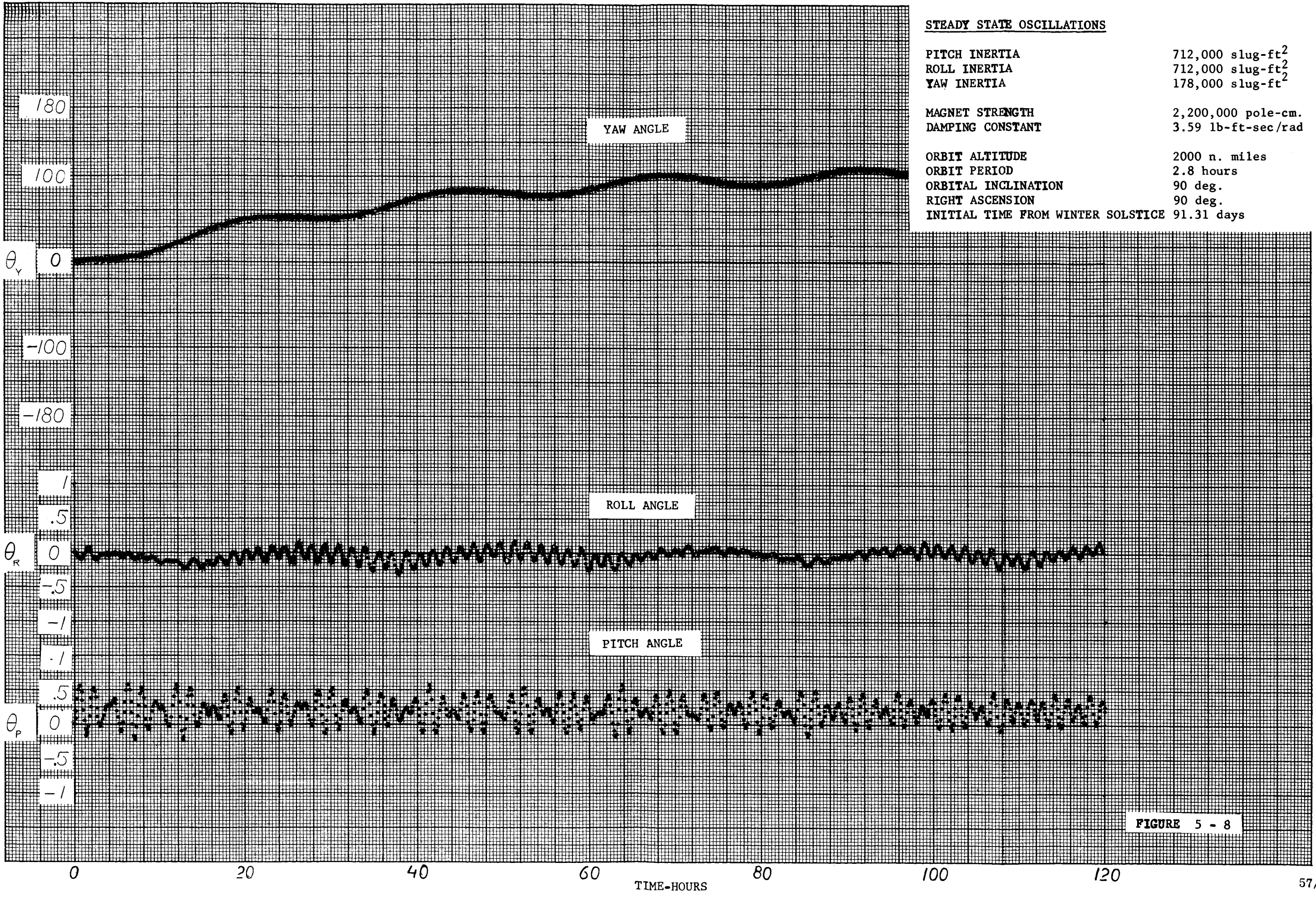

STEADY STATE OSCILLATIONS

PITCH INERTIA	712,000 slug-ft^2
ROLL INERTIA	712,000 slug-ft^2
YAW INERTIA	178,000 slug-ft^2
MAGNET STRENGTH	2,200,000 pole-cm.
DAMPING CONSTANT	3.59 lb-ft-sec/rad
ORBIT ALTITUDE	2000 n. miles
ORBIT PERIOD	2.8 hours
ORBITAL INCLINATION	90 deg.
RIGHT ASCENSION	90 deg.
INITIAL TIME FROM WINTER SOLSTICE	91.31 days

FIGURE 5 - 8

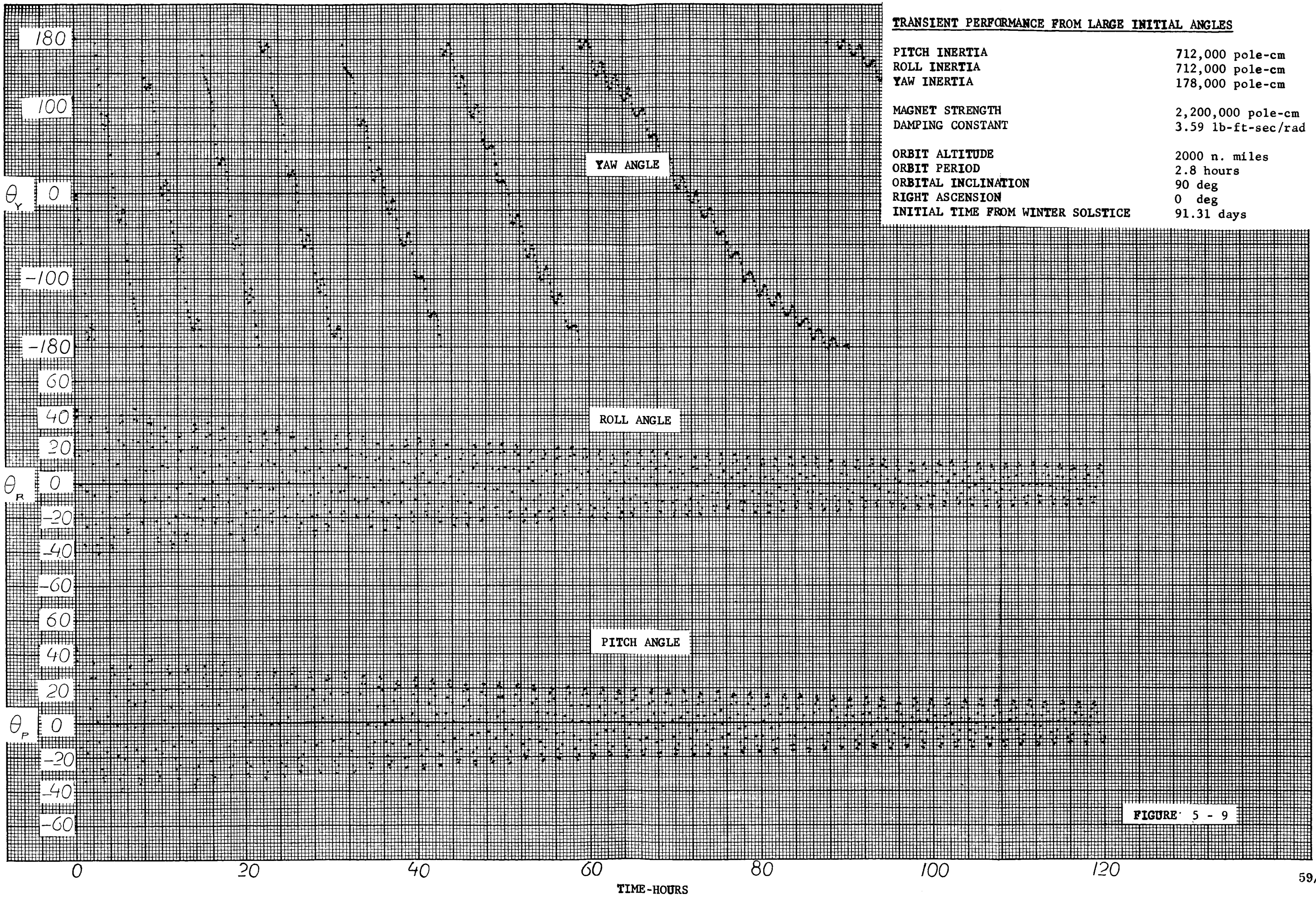

TRANSIENT PERFORMANCE FROM LARGE INITIAL ANGLES

PITCH INERTIA	712,000 pole-cm
ROLL INERTIA	712,000 pole-cm
YAW INERTIA	178,000 pole-cm
MAGNET STRENGTH	2,200,000 pole-cm
DAMPING CONSTANT	3.59 lb-ft-sec/rad
ORBIT ALTITUDE	2000 n. miles
ORBIT PERIOD	2.8 hours
ORBITAL INCLINATION	90 deg
RIGHT ASCENSION	0 deg
INITIAL TIME FROM WINTER SOLSTICE	91.31 days

FIGURE 5 - 9

EFFECT OF SOLAR TORQUE ON TRANSIENT DECAY

PITCH INERTIA	712,000 slug-ft^2
ROLL INERTIA	712,000 slug-ft^2
YAW INERTIA	178,000 slug-ft^2
MAGNET STRENGTH	2,200,000 pole-cm
DAMPING CONSTANT	3.59 lb-ft-sec/rad
ORBIT ALTITUDE	2000 n. miles
ORBIT PERIOD	2.8 hours
ORBITAL INCLINATION	90 deg.
RIGHT ASCENSION	90 deg.
INITIAL TIME FROM WINTER SOLSTICE	91.31 days

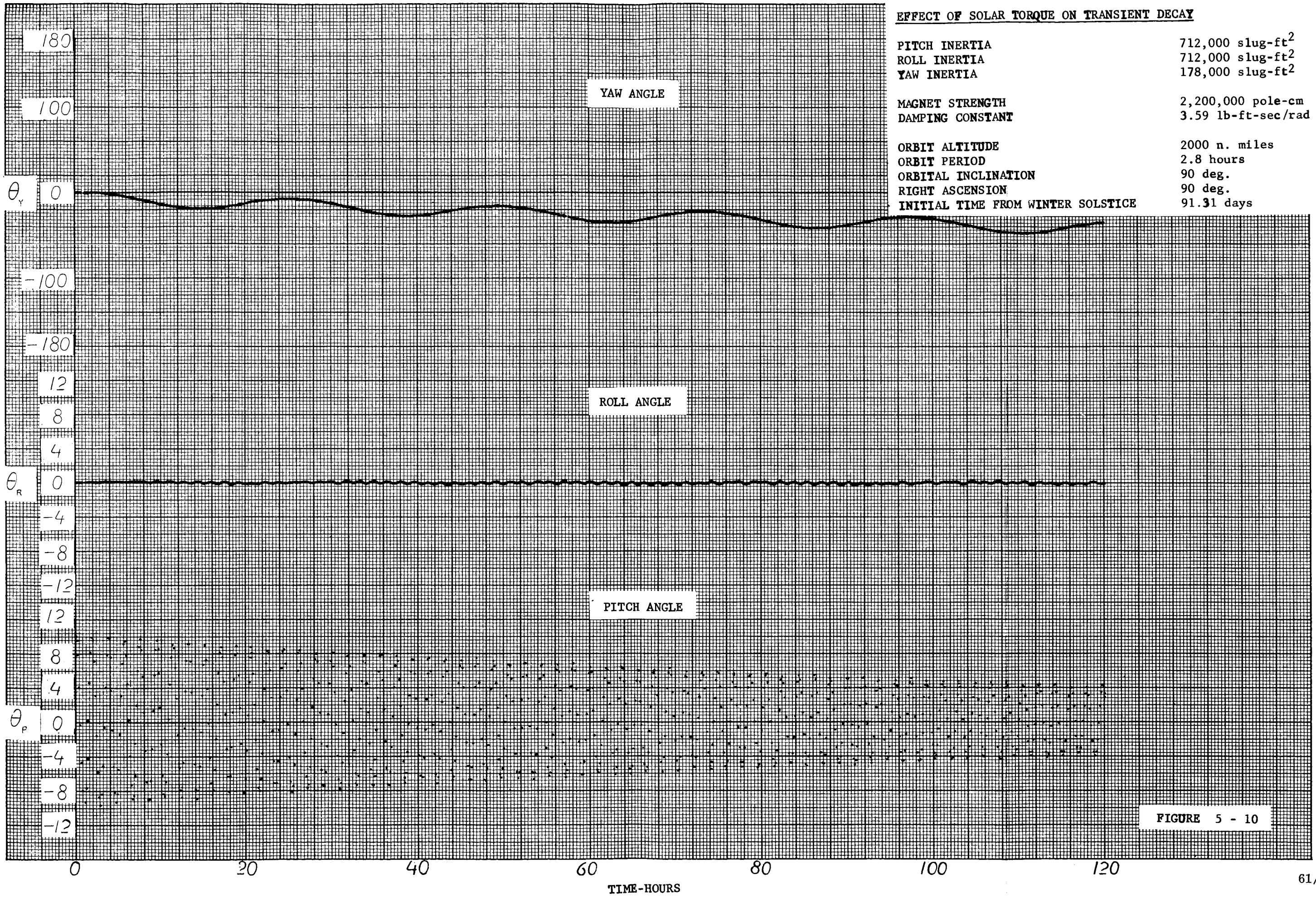

FIGURE 5 - 10

SOLAR TORQUE WITH SUN NORMAL TO ORBIT PLANE

PITCH INERTIA	712,000 slug-ft^2
ROLL INERTIA	712,000 slug-ft^2
YAW INERTIA	178,000 slug-ft^2
MAGNET STRENGTH	2,200,000 pole-cm
DAMPING CONSTANT	3.59 lb-ft-sec/rad
ORBIT ALTITUDE	2000 n. miles
ORBIT PERIOD	2.8 hours
ORBITAL INCLINATION	90 deg.
RIGHT ASCENSION	90 deg.
INITIAL TIME FROM WINTER SOLSTICE	91.31 days

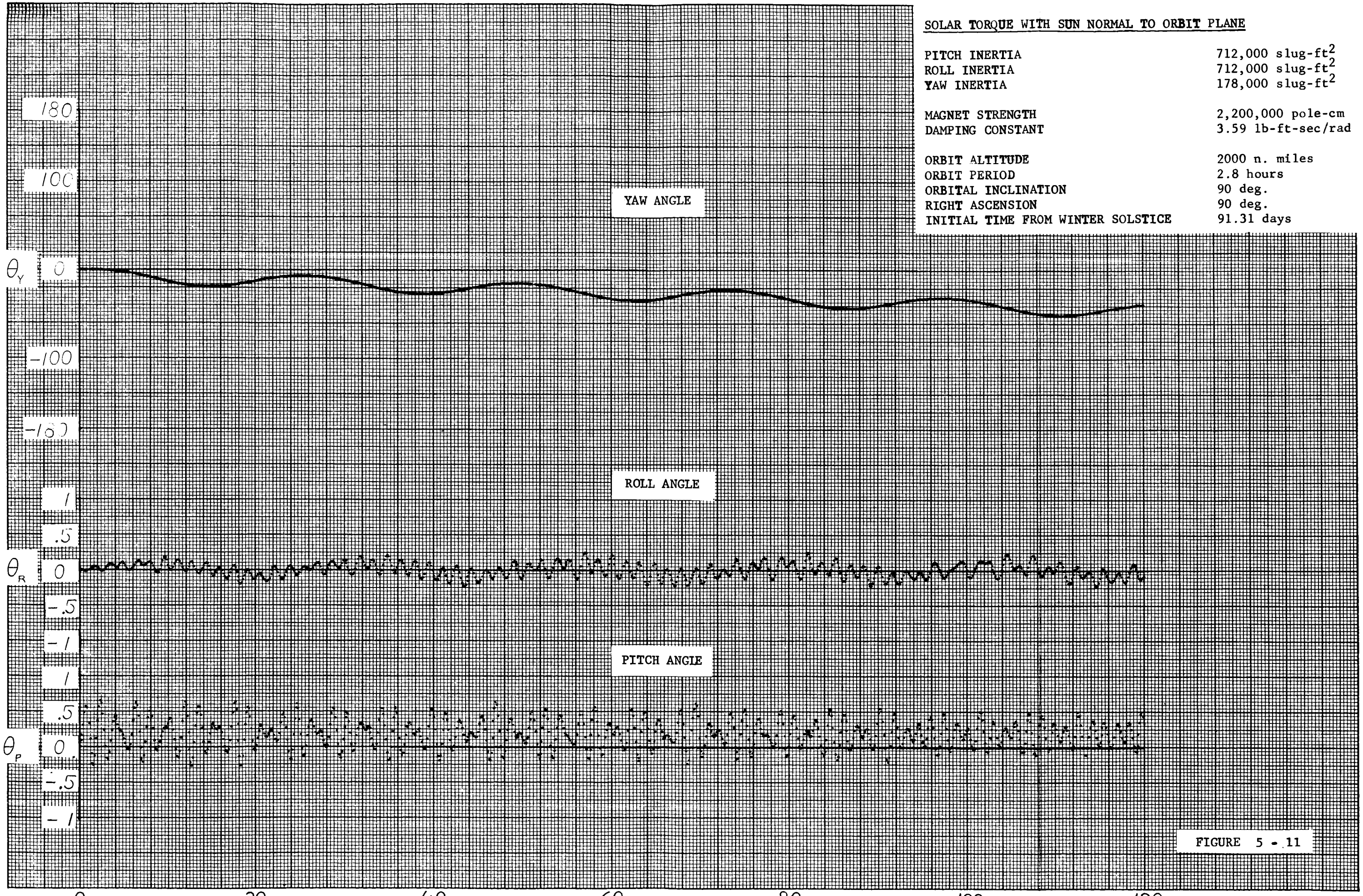

FIGURE 5 - 11

SOLAR TORQUE 45 DEGREE TO ORBIT PLANE

PITCH INERTIA	712,000 slug-ft^2
ROLL INERTIA	712,000 slug-ft^2
YAW INERTIA	178,000 slug-ft^2
MAGNET STRENGTH	2,200,000 pole-cm
DAMPING CONSTANT	3.59 lb-ft-sec/rad
ORBIT ALTITUDE	2000 n. miles
ORBIT PERIOD	2.8 hours
ORBITAL INCLINATION	90 deg.
RIGHT ASCENSION	45 deg.
INITIAL TIME FROM WINTER SOLSTICE	91.31 days

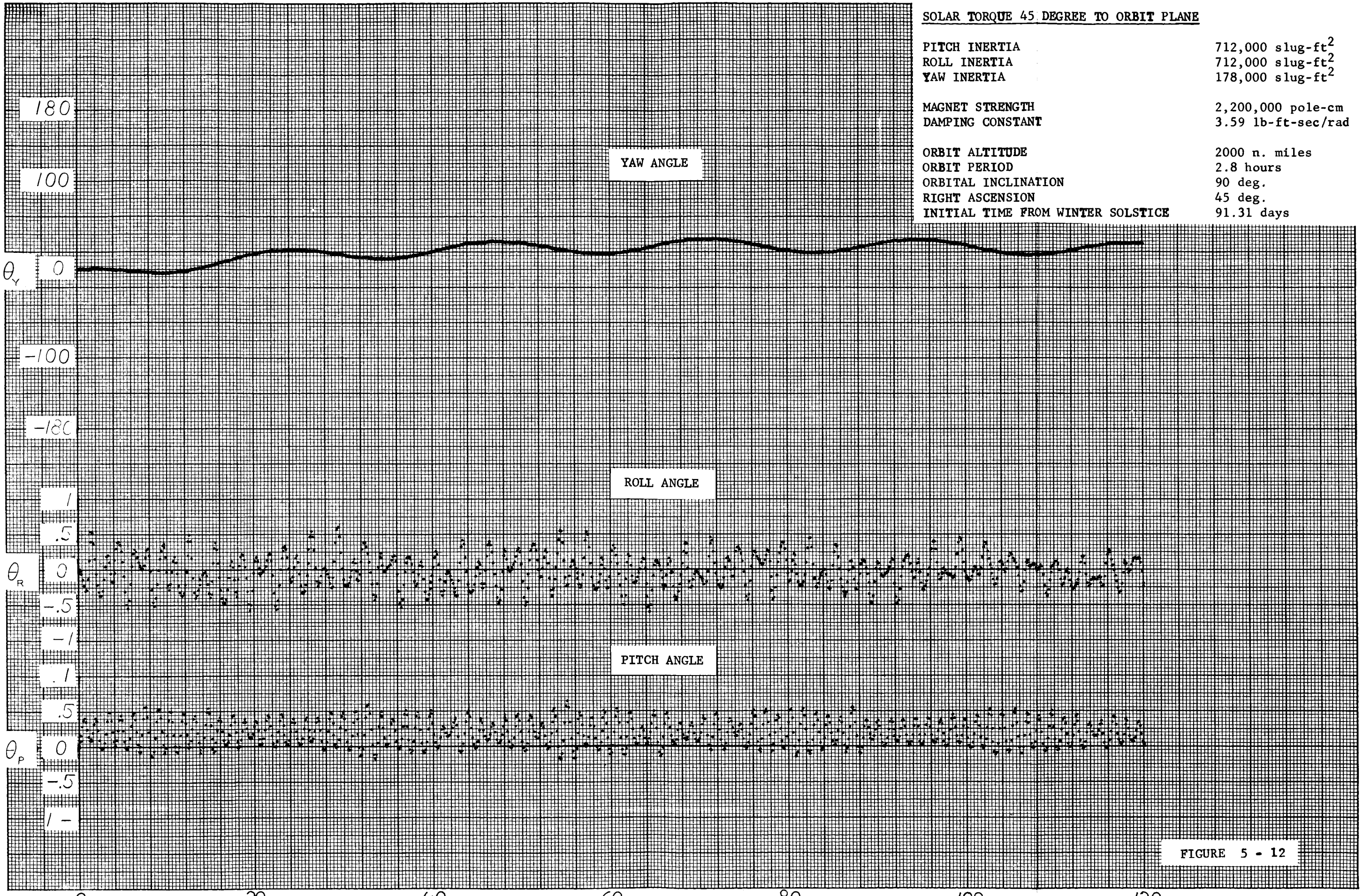

FIGURE 5 - 12

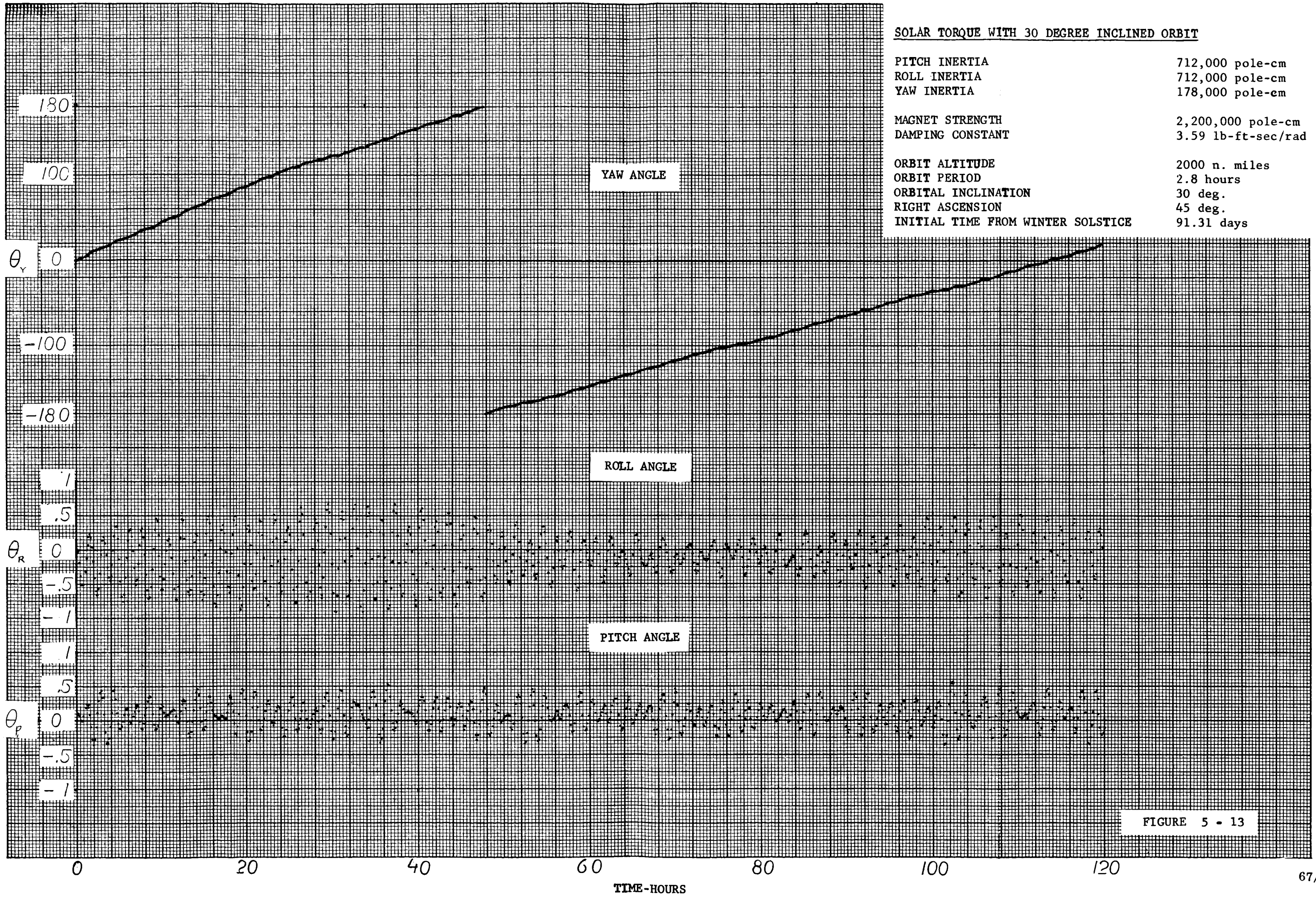

SOLAR TORQUE WITH 30 DEGREE INCLINED ORBIT

PITCH INERTIA	712,000 pole-cm
ROLL INERTIA	712,000 pole-cm
YAW INERTIA	178,000 pole-cm
MAGNET STRENGTH	2,200,000 pole-cm
DAMPING CONSTANT	3.59 lb-ft-sec/rad
ORBIT ALTITUDE	2000 n. miles
ORBIT PERIOD	2.8 hours
ORBITAL INCLINATION	30 deg.
RIGHT ASCENSION	45 deg.
INITIAL TIME FROM WINTER SOLSTICE	91.31 days

FIGURE 5 - 13

SOLAR TORQUES WITH 48 DEGREE INCLINED ORBIT

PITCH INERTIA	712,000 pole-cm
ROLL INERTIA	712,000 pole-cm
YAW INERTIA	178,000 pole-cm
MAGNET STRENGTH	2,200,000 pole-cm
DAMPING CONSTANT	3.59 lb-ft-sec/rad
ORBIT ALTITUDE	2000 n. miles
ORBIT PERIOD	2.8 hours
ORBITAL INCLINATION	48 deg
RIGHT ASCENSION	45 deg
INITIAL TIME FROM WINTER SOLSTICE	91.31 days

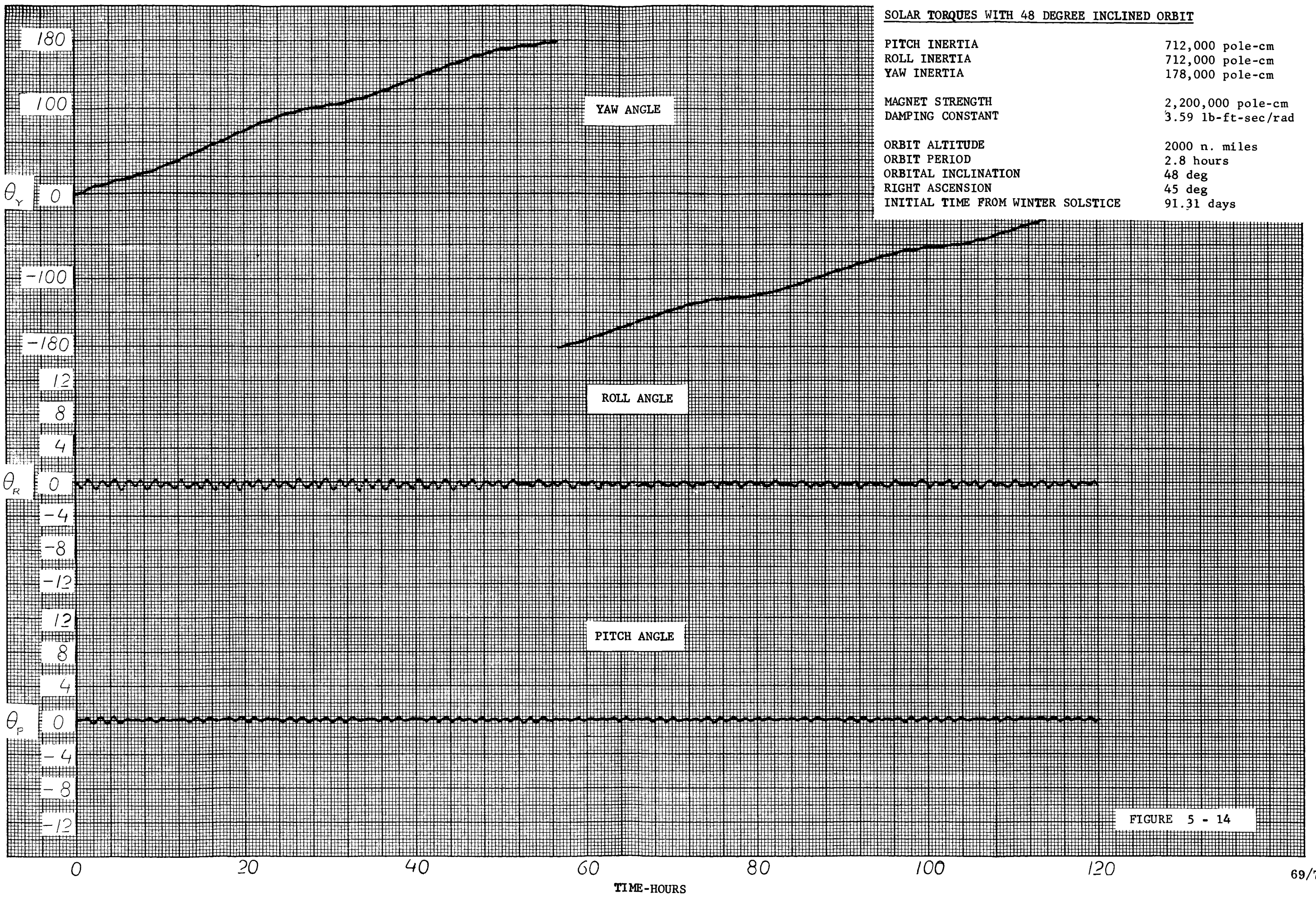

FIGURE 5 - 14

SOLAR TORQUE NORMAL TO ECCENTRIC ORBIT

ECCENTRICITY = .016

PITCH INERTIA	712,000 pole-cm
ROLL INERTIA	712,000 pole-cm
YAW INERTIA	178,000 pole-cm
MAGNET STRENGTH	2,200,000 pole-cm
DAMPING CONSTANT	3.59 lb-ft-sec/rad
ORBIT ALTITUDE	2000 n. miles
ORBIT PERIOD	2.8 hours
ORBITAL INCLINATION	90 deg
RIGHT ASCENSION	90 deg
INITIAL TIME FROM WINTER SOLSTICE	91.31 days

FIGURE 5 - 15

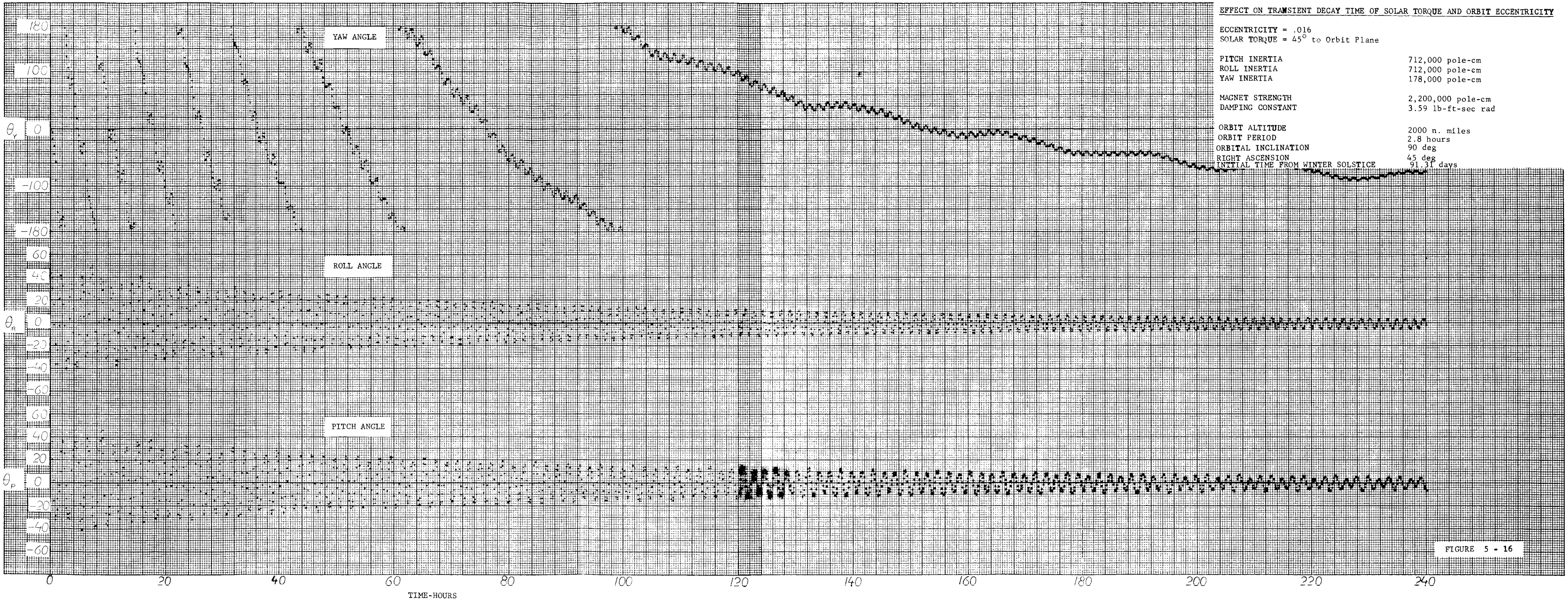

EFFECT ON TRANSIENT DECAY TIME OF SOLAR TORQUE AND ORBIT ECCENTRICITY

ECCENTRICITY = .016
SOLAR TORQUE = 45° to Orbit Plane

PITCH INERTIA	712,000 pole-cm
ROLL INERTIA	712,000 pole-cm
YAW INERTIA	178,000 pole-cm
MAGNET STRENGTH	2,200,000 pole-cm
DAMPING CONSTANT	3.59 lb-ft-sec rad
ORBIT ALTITUDE	2000 n. miles
ORBIT PERIOD	2.8 hours
ORBITAL INCLINATION	90 deg
RIGHT ASCENSION	45 deg
INITIAL TIME FROM WINTER SOLSTICE	91.31 days

FIGURE 5 - 16

6.0 DAMPER DESIGN ANALYSIS

6.1 MAGNETIC MATERIAL SELECTION

An analysis of permanent magnet materials obtained from several manufacturers indicated that Cast Alnico 5DG with its high B at peak energy would give the highest magnetic moment per unit mass of material. This material has been tentatively selected for the horseshoe magnets and the bar magnets.

To minimize the amount of bismuth in the outer shell and lower the weight of the supporting structure needed to withstand launch, it is desirable to have the inner sphere neutrally bouyant. This can be achieved by using a cylindrical magnet of approximately 4:1 ratio of length to diameter. This configuration provides a good magnetic moment, and permits the inner sphere to be of sufficient diameter to achieve neutrally bouyancy, even after addition of the extra retaining magnets and shell structure.

6.2 WEIGHT ESTIMATES

The weight of the inner sphere for neutral bouyancy is

$$Wt_s = \frac{\pi}{6} l_m^3 d_f \tag{6.1}$$

where d_f - density of fluid

l_m - length of magnet

The equation for magnetic moment is

$$M = \frac{BA_m}{4\pi} k l_m \tag{6.2}$$

where B - flux density

k - ratio of pole length to actual length

A_m - Area of magnet

For the magnet length equal to 4 times the magnet diameter.

$$A_m = \frac{\pi l_m^2}{64} \tag{6.3}$$

and

$$M = \frac{bkl_m^3}{256} \tag{6.4}$$

Solving for 1 and substituting into Equation 6.1

$$Wt = \frac{\pi d_f \, 256 \, M}{6 \, Bk} \tag{6.5}$$

$$= 134 \frac{d_f}{Bk} M \tag{6.6}$$

for $d_f = .97$ dynes/cm^2

$B = 11{,}000$ dynes/cm^2

$k = 0.7$

$Wt = .0169 \, M$ gr.

$$= 37.2 \, M \times 10^{-6} \text{ lbs.} \tag{6.7}$$

An assumption of 1/30 the radius of the sphere for thickness of Bismuth and the same for a supporting structure gives an external shell weight of

$$W_{to} = \pi(l_m + \frac{l_m}{60})^2 \frac{l_m}{60} d_{b_i} + \pi(l_m + \frac{31m}{60})^2 \frac{l_m}{60} d_{a_L} \tag{6.8}$$

where

d_{b_i} = Density of Bismuth = 9.75 gr/cc

d_{a_L} = Density of Aluminum = 2.7 gr/cc

Hence

$$W_{t_O} = .684 \, l_m^3 \text{ gr} \tag{6.9}$$

From Equation (6.4)

$$m^3 = \frac{256}{bk} M = .0227 \, M \tag{6.10}$$

And

$$Wt_O = .0235 \, M \text{ gr} \tag{6.11}$$

$$= 50 \, M \times 10^{-6} \text{ lbs.} \tag{6.12}$$

The total weight of the damper component can then be estimated to better than 10 percent accuracy by combining equations (6.6) and (6.10)

Total Weight = $87.2 \, M \times 10^{-6}$ lbs.

The above calculations are conservative. A decrease in length to diameter ratio of the magnet in the inner sphere, would decrease the weight by nearly the square in the change of that ratio. Tests of actual magnets in a shell of bismuth would indicate the minimum thickness required. The band of weight vs. magnet strength shown in Figure 4-5 takes into account the uncertainty in required bismuth.

7.0 SUN PRESSURE TORQUES

Solar torques arise from solar radiation pressure on the surfaces of a body. This pressure is the result of bombardment of the surfaces by photons. The pressure is exerted on both absorbing and reflecting surfaces.

If an elementary surface area dA is exposed to sunlight, the force exerted by the photons striking the surface is

$$d^2F=P_o dA \left[\bar{s} (1 - \rho) (\bar{s} \cdot \bar{n}) + 2\bar{n} \rho (\bar{s} \cdot \bar{n})^2 \right] \qquad (7.1)$$

The ratio of the solar power flux density to the velocity of light ($P_o=E/c$) is the pressure exerted on a perfectly absorbing surface normal to the incident radiation. At earth's distance from the sun this is 4.62×10^{-5} dynes per square centimeter or 9.65×10^{-8} pounds per square foot. The first term in the brackets is the contribution due to absorption, and the second term is that due to reflection. $\bar{s}$ is a unit vector in the direction of propagation of the radiation. $\bar{n}$ is a unit vector perpendicular to the surface and positive inward. (The radiation impinges on the "outer" side of the surface.) The quantity $(\bar{s} \cdot \bar{n})$ is the cosine of the angle of incidence. It is seen that the absorption contribution is along the incident ray and that the reflection contribution is along the normal into the surface. Both terms have a cosine factor $(\bar{s} \cdot \bar{n})$ because the projected area normal to the radiation is this cosine factor times the area dA. The reflection term has a factor 2 and a second cosine factor. These arise from taking the resultant of the forces due to the incident and reflected rays. In practical problems, all of the sun's rays at the satellite are assumed to be parallel, although the sun actually subtends about a half of a degree at 1 a.u.

In analyzing the attitude dynamics of a satellite or any other body, the torques about some particular center of rotation are of primary interest. The center of rotation generally has an arbitrary location with respect to any surface under consideration. Therefore, the calculation of the solar torques on the body, due to solar radiation on one of the body surfaces requires expression of the vector moment arm from the arbitrary location of the center of rotation to each element dA of the surface. If this moment arm is designated h, then the solar torque due to a surface is the integral of the vector cross-product $\vec{h} \times \vec{d^2F}$ over the portion of the surface illuminated by the solar radiation.

7.1 TWO DIMENSIONAL SKIN

Equations are derived for a two dimensional skin which neglect wire thickness; these equations are a first approximation to the much more complicated three dimensional equations. Figure 7.1 shows the coordinate system which was used to describe the POLES satellite for this analysis. The righthanded system of coordinates i, j, k is defined such that the sun is instantaneously in the i,k plane. The angle which the sun makes with the $\bar{i}$ axis is θ where $0 \leq \theta \leq 180$. The i axis is along the longitudinal axis of the balloon and directed as shown in the figure. The lens was assumed to be composed of portions of two spheres whose centers are 0 and 0' and whose radius is r_o. ϕ is the measured from the horizontal to the edge of the lens; thus, the lens central angle is $2(90-\phi)$. ψ is the integration variable along a "latitude" line of the sphere and λ along a "longitude" line. $\bar{n}$ is a vector normal to the surface which is directed toward the center.

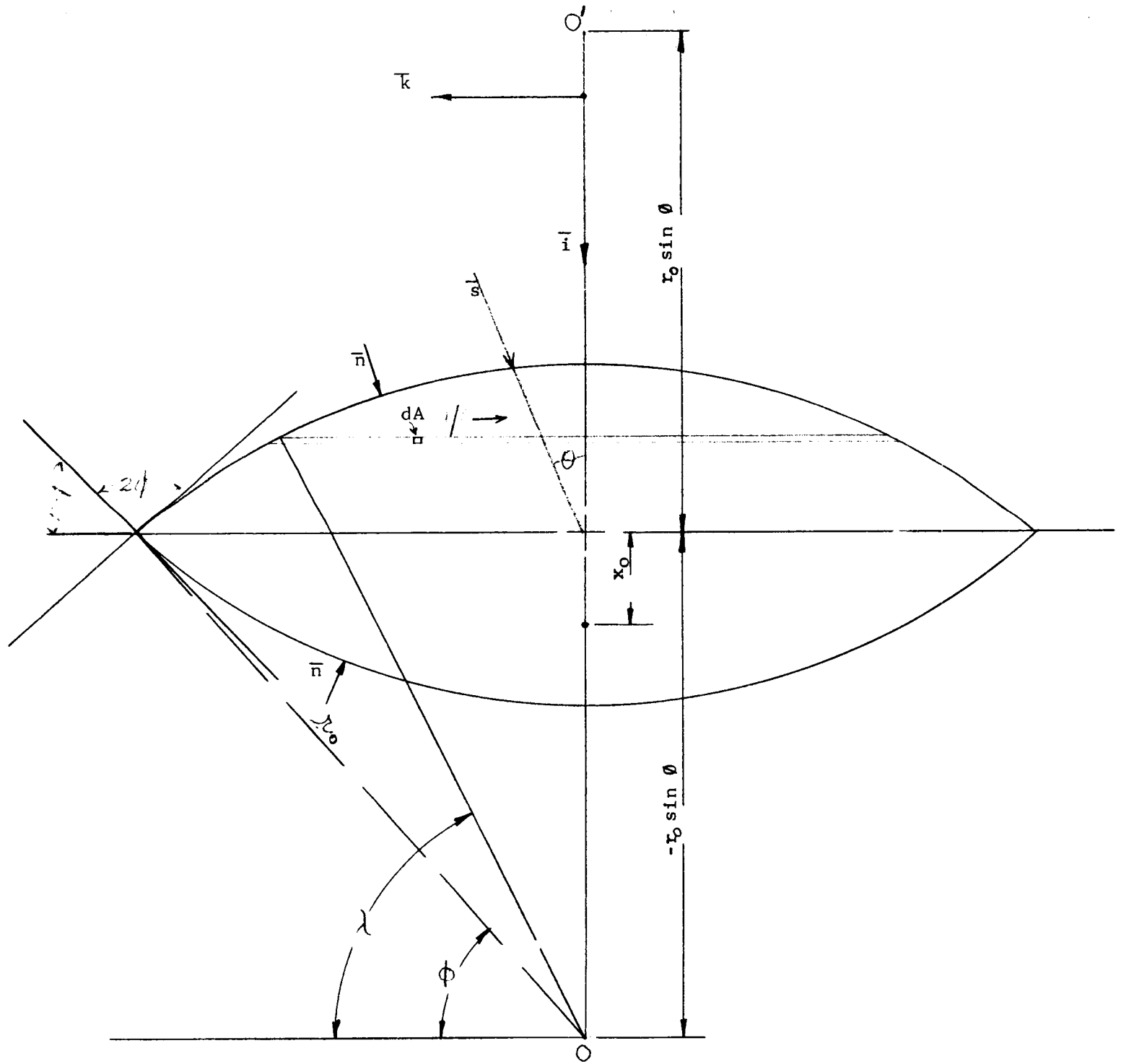

Figure 7-1 BALLOON COORDINATE SYSTEM WITH SUN IN i,k PLANE

It can be seen that the sun vector is

$$\bar{s} = \cos\theta\,\bar{i} - \sin\theta\,\bar{k} \tag{7.2}$$

and the normal to the surface of the sphere is

$$\bar{n} = \sin\lambda\,\bar{i} - \sin\psi\cos\lambda\,\bar{j} - \cos\psi\cos\lambda\,\bar{k} \tag{7.3}$$

The elementary surface area is

$$dA = r_o^2\cos\lambda\,d\lambda\,d\psi \tag{7.4}$$

When no shadows exist, the iluminated surface is defined by $-\pi \le \psi \le \pi$ and $0 \le \lambda \le \pi/2$. However, when the sun makes a certain angle ($\theta > \emptyset$) with the $\bar{i}$ axes, shadow will occur along two straight lines which are perpendicular to the sun vector. Along these lines,

$$\bar{s} \cdot \bar{n} = 0 \tag{7.5}$$

Therefore,

$$\cos\theta\sin\lambda + \sin\theta\cos\psi\cos\lambda = 0 \tag{7.6}$$

If ψ_c is defined as the angle at which the shadow occurs then, the sun-shadow line will be defined by

$$\cos\psi_c = -\frac{\tan\lambda}{\tan\theta} \tag{7.7}$$

A system of offsets must be defined such that the torques can be computed about any arbitrary point. Since the torques are computed about two spherical centers, two sets of offsets, x_L, y_L, z_L and x_L', y_L', z_L', are necessary. If x_o is the distance along the $\bar{i}$ axis from the geometrical center to the arbitrary center of torque (positive toward 0 in Figure 7.1) then

$$x_L = -r_o\sin\emptyset + x_o \tag{7.8}$$

$$x_L' = r_o\sin\emptyset + x_o \tag{7.9}$$

y_L and y_L' are offsets along the $\bar{j}$ axis and will be equal since the two spherical centers are along the $\bar{i}$ axis. Similiar reasoning follows for z_L and z_L', the offsets along the $\bar{k}$ axis. Therefore, only the offsets x_L, x_L', y_L and z_L will be considered. The moment arm from the point around which the torques are computed to dA for the spherical segment, 0, is

$$\vec{h} = i(-r_o\sin\lambda - x_L) + j(r_o\cos\lambda\sin\psi - y_L) + k(r_o\cos\lambda\cos\psi - z_L) \tag{7.10}$$

For the spherical segment, 0', the corresponding moment arm is

$$\vec{h}' = i(-r_o\sin\lambda - x_L') + j(r_o\cos\lambda\sin\psi' - y_L) + k(r_o\cos\lambda\cos\psi - z_L) \tag{7.11}$$

The element of torque about the arbitrary point, due to solar flux on dA, is

$$\vec{d^2T} = \vec{h} \times \vec{d^2F} \tag{7.12}$$

and

$$\vec{d^2T}' = \vec{h}' \times \vec{d^2F} \tag{7.13}$$

for the two spherical segments.

Thus far, in the discussion no mention has been made of the material which the balloon is made of. If the material is solid, then the previous discussion is sufficient and the equations may be integrated as they stand. However, if the material is a mesh type substance, further definition is necessary.

As a first approximation, the mesh is considered to be square and of negligible thickness. The percentage of the closed area is estimated. This percentage, K_1, is assumed to be the percentage of the torque on the surface of the balloon toward the sun which is experienced by the balloon. Since the surface is partly open $(1 - K_1)$ of the sun's rays will fall on the inside of the balloon. Of these rays, K_1 of them will cause torque on the balloon. Therefore, a factor of $K_1(1 - K_1)$ is applied to torques on the inside of the balloon.

The derivation of K_1 may be seen from the following illustration.

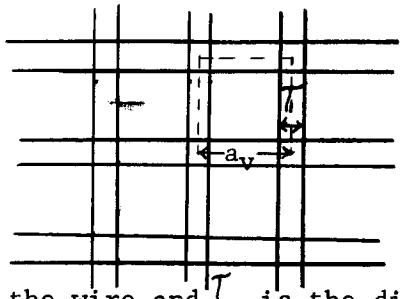

where a_v is the width of the wire and τ_1 is the distance from the center of one wire to the center of the next wire. The area of the solid material is $\tau_1(2\,a_v - \tau_1)$. The area of the total square is a_v^2

$$\text{Then } K_1 = \frac{\tau_1(2a_v - \tau_1)}{a_v^2} \tag{7.14}$$

but $2\,a_v >> \tau_1$, and

$$K_1 = \frac{2\,\tau_1}{a_v} \tag{7.15}$$

For example, if $\tau_1 = .001$ and $a_v = .1$, then $K_1 = .02$ or 2% of the balloon is solid material.

The derivation of the force equation assumes that $\bar{s} \cdot \bar{n}$ is positive which is to say that the sun looks into the surface as does the normal. For a porous inner surface, the normal must then be directed away from the center of the sphere or the force equation must be redefined such that the terms containing odd powers of $\bar{n}$ are switched in sign. Therefore, the new force equation becomes

$$\overrightarrow{d^2F_o} = dA\left[-\bar{s}(\bar{s}\cdot\bar{n})(1-\rho_s) + \frac{2}{3}\rho_d\,(\bar{s}\cdot\bar{n}) - 2\rho_s\,\bar{n}(\bar{s}\cdot\bar{n})^2\right] \tag{7.16}$$

where the subscript o will be used to distinguish this special case.

The following table shows the integration limits, mesh coefficient and force equation to be used for the four ranges of sun angle θ. Case I and IV represent no shadow condition while the balloon is partly in shadow for cases II and III.

Table 7.1 Integration Limits for $\iint \overrightarrow{d^2T}$

Case	Term	θ	ψ	λ	Center	Mesh Coefficient	Force Equation
I	1	0 to ϕ	$\pm\pi$	ϕ to $\pi/2$	0	K_1	d^2F
	2		$\pm\pi$	$-\pi/2$ to $-\phi$	0'	$K_1(1-K_1)$	d^2F_o
II	1	ϕ to $\pi/2$	$+\pi$	θ to $\pi/2$	0	K_1	d^2F
	2		$\pm\psi_c$	ϕ to θ	0	K_1	d^2F
	3		$\pm\psi_c$	$-\theta$ to $-\phi$	0'	K_1	d^2F
	4		$\pm\pi$	$-\pi/2$ to $-\theta$	0'	$K_1(1-K_1)$	d^2F_o
III	1	$\pi/2$ to $\pi-\phi$	$\pm\pi$	$-\pi/2$ to $-(\pi-\theta)$	0'	K_1	d^2F
	2		$\pm\psi_c$	$-(\pi-\theta)$ to $-\phi$	0'	K_1	d^2F
	3		$\pm\psi_c$	ϕ to $\pi-\theta$	0	K_1	d^2F
	4		$\pm\pi$	$\pi-\theta$ to $\pi/2$	0	$K_1(1-K_1)$	d^2F_o
IV	1	$\pi-\phi$ to π	$+\pi$	$-\pi/2$ to $-\phi$	0'	K_1	d^2F
	2		$\pm\pi$	ϕ to $\pi/2$	0	$K_1(1-K_1)$	d^2F_o

It is only necessary to consider $0 \leq \theta \leq \pi$ since the integration in the plane perpendicular to θ includes $\pm\pi$ if no shadow exists or $\pm\psi$ if a shadow exists where ψ_c defines the sun-shadow line.

Following is a summary of the torque equations which have been obtained by combining and integrating the equations defined in this section.

Intermediate functions:

$$F_1 = \sin\theta \cos\theta \cos^2\phi \,(1 - \sin^2\phi\rho_s) \tag{7.17}$$

$$F_2 = 2/9\,\rho_d \sin\theta(2 - 3\sin\phi + \sin^3\phi) \tag{7.18}$$

$$F_3 = \cos^2\theta\cos^2\phi + \tfrac{1}{2}\rho_s \cos^2\phi(2\cos^2\theta - 3\cos^2\theta\cos^2\phi + \cos^2\phi) \tag{7.19}$$

$$F_4 = 4/9\,\rho_d \cos\theta\,(1 - \sin^3\phi) \tag{7.20}$$

$$F_5 = \sin\theta\left[\frac{\pi}{2} - \sin^{-1}\left(\frac{\sin\phi}{\sin\theta}\right) - \sin\phi\sqrt{\sin^2\theta - \sin^2\phi} - \cos\theta\cos^2\phi(1-\sin^2\phi\rho_s)\cos^{-1}(\cot\theta\tan\phi)\right.$$
$$\left. - \rho_s\sin\phi\,(2/3 - \sin^2\phi + \frac{1}{3}\,\frac{\sin^2\phi}{\sin^2\theta})\,\sqrt{\sin^2\theta - \sin^2\phi}\,\right] \tag{7.21}$$

$$F_6 = \frac{2}{9}\rho_d\sin\theta\left[-2\cos^{-1}\left(\frac{\cos\theta}{\cos\phi}\right) + (3-\sin^2\phi)\sin\phi\,\cos^{-1}(\cot\theta\tan\phi) - \frac{\sin^2\phi}{\sin^2\theta}\cos\theta\sqrt{\sin^2\theta-\sin^2\phi}\,\right] \tag{7.22}$$

$$F_7=\pi \sin\theta\cos\theta\cos^2\phi(1-\sin^2\phi\rho_s) - \frac{2}{9}\rho_d\pi\sin\theta\sin\phi(3-\sin^2\phi)+\frac{4}{9}\rho_d\pi\sin\theta \quad (7.23)$$

$$F_8= -(1-K_1)\pi\sin\theta\left[\cos^3\theta(1-\sin^2\theta\rho_s) - \frac{4}{9}\rho_d + \frac{2}{9}\rho_d \sin\theta(3-\sin^2\theta)\right] \quad (7.24)$$

$$F_9= \cos\theta\left[\frac{\pi}{2} -\sin^{-1}\left(\frac{\sin\phi}{\sin\theta}\right)-\sin\phi\sqrt{\sin^2\theta-\sin^2\phi}-\cos\theta\cos^2\phi\cos^{-1}(\cot\theta\tan\phi)\right] \quad (7.25)$$

$$+\rho_s\left[\frac{3}{2}\cos\theta\sin\phi\cos^2\phi\sqrt{\sin^2\theta-\sin^2\phi} - \frac{1}{2}\cos2\phi\ (\cos^2\phi-3\cos^2\theta\cos^2\phi+2\cos^2\theta)\cos^{-1}(\cot\theta\tan\phi)\right] \quad (7.26)$$

$$F_{10}=\pi\cos^2\phi\cos^2\theta+\frac{1}{2}\pi\rho_s\cos^2\phi(\cos^2\phi-3\cos^2\theta\cos^2\phi+2\cos^2\theta)+\frac{4}{9}\rho_d\pi\cos\theta(1-\sin^3\phi) \quad (7.27)$$

$$F_{11}= -\pi(1-K_1)\cos\theta\left[\cos^3\theta(1+\frac{3}{2}\rho_s\sin^2\theta) - \frac{4}{9}\rho_d(1-\sin^3\theta)\right] \quad (7.28)$$

$$F_{12}= -(1-K_1)\pi\sin\theta\left[\cos^3\theta(1-\sin^2\theta\rho_s) + \frac{4}{9}\rho_d - \frac{2}{9}\rho_d\sin\theta(3-\sin^2\theta)\right] \quad (7.29)$$

$$F_{13}= -(1-K_1)\pi\cos\theta\left[\cos^3\theta(1+\frac{3}{2}\rho_s\sin^2\theta) + \frac{4}{9}\rho_d(1-\sin^3\theta)\right] \quad (7.30)$$

Torque Equations:

Case I: $0 \le \theta \le \phi$

$$T_i = K_1(2-K_1)P_o r_o^2 y_L \pi (F_1 + F_2) \quad (7.31)$$

$$T_k = K_1(2-K_1)P_o r_o^2 y_L \pi (F_3 + F_4) \quad (7.32)$$

$$T_y = -K_1^2 P_o r_o^3 \pi(1-\rho_s)\sin\phi\cos^2\phi\sin\theta\cos\theta$$
$$-K_1 P_o r_o^2 \pi\left[(x_L + x_L' - K_1 x_L')(F_1+F_2)+(2-K_1)(F_3+F_4)z_L\right] \quad (7.33)$$

Case II: $\phi < \theta \le 90^\circ$

$$T_i = K_1 P_o r_o^2 y_L (2F_5 + F_7 - F_{12}) \quad (7.34)$$

$$Tk = K_1 P_o r_o^2 y_L (2F_9 + F_{10} - F_{13}) \quad (7.35)$$

$$T_j = -K_1 P_o r_o^3 \pi(1-\rho_s)\sin\theta\cos\theta\left[\sin\phi\cos^2\phi - \sin\theta\cos^2\theta(1-K_1)\right]$$
$$-K_1 P_o r_o^2\left[(x_L + x_L')F_5 + (x_L - x_L')F_6 + x_L F_7 - x_L' F_{12}\right.$$
$$\left. + 2z_L F_9 + z_L F_{10} - z_L F_{13}\right] \quad (7.36)$$

Case III $90^\circ < \theta < \pi - \phi$

$$T_i = K_1 P_o r_o^2 y_L (2F_5 + F_7 + F_8) \quad (7.37)$$

$$T_k = K_1 P_o r_o^2 y_L (2F_9 + F_{10} + F_{11}) \quad (7.38)$$

$$T_j = -K_1 P_o r_o^3 \pi(1-\rho_s)\sin\theta\cos\theta\left[\sin\phi\cos^2\phi - \sin\theta\cos^2\theta(1-K_1)\right]$$
$$-K_1 P_o r_o^2\left[(x_L + x_L')F_5 + (x_L - x_L')F_6 + x_L F_7 + x_L F_8\right.$$
$$\left. + 2z_L F_9 + z_L F_{10} + z_L F_{11}\right] \quad (7.39)$$

Case IV: $\pi - \phi \leq \theta \leq \pi$

$$T_i = K_1(2 - K_1)\, P_o r_o^2 y_L \pi (-F_1 + F_2) \tag{7.40}$$

$$T_k = K_1(2 - K_1)\, P_o r_o^2 y_L \pi (-F_3 + F_4) \tag{7.41}$$

$$T_j = -K_1^2\, P_o r_o^3 \pi (1 - \rho_s) \sin\phi\cos^2\phi\sin\theta\cos\theta$$
$$-K_1 P_o r_o^2 \pi \left[(x_L + x_L' - K_1 x_L)(-F_1 + F_2) + (2 - K_1)(-F_3 + F_4) z_L\right] \tag{7.42}$$

The preceding equations were programmed separately so that solar torques could be easily evaluated as a function of sun angle for set vehicle configurations. Figures 7-2, 7-3, 7-4 show solar torque versus sun angle for $\rho_s = .65, \rho_d = .05$ and mesh coefficients of 100%, 5% and 2%. Both symmetric and unsymmetric satellites are included.

7.2 THREE DIMENSIONAL SKIN

The preceding analysis considered solar torques on mesh wires whose surfaces are parallel to the spherical surfaces. These wires were considered to be of negligible thickness. Appendix III contains the derivation of the solar torques on the radial areas of a mesh satellite composed of square cross-sectional wires. Therefore the total solar torque on a mesh satellite with square cross-sectional wires is the sum of the solar torques on the parallel and radial surfaces. At present, the equations contained in Appendix III have not been programmed.

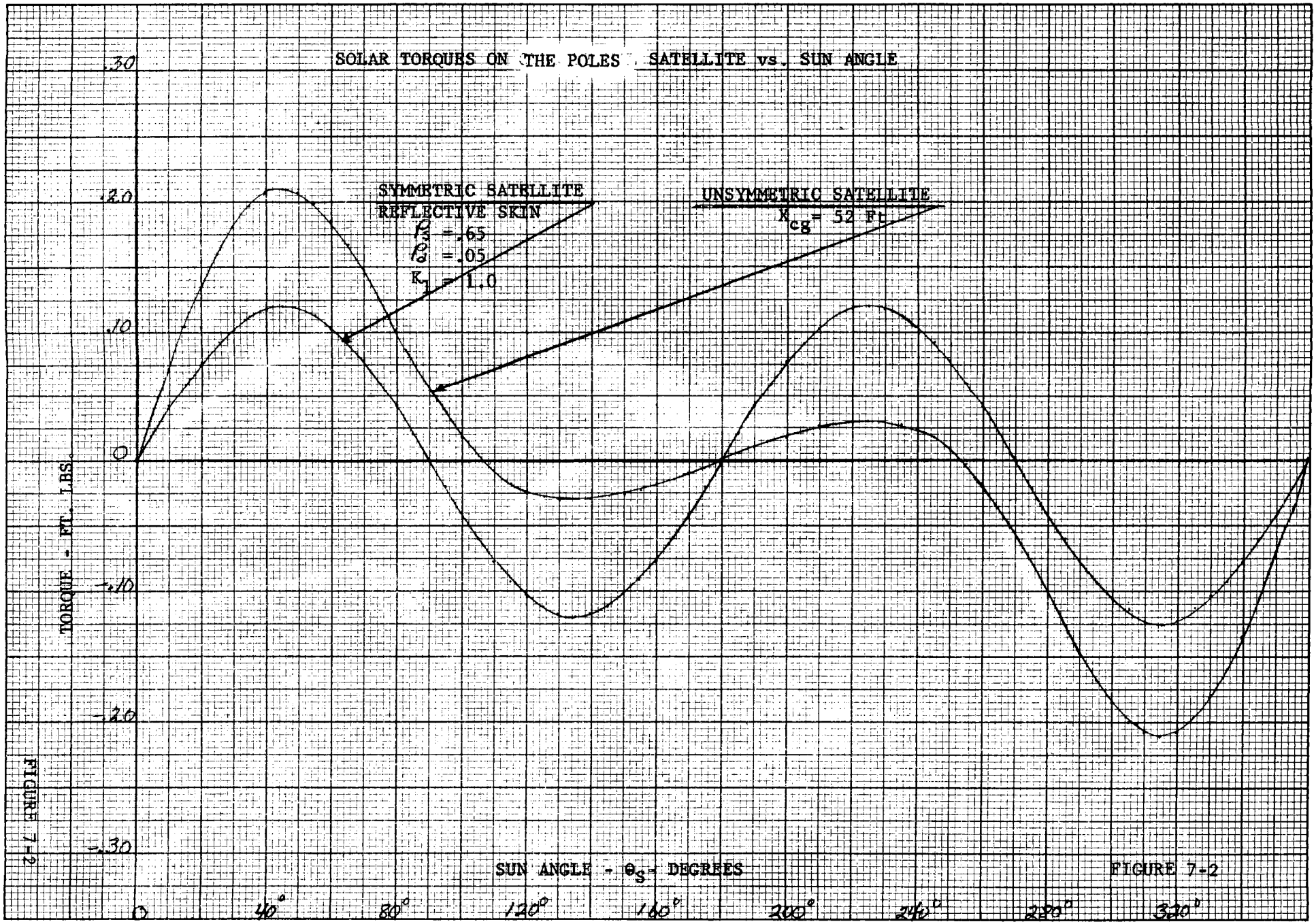

FIGURE 7-2

FIGURE 7-2

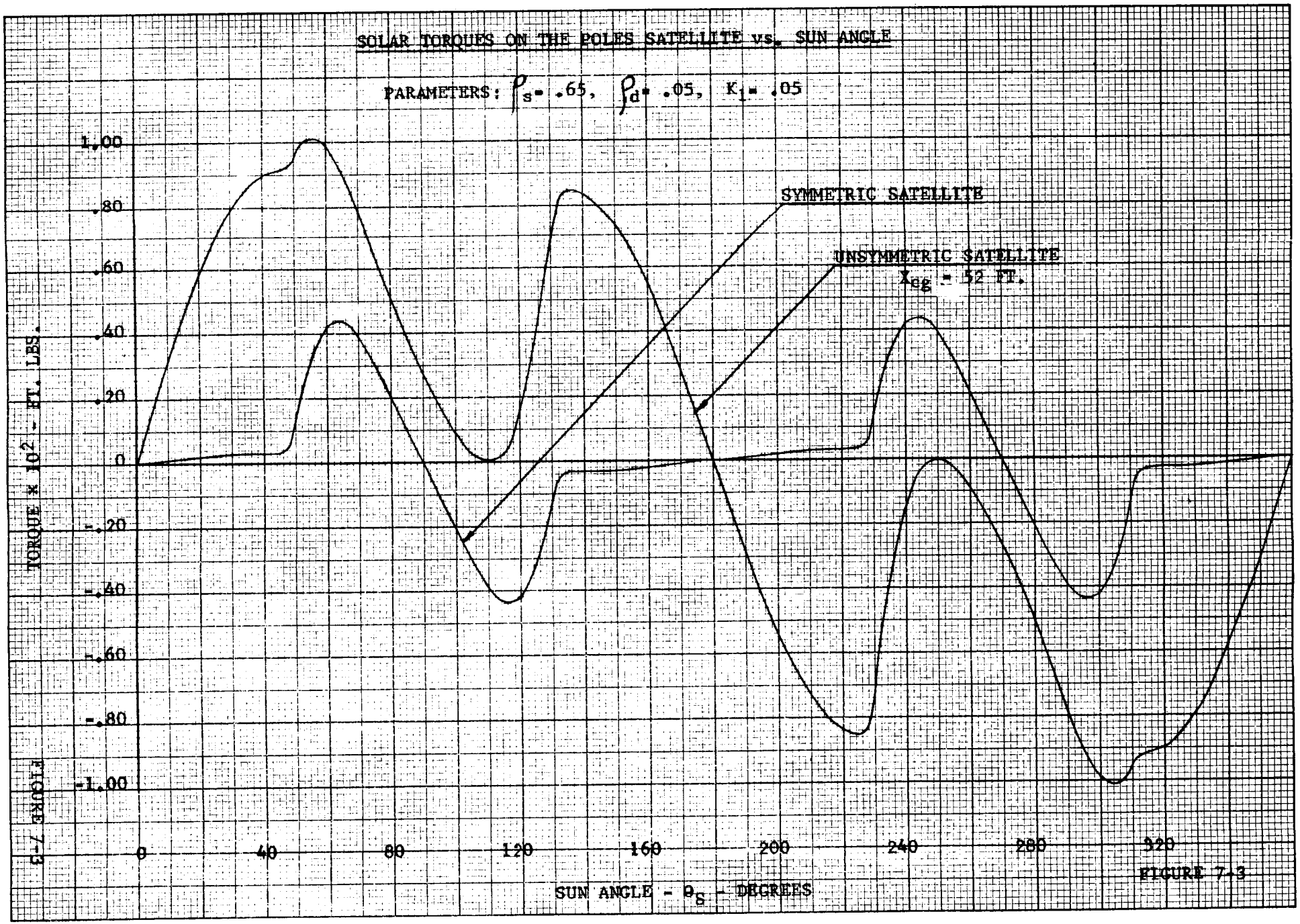
SOLAR TORQUES ON THE POLES SATELLITE vs. SUN ANGLE
PARAMETERS: ρ_s = .65, ρ_d = .05, K_1 = .05
SYMMETRIC SATELLITE
UNSYMMETRIC SATELLITE
X_{cg} = 52 FT.
TORQUE * 10^2 - FT. LBS.
1.00
.80
.60
.40
.20
0
-.20
-.40
-.60
-.80
-1.00
0
40
80
120
160
200
240
280
320
SUN ANGLE - θ_S - DEGREES

FIGURE 7-3

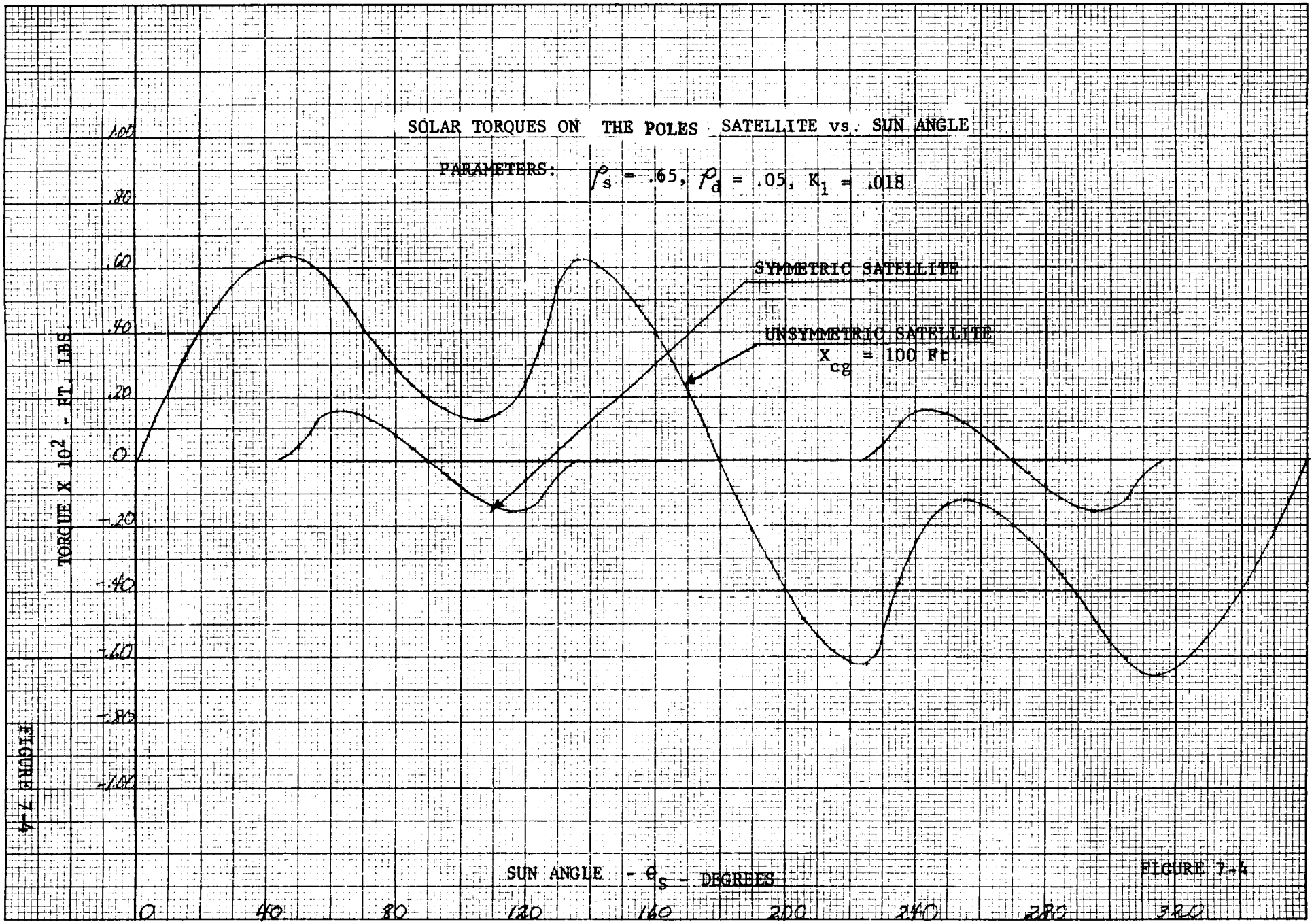
SOLAR TORQUES ON THE POLES SATELLITE vs. SUN ANGLE
PARAMETERS: ρ_s = .65, ρ_d = .05, K_1 = .018
SYMMETRIC SATELLITE
UNSYMMETRIC SATELLITE
X_{cg} = 100 Ft.
TORQUE X 10^2 - FT. LBS.
100
80
60
40
20
0
-20
-40
-60
-80
-100
0
40
80
120
160
200
240
280
320
SUN ANGLE - θ_s - DEGREES

FIGURE 7-4

8.0. EDDY CURRENT TORQUES

This analysis pertains to an investigation of the torques due to eddy currents of a lenticular balloon satellite in orbit. The balloon is composed of a large lens-shaped wire mesh. This conducting material is in motion in the magnetic field of the earth; therefore, eddy currents will be induced into the material. The eddy current loops produce a magnet moment which interacts with the earth's magnetic field, producing a torque on the satellite. We shall try to give a good estimate of the magnitude and frequency of this torque for the worst possible case. Two cases will be considered as an approximation: (a) a circular wire loop and (b) a thin conducting disc.

Faraday's Law states that the induced emf around a closed path is equal to the negative rate of change of flux through the loop. (reference 2, 3 and 4)

$$\mathcal{E} = -\frac{d\Phi}{dt} \tag{8.1}$$

$$\Phi = \int_{\text{area enclosed by loop}} \vec{B} \cdot d\vec{S} \tag{8.2}$$

where: $\mathcal{E}$ = emf produced in loop (volts)
Φ = magnetic flux through the loop (webers)
B = flux density (webers/M^2)

Equation (8.1) considers only the emf due to a flux change and does not take into account the motion of a conductor such as a straight wire moving in a constant magnetic field. This motional emf is correctly given by

$$\mathcal{E} = -\int \vec{B} \cdot \vec{v}_o \times d\vec{l}_o \tag{8.3}$$

where: $\vec{v}_o$ = velocity of the element of wire
$d\vec{l}_o$ = element of wire

We shall show immediately that the emf produced by equation (8.3) is zero for the case of a rigid wire loop moving in a uniform magnetic field. (Uniform field means that the instantaneous value of the field is the same at all parts of the circuit.) The motion considered is that of translation only.

The dot and the cross in equation (8.3) may be interchanged to give

$$\mathcal{E} = -\oint \vec{B} \times \vec{v}_o \cdot d\vec{l}_o$$

and since $\vec{B}$ and $\vec{v}_o$ are constant vectors during the integration, they may be taken outside of the integral, giving

$$\mathcal{E} = -\vec{B} \times \vec{v}_o \cdot \oint d\vec{l}_o$$

But $\oint \vec{dl}_o = 0$ for a closed loop, hence

$$\mathcal{E} = 0 \text{ for translational motion.}$$

From now on we concern ourselves only with the emf produced by equations (8.1) and (8.2).

The magnetic field of the earth may be approximated by a dipole. The description of a dipole field is

$$H = \frac{Me}{r^3}\left[\, 2\cos\xi\ \vec{r} + \sin\xi\ \vec{\xi}\,\right] \tag{8.4}$$

where: H is the magnetic field intensity (amp/m), $\vec{r}$ and $\vec{\xi}$ are unit vectors and the coordinates r (geocentric radius) and ξ (polar angle) are shown in Figure 8-1.

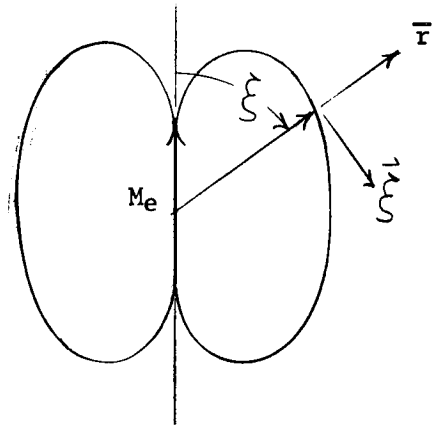

Figure 8-1

Description of Dipole Field

M_e is the strength of the earth's magnetic dipole and is equal to, cf (reference 5),

$$M_e = 6.43 \times 10^{21} \text{ amp - meter}^2 \tag{8.5}$$

The satellite is oriented so as to always point down along the local vertical.

A circular loop of wire, or a disc, is in a circular orbit as in Figure 8-2, and we wish to find the torque due to eddy currents on the wire and disc respectively.

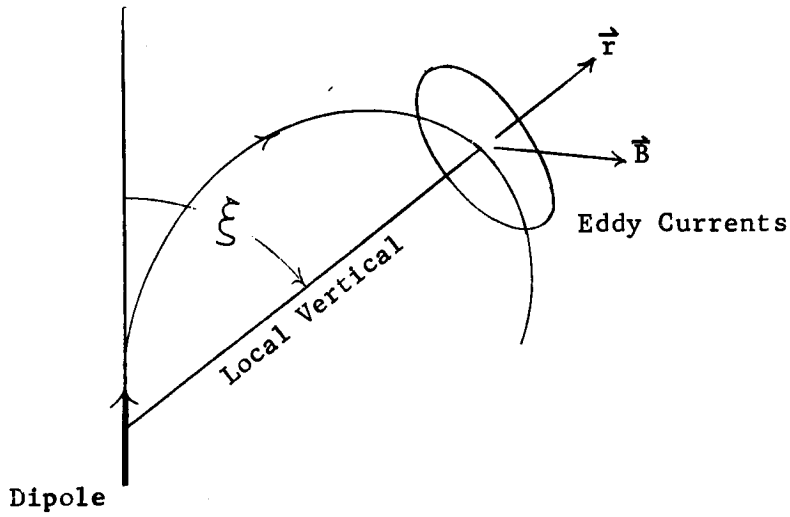

Figure 8-2

Loop in Orbit Around Magnetic Dipole

A polar orbit is chosen because this would produce the maximum flux change through the loop.

8.1. EDDY CURRENT TORQUE ON A WIRE LOOP

The flux density at the position of the loop is

$$\vec{B} = \mu_o \vec{H}$$

$$\vec{B} = \frac{\mu_o M_e}{r^3} \left[2 \cos\xi \ \vec{r} + \sin\xi \ \vec{\xi} \right] \qquad (8.6)$$

where: $\mu_o = 4\pi \times 10^{-7}$ Henry/meter

B is assumed to have the same value at all points along the loop.

The flux through the loop is

$$\Phi = \int \vec{B} \cdot d\vec{S} = A \vec{B} \cdot \vec{r}$$

$$\Phi = 2\pi a_o^2 \frac{\mu_o M_e}{r^3} \cos\xi \qquad (8.7)$$

where: a_o and A are the radius and area of the loop respectively.

The emf induced in the loop due to the flux change through the loop becomes

$$\mathcal{E} = \frac{2\pi a_o \mu_o M_e}{r^3} \omega_o \sin \omega_o t \qquad (8.8)$$

where: ξ has been replaced by $\omega_o t$ and ω_o is the orbital angular velocity.

The above emf produces a current in the loop of magnitude

$$i_o = \frac{\mathcal{E}}{2\pi a_o \sigma_o} \qquad (8.9)$$

where: σ_o = resistance per unit length of wire (ohm/meter)

The current in turn produces a magnetic moment of $\vec{M}$ of

$$\vec{M} = i_o A \vec{r} \qquad (8.10)$$

which interacts with the magnetic field to produce a torque $\vec{T}$

$$\vec{T} = \vec{M} \times \vec{B}$$

$$\vec{T} = i_o A \vec{r} \times \vec{B}$$

$$T = \frac{\pi a_o^3}{\sigma_o} \left[\frac{\mu_o M_e}{r^3} \right]^2 \omega_o \sin^2 \omega_o t \, (\vec{r} \times \vec{\xi}) \qquad (8.11)$$

For the circular orbit considered here, the geocentric radius is related to the angular velocity by

$$\omega_o^2 = \frac{K}{r^3} \qquad (8.12)$$

where: $K = (3.98 \times 10^{14}\ m^3/sec^2)$ is the product of the gravitational constant and the mass of the earth.

With the above substitution into equation (8.11) the eddy current torque becomes

$$\vec{T} = \frac{\pi}{2} \left[\frac{\mu_o M_e}{K} \right]^2 \frac{a_o^3 \omega_o^5}{\sigma_o} \left[1 - \cos 2\omega_o t \right] (\vec{r} \times \vec{\xi}) \qquad (8.13)$$

normal to orbit plane (along pitch axis).

The eddy current torque is seen to depend upon the third power of the radius of the loop, the fifth power of the orbital angular velocity and inversely upon the resistance per unit length of wire.

The eddy current torque, equation (8.13), has a frequency of $2\omega_o$; but it is always in the same direction normal to the orbital plane in the sense of the orbital rotation (pitch direction). This is due to the fact that when the radial component of the field is increasing, the tangential component is negative, while when the radial component is decreasing, the tangential component is positive. The interaction of the eddy current with the field produces a torque that is always in the same direction.

8.2. EDDY CURRENT TORQUE ON A THIN CONDUCTING DISC

Next we consider the torque on a thin conducting disc. The analysis is similar to the wire loop except now the medium is continuous. The disc is thin to allow the magnetic field to penetrate without significant loss in field intensity. Also, the eddy currents are assumed to be circles concentric with the center of the disc as in Figure 8-2.

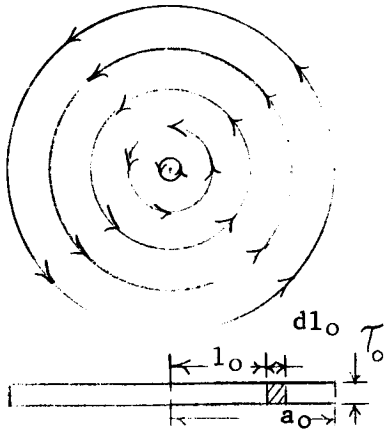

Figure 8-3

Eddy Currents in Thin Conducting Disc

Circular currents are a plausible assumption because if one starts at the edge of the disc the continuity of current imposes the condition that the current must be tangent to the edge. From symmetry the current must be the same magnitude all the way around the edge. In this manner one can work from the edge to the center where the current must become zero.

The flux through the area enclosed by a circle at a distance l_o from the center of the disc is the same as equation (7) with a_o replaced by l_o. The emf is similar to equation (8).

$$\mathcal{E} = 2\pi l_o^2 \frac{\mu_o M_e}{r^3} \omega_o \sin \omega_o t \tag{8.14}$$

The current flowing through the small cross section of thickness and width dl_o at a distance l_o from the center is

$$di_o = \frac{\mathcal{E} \tau_o \, dl_o}{2\pi l_o \rho_o} \tag{8.15}$$

where: ρ_o is the resistivity of the material (ohm-meter).

The magnetic moment of this current is

$$\vec{dM} = \pi l_o^2 \, di_o \, \vec{r} \tag{8.16}$$

and the total magnetic moment due to all eddy current loops is found by integrating equation (8.16)

$$\vec{M} = \frac{\pi \tau_o}{\rho_o} \left[\frac{\mu_o M_e}{r^3} \right] \omega_o \sin\left[\omega_o t\right] \vec{r} \int_o^{a_o} l_o^3 \, dl_o$$

Upon performing the integration and making the circular orbit substitution, equation (8.12), the magnetic moment becomes

$$\vec{M} = \frac{\pi a_o^4 \tau_o}{4\rho_o} \left[\frac{\mu_o M_e}{K} \right] \omega_o^3 \sin\left[\omega_o t\right] \vec{r} \tag{8.17}$$

The torque ($\vec{T} = \vec{M} \times \vec{B}$) on the conducting disc is found to be

$$T = \frac{\pi}{8} \left[\frac{\mu_o M_e}{K}\right]^2 \frac{\tau_o a_o^4 \omega_o^5}{\rho_o} \left[1 - \cos 2\omega_o t\right] (\vec{r} \times \vec{\xi}) \tag{8.18}$$

Equation (8.18) is similar to equation (8.13) except now the torque depends upon the fourth power of the radius instead of the third power as in the case for a circular wire loop. It also depends linearly on the thickness of the disc as would be expected.

If the lenticular satellite is composed of a wire mesh, it is possible to show that the total torque is due only to the contribution of the outside ring. A flat wire mesh as shown in Figure 8-4 is composed of many small conducting loops, each of which has an emf induced by the magnetic field.

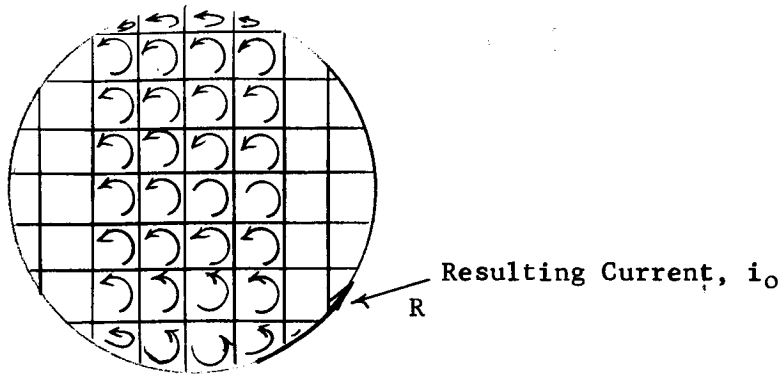

Figure 8-4

Eddy Current Loops in a Wire Mesh

The current in any one loop is completely cancelled by the currents in adjacent loops surrounding the given loop unless, of course, the loop happens to be next to the edge. In that case current will flow around the outside edge only. Thus, the torque on a wire mesh is the same as the torque on a wire loop that coincides with the perifery of the mesh.

8.3. RELATIVE MAGNITUDES OF EDDY CURRENT TORQUES

The lenticular balloon will be approximated by (1) a thin wire mesh and (2) a thin conducting copper disc. The torque on the wire mesh is given by equation (8.13) and the torque on the conducting disc is given by equation (8.18). The constant $\mu_o M_e/K$ appearing in both equations has a magnitude of

$$\frac{\mu_o M_e}{K} = 20.3 \ \frac{\text{volt sec}^3}{M^2} \qquad (8.19)$$

The emf induced into a loop is given by equation (8.8) with r^3 replaced by K/ω_o^2.

$$\mathcal{E} = 2\pi\left[\frac{\mu_o M_e}{K}\right] a_o^2 \omega_o^3 \sin\left[\omega_o t\right] \qquad (8.20)$$

The amplitude of equation (8.20) is shown in Figure 8-5. The emf is plotted versus orbital rate for different values of loop radius.

8.3.1. Torque on Wire Loop

The lenticular balloon will be made of a mesh material with wires that are 1 mil to 3.5 mils square cross section. To establish an upper limit, the larger value of 3.5 mils is assumed. This cross sectional area corresponds to that of 38 gauge wire for which the resistance per unit length, σ_o, is approximately 0.7 ohms per foot. Equation (8.13) may be written as

$$T = T_{ave}\ (1 - \cos 2\omega_o t) \qquad (8.21)$$

where: $$T_{ave} = \frac{\pi}{2}\left[\frac{\mu_o M_e}{K}\right]^2 \frac{a_o^3 \omega_o^5}{\sigma_o} \qquad (8.22)$$

A plot of equation (8.22) is shown in Figure 8-6 for various values of T_{ave}, a_o and ω_o for the 38 gauge wire described above. As can be seen from the graph, the torque on a single wire loop is completely negligible. The gravity gradient restoring torque per degree of deviation from the vertical is about 10^{-2} foot pounds.

8.3.2. Torque on a Thin Conducting Disc

Let the conducting material be copper of thickness 1 mil (.001 in), then τ_o = .001 inches and $\sigma_o = 1.72 \times 10^{-6}$ ohm-cm.

The torque on the disc is given by equation (8.18) which can be written as

$$T = T_{ave}\ (1 - \cos 2\omega_o t) \qquad (8.23)$$

where: $$T_{ave} = \frac{\pi}{8}\left[\frac{\mu_o M_e}{K}\right]^2 \frac{\tau_o a_o^4 \omega_o^5}{\rho_o} \qquad (8.24)$$

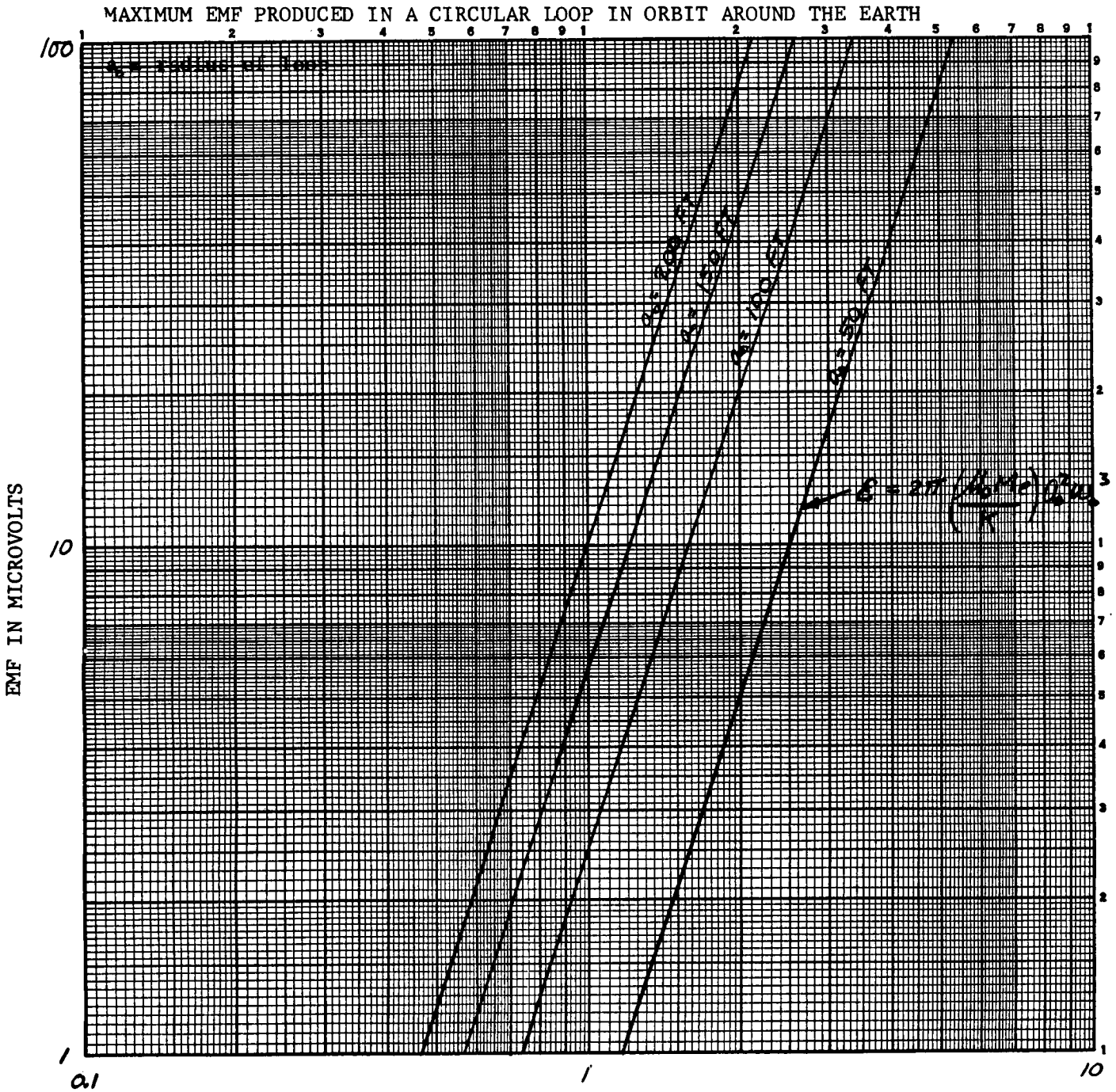
MAXIMUM EMF PRODUCED IN A CIRCULAR LOOP IN ORBIT AROUND THE EARTH
EMF IN MICROVOLTS
100
10
1
0.1
1
10
ORBITAL ANGULAR VELOCITY, ω_o, IN RAD./HR.

Figure 8-5

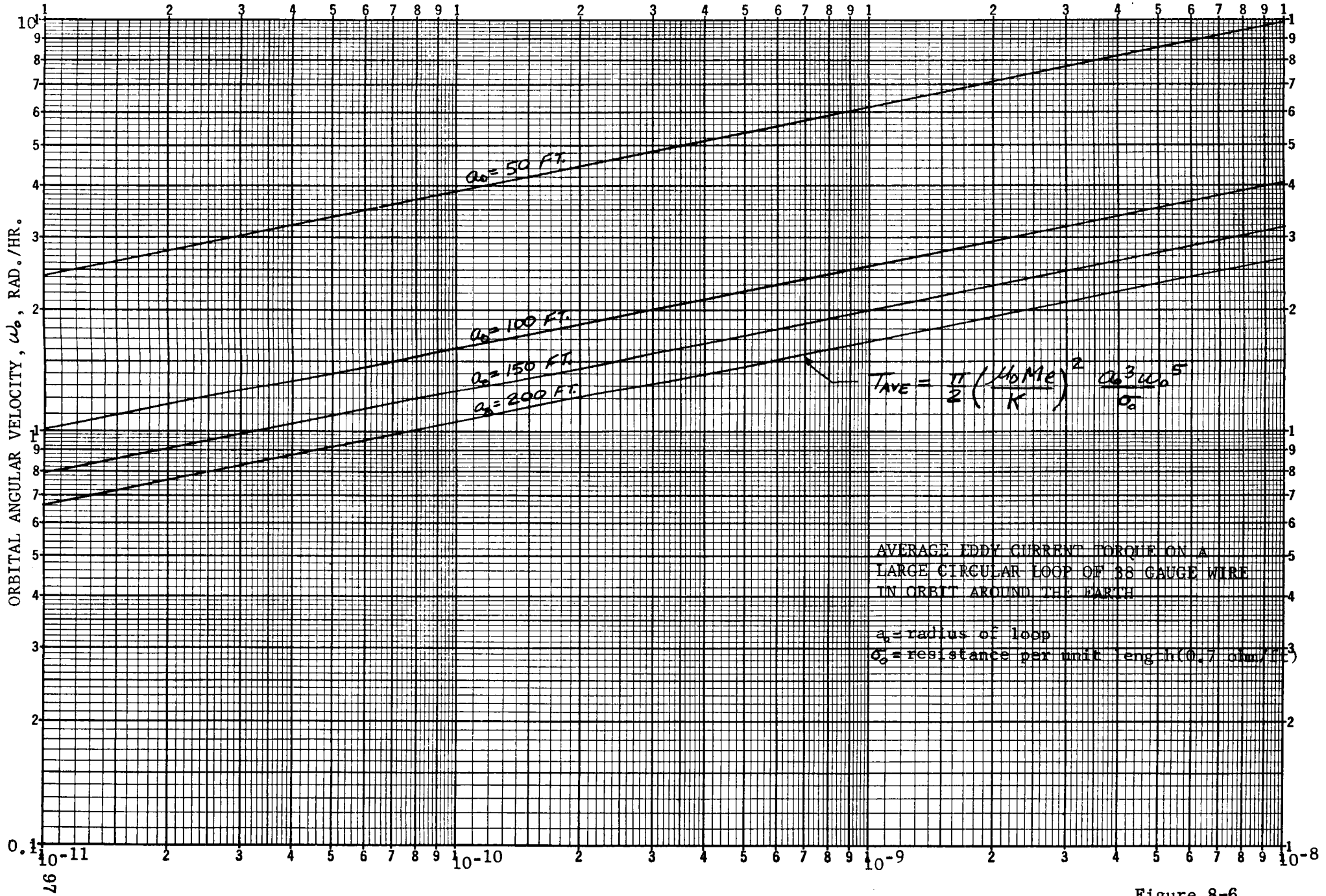
ORBITAL ANGULAR VELOCITY, ω_o, RAD./HR.
AVERAGE TORQUE - FOOT-POUNDS
a_o = 50 FT.
a_o = 100 FT.
a_o = 150 FT.
a_o = 200 FT.
$T_{AVE} = \frac{\pi}{2}\left(\frac{\mu_0 M_e}{K}\right)^2 \frac{a_o^3 \omega_o^5}{\sigma_o}$
AVERAGE EDDY CURRENT TORQUE ON A LARGE CIRCULAR LOOP OF 38 GAUGE WIRE IN ORBIT AROUND THE EARTH
a_o = radius of loop
σ_o = resistance per unit length (0.7 ohm/FT)

Figure 8-6

AVERAGE EDDY CURRENT TORQUE PER MIL THICKNESS OF A LARGE THIN COPPER DISC IN ORBIT AROUND THE EARTH.

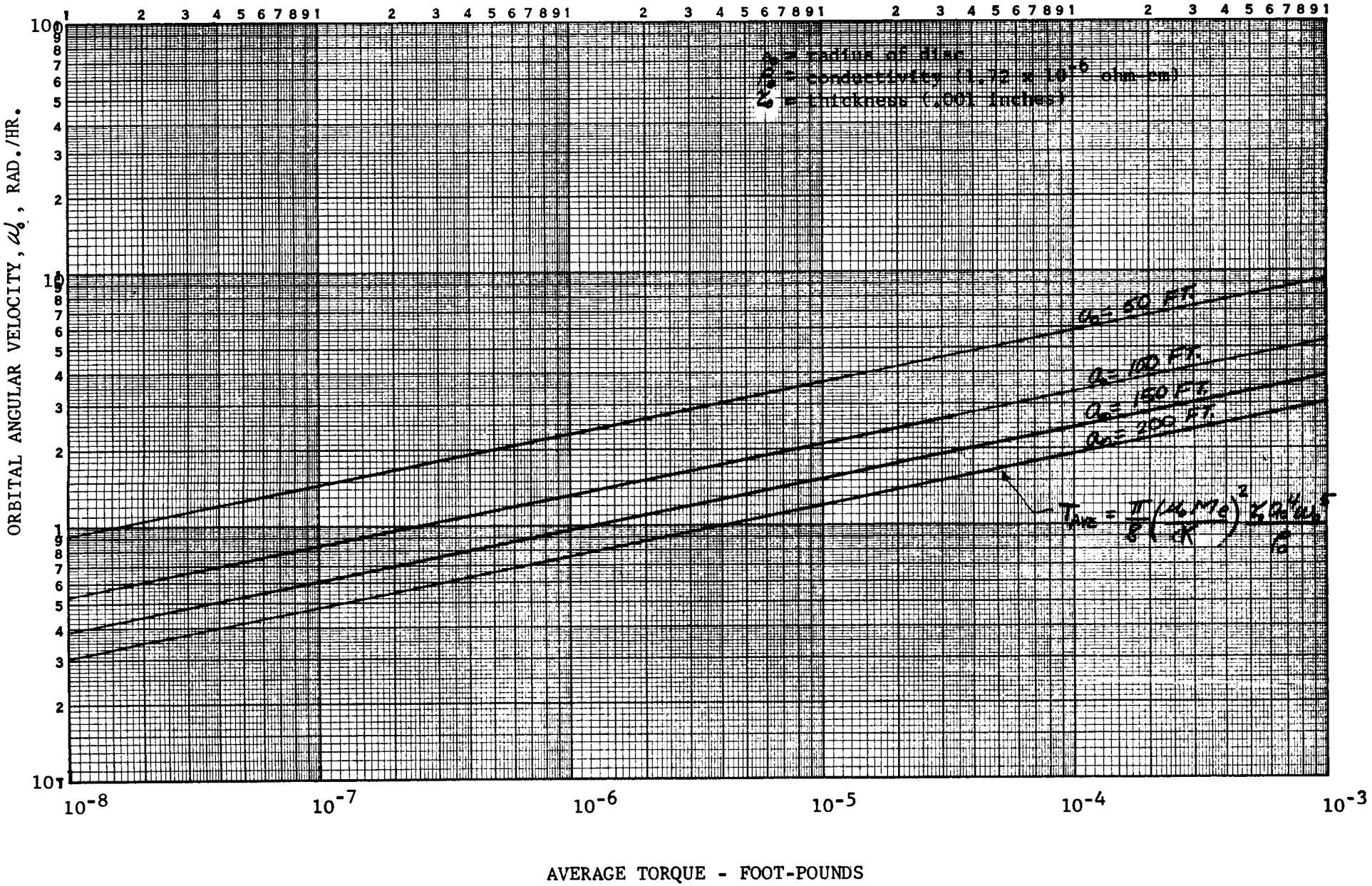

Figure 8-7

A plot of equation (8.24) is shown in Figure (8-7) for various values of T_{ave}, a_o and ω_o for the copper disc described above. This torque represents the maximum value that could be developed by any large surface of material in orbit around the earth.

8.4. EDDY CURRENT TORQUES ON GRAVITY GRADIENT RODS

A satellite moving in the magnetic field of the earth will experience induced eddy currents from the field. The eddy current loops produce a magnetic moment which then interacts with the magnetic field to produce a torque. We will consider the eddy current torques on the gravity gradient rods of a gravity gradient stabilized satellite. The satellite is assumed to be in steady state motion (pointing along local vertical) in a circular orbit over the magnetic poles.

The rod is in a circular orbit as shown in Figure (8-8), always pointing down along the local vertical.

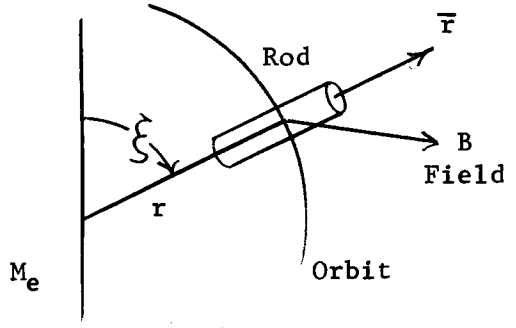

Figure 8-8)

Rod in Orbit Around a Magnetic Dipole

The rods are actually thin walled tubes. The eddy currents will be produced on the surface of the rod and travel in circular paths as shown in Figure 8-9.

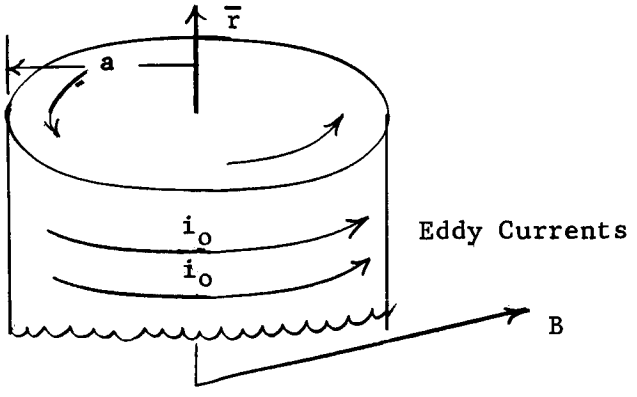

Figure 8-9)

Eddy Currents in Gravity-Gradient Rod

The flux density at the position of the rod is

$$\vec{B} = \mu_o \vec{H} \tag{8.25}$$

where: $\vec{H}$ is given by equation (4) and

$$\mu_o = 4\pi \times 10^{-7} \text{ Henry/meter}$$

$\vec{B}$ is assumed to have the same value at all points along the rod.

If we take a closed path of radius a_o on the surface of the rod, the flux through the enclosed area would be

$$\Phi = \int \vec{B} \cdot \vec{dS} = \pi a_o^2 \vec{B} \cdot \vec{r}$$

$$\Phi = \int \pi a_o^2 \frac{2 \mu_o M_e}{r^3} \cos \xi \tag{8.26}$$

In a circular orbit the geocentric radius is related to the angular velocity by the equation

$$\omega_o^2 = \frac{K}{r^3} \tag{8.27}$$

where: ω_o = orbital angular velocity
K = gravitational constant times mass of the earth

Also, the polar angle ξ is a function of time through the relation.

$$\xi = \omega_o t \tag{8.28}$$

The negative time rate of change of flux is the emf, namely

$$\mathcal{E} = 2\pi a_o^2 \left[\frac{\mu_o M_e}{K} \right] \omega_o^3 \sin\left[\omega_o t \right] \tag{8.29}$$

The current flowing around the rod is equal to the emf divided by the resistance of the rod along the path of the circular current. Total current in the rod is, therefore,

$$i_o = \frac{\mathcal{E} \tau_o' L}{2\pi a_o \rho_o} \tag{8.30}$$

where: τ_o' = wall thickness of tube
L = length of gravity rod
ρ_o = resistivity of the material (ohm-meter)

The total magnetic moment of the rod due to this current is

$$\vec{M} = \pi a_o^2 i_o \vec{r} \tag{8.31}$$

and the torque on the rod is

$$\vec{T} = \vec{M} \times \vec{B} \tag{8.32}$$

After combining all of the above equations we find the following result for the torque on a single gravity gradient rod.

$$\vec{T} = \frac{\pi \tau_o' L a_o^3}{2\rho_o} \left[\frac{\mu_o M_e}{K}\right]^2 \omega_o^5 (1 \cos 2\omega_o t) (\vec{r} \times \vec{\xi}) \tag{8.33}$$

The constant $\mu_o M_e/K$ appearing in equation (8.33) has a value of

$$\frac{\mu_o M_e}{K} = 20.3 \ \frac{\text{volt sec}^3}{M^2} \tag{8.34}$$

Magnitude of Eddy Current Torque

The gravity gradient rods have the following properties:

a_o (radius of rod) = .45 inches
τ_o' (wall thickness) = .005 inches
ρ_o (resistivity of copper) = 1.72×10^{-6} ohm-cm.

The eddy current torque, equation (8.33), is seen to be always positive with an average value of

$$T_{ave} = \frac{\pi \tau_o' L a_o^3}{2\rho_o} \left[\frac{\mu_o M_e}{K}\right]^2 \omega_o^5 \tag{8.35}$$

Upon conversion of units, the square of equation (8.35) becomes

$$\left[\frac{\mu_o M_e}{K}\right]^2 = 1.5 \times 10^{-11} \ \frac{\text{ohm}}{M^3} \frac{\text{hr}^5}{\text{ft}} \ \text{(ft-lbs)}$$

and combination of constants for the gravity rods produces the factor

$$\frac{\pi \tau_o' a_o^3}{2\rho_o} = 1.726 \times 10^{-2} \frac{M^3}{\text{ohm}}$$

Therefore, the average torque in terms of orbital rate and length of rod becomes

$$T_{ave} = 2.58 \times 10^{-13} \; L \; \omega_o^5 \qquad (8.36)$$

An inspection of the average torque reveals that the torque is very small and completely negligible in satellite dynamics. A plot of the average torque versus orbital rate for various rod lengths in shown in Figure 8-10.

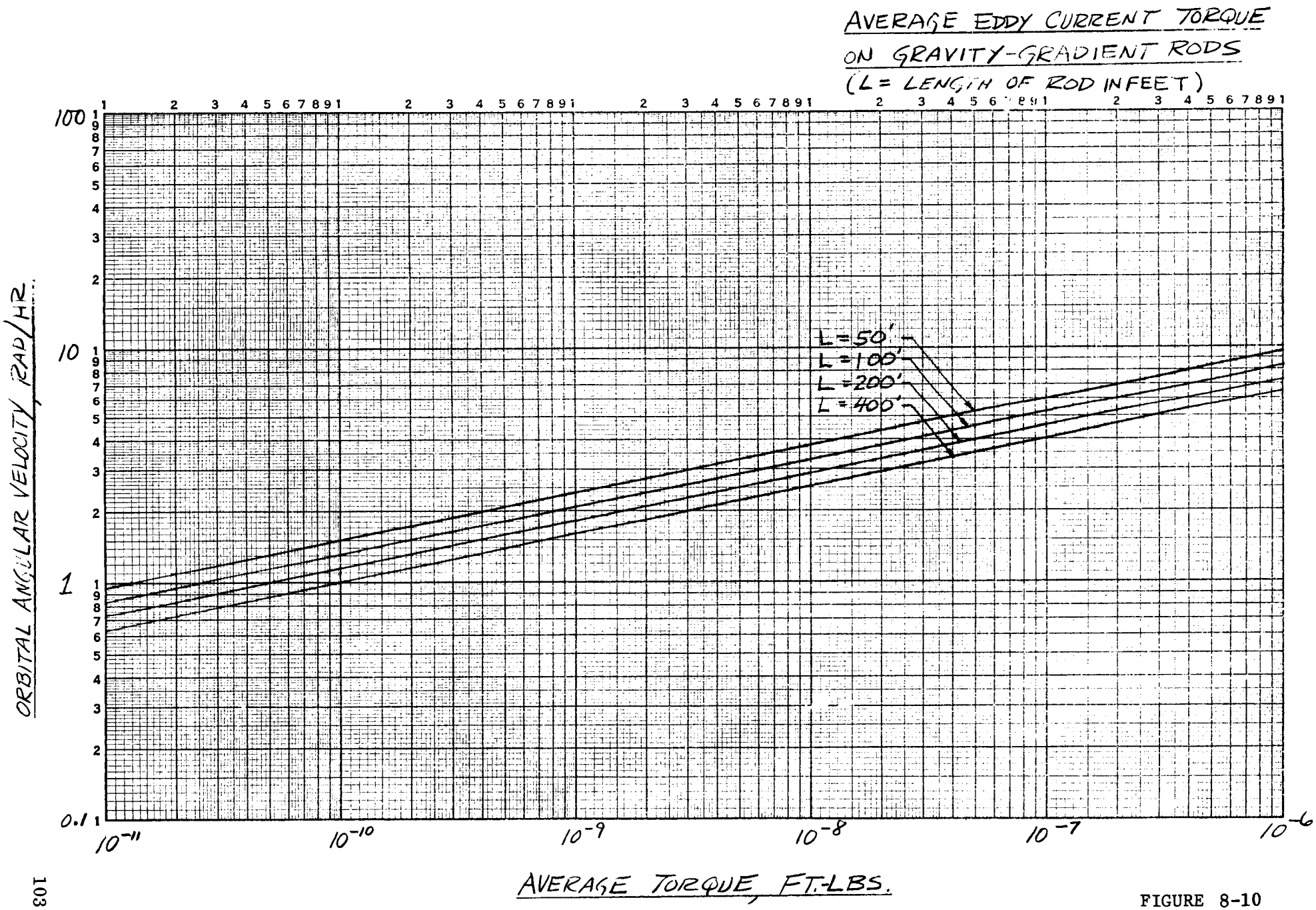
AVERAGE EDDY CURRENT TORQUE
ON GRAVITY-GRADIENT RODS
(L = LENGTH OF ROD IN FEET)
L=50'
L=100'
L=200'
L=400'
ORBITAL ANGULAR VELOCITY, RAD/HR
100
10
1
0.1
10^{-11}
10^{-10}
10^{-9}
10^{-8}
10^{-7}
10^{-6}
AVERAGE TORQUE, FT-LBS.

FIGURE 8-10

REFERENCES

1. General Electric Co., Passively Oriented Lenticular Satellite Study (letter proposal) 8 March 1963.

2. Pugh and Pugh "Principles of Electricity and Magnetism" p. 223, 224, and Problem 7-21 p. 239.

3. G. P. Harnwell "Principles of Electricity and Electromagnetism" p. 330-347.

4. W. Panofsky and M. Phillips "Classical Electricity and Magnetism", chapter 9.

5. R. Clayton "Passive Magnetic Damping of Communications Satellites", G. E. Technical Information Series No. 63SD268.

6. Levinson, Moris M., NCEP ANALYSIS AND SYNTHESIS MEMO NO. 131-098, "A Comparative Study of Magnetic Unloading Schemes for the OAO Vehicle", 24 March 1961.

DEFINITION OF SYMBOLS FOR APPENDICES I AND II

English Capital Letters

B = Magnetic Field Strength in Gauss

D = Operator Symbol - $\frac{d}{df}$

H = Magnetic Intensity in Oersted

I = Moment of Inertia in slug-ft^2

$I_B{}^o$ = Yaw Moment of Inertia of Satellite in Slug-ft^2

M = Magnetic Moment of Dipole in pole-cm

M_e = Earth's Magnetic Moment in pole-cm

Q = Internal Torques on Vehicle in lb-ft.

T = External Torques on Vehicle in lb-ft.

English Small Letters

a = Real Part of Quartic Root

b = Damping Constant in lb-ft-sec/rad

m = Average of Magnetic Field Variation

q = Imaginary Part of Quartic Root

r = Radius From Center of Earth in cm. or ft.

t = Time in sec.

Greek Capital Letters

Λ = Magnetic Colatitude in Deg. or Rad.

$\mathcal{M}$ = Mass of Earth, used only as $\mu\mathcal{M} = 1.41 \times 10^{16}$ ft^3/sec^2

Ξ = Magnetic Latitude in Deg. or Rad.

Greek Small Letters

γ = Angle Between Magnet and Magnetic Field in Deg. or Rad.

δ = Angle Between North Geographic Pole and North Magnetic Pole in Deg. or Rad.

ζ = Damping Fraction

θ = Pitch Angle in Deg. or Rad.

μ = Gravitational Constant Used Only As $= 1.41.10^{16}$ ft^3/sec^2

ν = Orbital Inclination in Deg. or Rad.

τ = Time Constant in Orbits or Hours

ϕ = Angle Between Local Vertical and Magnetic Field in Deg. or Rad.

ω_n = Undamped Natural Frequency of Satellite

ω_o = Orbital Frequency or rate in Rad/sec

Subscripts

B = Satellite

D = Damper

f = Final or steady state position

Dyn = Dynamic

Max = Maximum

Min = Minimum

To avoid excessive use of subscripts, words will be used as subscripts for variables which are transient or intermediate

I. PLANAR ANALYSIS

For simplicity, the magnetically anchored satellite can be assumed to have the Damper located at the center of the vehicle. Considering the earth as being located on the negative x axis, the coordinate system will be described by Figure I-1.

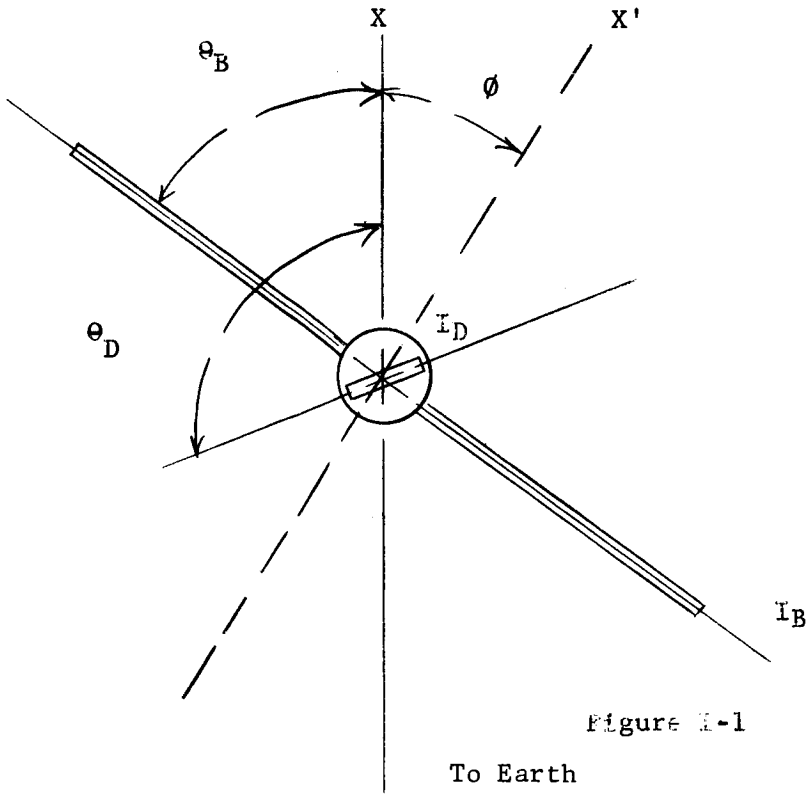

Figure I-1

where:

the x axis is the local vertical (positive away from the earth),

the x' axis is the direction of the magnetic field (positive away from the earth). as shown

θ_B = Angle between axis of least inertia of the satellite and x axis

θ_D = Angle between magnetic moment of the damper and the x axis

ϕ = Angle between the x axis and the x' axis

I_B = Pitch and Roll Inertia of Satellite in Slug-Ft^2

I_B^o = Yaw inertia of satellite in Slug-Ft^2

The analysis is planar and a magnetic polar orbit has been assumed. In addition the vehicle is assumed symmetrical with the satellite pitch inertia equal to its roll inertia.

Since only a planar analysis is being performed, cross coupling can be ignored and Euler's dynamical equations become

$$T_B - Q_B = I_B \ddot{\theta}_B \qquad \text{I-1}$$

$$T_D - Q_D = I_D \ddot{\theta}_D \qquad \text{I-2}$$

where T is the external torque, and Q the internal torque. The subscripts B refers to the satellite, and D the magnet.

Only one axis is being analysed and by Newton's Third Law.

$$Q_B = - Q_D \qquad \text{I-3}$$

The internal torque is the damping torque and is

$$Q_B = b\,(\dot{\theta}_B - \dot{\theta}_D) \qquad \text{I-4}$$

where b is the damping constant (ft-lb-sec). After Substitution, Equation I-1 and I-2 becomes

$$T_B - b(\dot{\theta}_B - \dot{\theta}_D) = I_B \ddot{\theta}_B \qquad \text{I-5}$$

$$T_D + b(\dot{\theta}_B - \dot{\theta}_D) = I_D \ddot{\theta}_D \qquad \text{I-6}$$

The only external torque experienced by the satellite is that due gravity gradient which is calculated from

$$T_B = -\frac{3\omega_o^2}{2} (I_B - I_B) \sin 2\theta_B \qquad \text{I-7}$$

where ω_o is orbital rate

The torque on the damper is predominately magnetic and is computed from

$$T_D = -M\,Ho \sin (\theta_D + \phi) \qquad \text{I-8}$$

where M is the magnetic moment of the satellite in pole-cm

H_o is the magnetic intensity in Oersted

with a permeability of one, the magnetic intensity equals the magnetic field B, in gauss, hence

$$T_D = - MB \operatorname{Sin} (\theta_D + \phi) \qquad \text{I-9}$$

Representing the earths magnetic field by a dipole, the magnetic intensity can be computed from

$$H = \frac{Me}{r^3}\sqrt{1 + 3\ \mathrm{Sin}^2\ \lambda} = B \qquad \text{I -10}$$

where

Me is the Earths magnetic moment in pole-cm

r is the radius from the magnet in cm

λ is the magnetic latitude

combining with Equation I-9

$$T_D = - M \frac{Me}{r^3}\sqrt{1 + 3\ \mathrm{Sin}^2\ \lambda}\ \mathrm{Sin}\ (\theta_D + \phi) \qquad \text{I -11}$$

To linearize the dynamical equations, it is necessary to define an average value of $\sqrt{1 + 3\ \mathrm{Sin}^2\ \lambda}$

An average value will be determined by the method suggested by M. Levinson in NCEP Memo 131-098. The average is

$$\bar{m} = \sqrt{\frac{1}{\Lambda_{max} - \Lambda_{min}} \int_{\Lambda_{min}}^{\Lambda_{max}} (3\ \cos^2 \Lambda + 1)\ d\Lambda} \qquad \text{I-12}$$

where Λ is the magnetic colatitude. Integrating

$$\bar{m} = \sqrt{\frac{1}{\Lambda_{max} - \Lambda_{min}} \left[\frac{5\Lambda}{2} + \frac{3}{4}\ \mathrm{Sin}\ 2\Lambda \right]_{\Lambda_{min}}^{\Lambda_{max}}} \qquad \text{I -13}$$

$$\Lambda_{max} = 90^\circ + (\nu + \delta) \qquad \text{I -14}$$

$$\Lambda_{min} = 90^\circ - (\nu + \delta)$$

where δ equals the angle between the north geographic pole and the north magnetic pole, and ν equals the orbital inclination

Representing the earth as a dipole, $\delta = 0$, and for a polar orbit, $\nu = 90^\circ$

Hence $\Lambda_{max} = 180^\circ = \pi$

$\Lambda_{min} = 0$

And

$$M = \sqrt{\frac{5}{2} + \frac{3}{4}(0)} = 1.58$$

Substituting into Equation I-11

$$T_D = -1.58 \; M \frac{Me}{r^3} \; \text{Sin} \; (\theta_D + \phi) \qquad \text{I-15}$$

As given, T_D would be in dyne-cm. It is necessary to convert from dyne-cm to lb-ft.

$$T_D = - \frac{1}{1.35581.10^7} \; \frac{\text{dyne-cm}}{\text{lb-ft}} \times 1.58 \; M \frac{Me}{r^3} \; \text{Sin}(\theta_D + \phi) \qquad \text{I-16}$$

$$T_D = - \; 1.165 \; .10^{-7} \; M \frac{Me}{r^3} \; \text{Sin} \; (\theta_D + \phi) \qquad \text{I-17}$$

The strength of the magnetic field is inversely proportional to the cube of the orbital period.

$$\omega_o^2 = \frac{\mu m}{r^3} \qquad \text{I-18}$$

where $\mu m = 1.41.10^{16}$ ft^3/sec^2 and r is in ft

With r in cm,

$$\mu m = 1.41.10^{16} \; (30.48 \text{ cm})^3/\text{sec}^2 = 3.993.10^{20} \text{ cm}^3/\text{sec}^2$$

And

$$\frac{1}{r^3} = \frac{\omega_o^2}{\mu m} \qquad \text{I-19}$$

Substituting into Equation I-17

$$T_D = - \; 1.165.10^{-7} \; \frac{\omega_o^2}{3.993.10^{20}} \; Me \; M \; \text{Sin} \; (\theta_D + \phi) \qquad \text{I-20}$$

Simplifying

$$T_D = -2.918.10^{-28} \; \omega_o^2 \; Me \; M \; \text{Sin} \; (\theta_D + \phi) \qquad \text{I-21}$$

The magnetic moment of the earth is

$$M_e = 8.064.10^{25} \text{ pole-cm} \quad \text{(Ref G.E. TIS 63SD268)}$$

Hence

$$T_D = -23.53.10^{-3}\omega_o^2 \text{ M Sin}(\theta_D + \phi) \qquad \text{I-22}$$

$$T_D = -.0235\omega_o^2 \text{ M Sin}(\theta_D + \phi) \qquad \text{I-23}$$

Combining Equations I-5, I-6, I-7, and I-23

$$I_B \ddot{\theta}_B + b(\dot{\theta}_B - \dot{\theta}_D) + \frac{3\omega_o^2}{2}(I_B - I_B^\circ) \text{ Sin } 2\theta_B = 0 \qquad \text{I-24}$$

$$I_D \ddot{\theta}_D - b(\dot{\theta}_B - \dot{\theta}_D) + .0235\omega_o^2 \text{ M Sin } (\theta_D + \phi) = 0 \qquad \text{I-25}$$

A new angle γ will be defined to be

$$\gamma = \theta_D + \phi \qquad \text{I-26}$$

Where γ is the angle between the magnetic moment of the magnet and the field. Then

$$\dot{\gamma} = \dot{\theta}_D + \dot{\phi} \qquad \text{I-27}$$

In a Polar orbit, the field makes two rotations for every single rotation of the satellite. Hence the average relative velocity between them is one orbital rate. With ϕ defined as shown

$$\dot{\gamma} = \dot{\theta}_D - \omega_o \qquad \text{I-28}$$

$$\ddot{\gamma} = \ddot{\theta}_D \qquad \text{I-29}$$

Substituting into equations I-24 and I-25

$$I_B \ddot{\theta}_B + b(\dot{\theta}_B - \dot{\gamma} - \omega_o) + \frac{3\omega_o^2}{2} (I_B - I_B^\circ) \text{ Sin } 2\theta_B = 0 \qquad \text{I-30}$$

$$I_D \ddot{\gamma} - b(\dot{\theta}_B - \dot{\gamma}\omega_o) + .0235\omega_o^2 \text{M Sin}\gamma = 0 \qquad \text{I-31}$$

To linearize these equations, it is necessary to find the final angle in steady state. In steady state, the vehicle and damper are in static equilibrium and

$$\dot{\theta}_B = \dot{\gamma} = \ddot{\theta}_B = \ddot{\gamma} = 0$$

Hence equations I-30 and I-31 become

$$b\omega_o = \frac{3\omega_o^2}{2} (I_B - I_B^\circ) \text{ Sin } 2\theta_{Bf} \qquad \text{I-32}$$

$$-b\omega_o = .0235\omega_o^2 \text{ M Sin}\gamma_f \qquad \text{I-33}$$

Where the subscript f means final position.

Considering θ_B and γ to be small variations about θ_{Bf} and γ_f respectively

$$\text{Sin } 2\theta_B \text{ can be replaced by Sin } 2(\theta_B + \theta_{Bf}) \qquad \text{I-34}$$

$$\text{Sin } \gamma \text{ can be replaced by Sin } (\gamma + \gamma_f) \qquad \text{I-35}$$

Expanding

$$\text{Sin } 2(\theta_B + \theta_{Bf}) = \text{Sin } 2\theta_B \text{ Cos } 2\theta_{Bf} + \text{Cos } 2\theta_B \text{ Sin } 2\theta_{Bf} \qquad \text{I-36}$$

$$\text{Sin } (\gamma + \gamma_f) = \text{Sin } \gamma \text{ Cos } \gamma_f + \text{Cos } \gamma \text{ Sin } \gamma_f \qquad \text{I-37}$$

For θ_B and γ small

$$\text{Sin } 2(\theta_B + \theta_{Bf}) = 2\theta_B \text{ Cos } 2\theta_{Bf} + \text{Sin } 2\theta_{Bf} \qquad \text{I-38}$$

$$\text{Sin } (\gamma + \gamma_f) = \gamma \text{ Cos } \gamma_f + \text{Sin } \gamma_f \qquad \text{I-39}$$

Substituting into equations I-30, and I-31,

$$I_B \ddot{\theta}_B + b(\dot{\theta}_B - \dot{\gamma}) + 3\omega_o^2(I_B - I_B^\circ)\theta_B \text{ Cos } 2\theta_{Bf} + \frac{3\omega_o^2}{2}(I_B - I_B^\circ) \text{ Sin } 2\theta_{Bf} - b\omega_o = 0 \qquad \text{I-40}$$

$$I_D \ddot{\gamma} - b(\dot{\theta}_B - \dot{\gamma}) + .0235\omega_o^2 \text{ M } \gamma \text{ Cos } \gamma_f + .0235\omega_o^2 \text{ M Sin } \gamma_f + b\omega_o = 0 \qquad \text{I-41}$$

In both of the above equations, the last two terms add to zero by equations I-32, and I-33,

Hence

$$I_B \ddot{\theta}_B + b(\dot{\theta}_B - \dot{\gamma}) + 3\omega_o^2 (I_B - I_B^\circ)\theta_B \text{ Cos } 2\theta_{Bf} = 0 \qquad \text{I-42}$$

$$I_D \ddot{\gamma} - b(\dot{\theta}_B - \dot{\gamma}) + .0235\omega_o^2 \text{ M } \gamma \text{ Cos } \gamma_f = 0 \qquad \text{I-43}$$

These equations can be non-dimensionalized if a change of time scale is performed. Let

$$\tau = \omega_o t \qquad \text{I-44}$$

Then

$$\frac{d}{d\tau} = \frac{d}{dt}\frac{dt}{d\tau} = \frac{1}{\omega_o}\frac{d}{dt} \qquad \text{I-45}$$

$$\frac{d^2}{d\tau^2} = \frac{1}{\omega_o^2}\frac{d}{dt^2} \qquad \text{I-46}$$

Using the ^{oo} notation to mean with respect to τ

$$\omega_o^2 I_B \overset{oo}{\theta}_B + \omega_o b(\overset{o}{\theta}_B - \overset{o}{\gamma}) + 3\omega_o^2(I_B - I_B^o)\theta_B \cos 2\theta_{Bf} = 0 \qquad \text{I-47}$$

$$\omega_o^2 I_D \overset{oo}{\gamma} - b\omega_o(\overset{o}{\theta}_B - \overset{o}{\gamma}) + .0235\omega_o^2 M\gamma \cos\gamma_f = 0 \qquad \text{I-48}$$

Simplifying

$$\overset{oo}{\theta}_B + \frac{b}{I_B\omega_o}(\overset{o}{\theta}_B - \overset{o}{\gamma}) + 3\left(1 - \frac{I_B^o}{I_B}\right)\theta_B \cos 2\theta_{Bf} = 0 \qquad \text{I-49}$$

$$\overset{oo}{\gamma} - \frac{b}{I_D\omega_o}(\overset{o}{\theta}_B - \overset{o}{\gamma}) + .0235\frac{M}{I_D}\gamma \cos\gamma_f = 0 \qquad \text{I-50}$$

In operator notation

$$\left[D^2 + \frac{b}{I_B\omega_o} D + 3\left(1 - \frac{I_B^o}{I_B}\right)\cos 2\theta_{Bf}\right]\theta_B \left[-\frac{b}{I_B\omega_o} D\right]\gamma = 0 \qquad \text{I-51}$$

$$\left[-\frac{b}{I_D\omega_o} D\right]\theta_B + \left[D^2 + \frac{b}{I_D\omega_o} D + .0235\frac{M}{I_D}\cos\gamma_f\right]\gamma = 0 \qquad \text{I-52}$$

These equations are linear and homogeneous, and for a solution, the determinant of the coefficients of the variables must be zero (Cramer's rule)

Hence

$$\begin{vmatrix} \left[D^2 + \frac{b}{I_B\omega_o} D + 3\left(1 - \frac{I_B^o}{I_B}\right)\cos 2\theta_{Bf}\right] & \left[-\frac{b\,D}{I_B\omega_o}\right] \\ \left[-\frac{b\,D}{I_D\omega_o}\right] & \left[D^2 + \frac{b}{I_D\omega_o} + .0235\frac{M}{I_D}\cos\gamma_f\right] \end{vmatrix} = 0 \qquad \text{I-53}$$

$$\begin{aligned} & D^4 \\ & + D^3\left[\frac{b}{I_B\omega_o} + \frac{b}{I_D\omega_o}\right] \\ & + D^2\left[3\left(1 - \frac{I_B^o}{I_B}\right)\cos 2\theta_{Bf} + \frac{b^2}{I_B I_D\omega_o^2} - \frac{b^2}{I_B I_D\omega_o^2} + .0235\frac{M}{I_D}\cos\gamma_f\right] \\ & + D\left[\frac{b}{I_B\omega_o}\left(.0235\frac{M}{I_D}\cos\gamma_f\right) + \frac{3b}{I_D\omega_o}\left(1 - \frac{I_B^o}{I_B}\right)\cos 2\theta_{Bf}\right] \\ & + \left[3\left(1 - \frac{I_B}{I_B}\right)\cos 2\theta_{Bf}\ .0235\frac{M}{I_D}\cos\gamma_f\right] \end{aligned} \qquad \text{I-54}$$

Which can be reduced to four non-dimensional parameters

$$\frac{b}{I_B \omega_o}, \quad \frac{M}{I_B}, \quad \frac{I_B}{I_D}, \quad \frac{I_B^\circ}{I_B}$$

$$D^4$$

$$+ D^3\left[\frac{b}{I_B\omega_o}\left(1 + \frac{I_B^\circ}{I_D}\right)\right]$$

$$+D^2\left[3\left(1 - \frac{I_B^\circ}{I_B}\right)\cos 2\theta_{Bf} + .0235\left(\frac{M}{I_B}\right)\left(\frac{I_B}{I_D}\right)\cos\gamma_f\right]$$

$$+ D\left[\frac{b}{I_B\omega_o}\left(\frac{I_B}{I_D}\right)\left\{.0235\,\frac{M}{I_B}\cos\gamma_f + 3\left(1 - \frac{I_B^\circ}{I_B}\right)\cos 2\theta_{Bf}\right\}\right]$$

$$+ \left[3\left(1 - \frac{I_B^\circ}{I_B}\right)\cos 2\theta_{Bf}\right]\left[.0235\left(\frac{M}{I_B}\right)\left(\frac{I_B}{I_D}\right)\cos\gamma_f\right] \qquad \text{I-55}$$

Where

$$\cos 2\theta_{Bf} = \cos\left[\text{Arc Sin}\left\{\frac{2b}{3I_B\omega_o}\,\frac{1}{\left(1 - \frac{I_B^\circ}{I_B}\right)}\right\}\right] \qquad \text{I-56}$$

$$\cos\gamma = \cos\left[\text{Arc Sin}\left\{-\frac{b}{I_B\omega_o}\left(\frac{I_B}{M}\right)\frac{1}{.0235}\right\}\right] \qquad \text{I-57}$$

Solution of equation I-55 will yield the damped natural frequency and decay times of the system as a function of ω_o. The roots will be of the form

$$a \pm qi \qquad \text{I-58}$$

Where

$$a = \zeta\omega_n/\omega_o \qquad \text{I-59}$$

$$q = \left[\omega_n/\omega_o\right]\sqrt{1 - \zeta^2} \qquad \text{I-60}$$

The time constant is

$$\frac{1}{\zeta\omega_n} = \frac{1}{a\omega_o} \qquad \text{I-61}$$

In terms of orbits

$$\text{Time Constant} = \frac{1}{a\,\frac{2\pi}{\tau_{orbit}}} = \frac{\frac{1}{a}}{2\pi}\,\tau_{orbit} \qquad \text{I-62}$$

B. Steady State Analysis

The equations describing steady state are equation I-32 and I-33

$$b\omega_o = \frac{3\omega_o^2}{2} (I_B - I_B^\circ) \sin 2\theta_{Bf} \qquad \text{I-32}$$

$$- b\omega_o = .0235\, \omega_o^2\, M \sin \gamma_f \qquad \text{I-33}$$

These can be rearranged to

$$\sin 2\theta_{Bf} = \frac{2b}{3\omega_o(I_B - I_B^\circ)} = \frac{2b}{3I_B\omega_o}\left(\frac{1}{(1 - I_B^\circ/I_B)}\right) \qquad \text{II-1}$$

$$\sin \gamma_f = \frac{-b}{.0235\omega_o M} = -\frac{b}{I_B\omega_o}\left(\frac{I_B}{M}\right)\frac{1}{.0235} \qquad \text{II-2}$$

Since the yaw position of the vehicle is irrelevant, θ_{Bf} may be considered an error. The position of the magnet is totally irrelevant, and γ_f is merely an offset. However for reasons of stability the value of γ_f should not be too large. "Large" will not be defined here.

Considering θ_{Bf} as an error, it should be kept small, hence

$$2\theta_{Bf} = \frac{2b}{3I_B\omega_o}\,\frac{1}{1-I_B^\circ/I_B} \qquad \text{II-3}$$

$$\theta_{Bf} = \frac{1}{3}\left(\frac{b}{I_B\omega_o}\right)\frac{1}{(1-I_B^\circ/I_B)} \qquad \text{II-4}$$

Since damping must be kept small, the natural frequency of the satellite is unchanged by the damping. Hence dividing the gravity gradient torque by the inertia

$$\omega_n = \omega_o\sqrt{3\,(1 - I_B^\circ/I_B)} \qquad \text{II-5}$$

The magnetic disturbing torque occurs at a frequency of $2\omega_o$ and, with light damping the dynamic amplification is

$$\frac{\theta_{Bf}}{\theta_{Bf}}_{dyn} = \frac{1}{\sqrt{\left[1 - (\omega_f/\omega_n)^2\right]^2}} = \frac{1}{\left|1 - \left(\frac{\omega_f}{\omega_n}\right)^2\right|} \qquad \text{II-6}$$

$$\frac{\theta_{Bf\ dyn}}{\theta_{Bf}} = \frac{1}{\left|1 - \left(\frac{2\omega_o}{\omega_o\ 3(1-I_B^\circ/I_B)}\right)^2\right|} \qquad \text{II-7}$$

which reduces to

$$\frac{\theta_{Bf\ dyn}}{\theta_{Bf}} = \frac{1}{\left|\frac{3(1-I_B^\circ/I_B)-4}{3(1-I_B^\circ/I_B)}\right|} = \frac{1}{\left|\frac{-1-3\ I_B^\circ/I_B}{3(1\ -\ I_B/I_B)}\right|} \qquad \text{II-8}$$

$$= \frac{3(1\ -\ I_B^\circ\ /I_B)}{1+3\ I_B^\circ/I_B} \qquad \text{II-9}$$

The maximum error occurs when the static error and the dynamic error add

$$\theta_{Bfmax} = \theta_{Bf}\ (1 + \frac{\theta_{Bf\ dyn}}{\theta_{Bf}}) \qquad \text{II-10}$$

$$= \theta_{Bf} \left(\frac{1 + 3\ I_B^\circ\ /I_B + 3\ -3\ I_B^\circ/I_B}{1 + 3\ I_B^\circ/I_B}\right) \qquad \text{II-11}$$

$$= \theta_{Bf} \left(\frac{4}{1 + 3\ I_B^\circ/I_B}\right) \qquad \text{II-12}$$

Finally

$$\theta_{Bfmax} = \frac{4}{3}\left(\frac{b}{I_B\,\omega_o}\right) \frac{1}{(1-I_B^\circ/I_B)(1 + 3\ I_B^\circ/I_B)} \qquad \text{II-13}$$

This equation is plotted in Figure 4-2

Considering γ_f as an offset, it will not be considered small. The natural frequency of the magnet is approximately

$$\omega_n = \omega_o \sqrt{\frac{.0235\ M}{I_D}} \qquad \text{II-14}$$

For a magnetic moment of 2000 pole cm, and a damper inertia of .01 slug-ft^2

$$\omega_n = \omega_o \sqrt{\frac{2.35.10^{-2}\ \ .2\ .10^3}{1.10^{-2}}} = 68.6\,\omega_o \qquad \text{II-15}$$

Considering the magnet to be critically damped

$$\frac{\gamma_{f\,dyn}}{\gamma_f} = \frac{1}{\sqrt{(2\omega_f/\omega_n)^2 + \left[1-\omega_f/\omega_n)^2\right]^2}} \qquad \text{II-16}$$

The disturbance torque on the magnet is also $2\omega_o$

$$\frac{\gamma_{f\ dyn}}{\gamma_f} = \frac{1}{\sqrt{\left(\frac{2 \times 2\omega_o}{68.6\omega_o}\right)^2 \left[1+\left(\frac{2\omega_o}{68.6\,\omega_o}\right)^2\right]^2}} \qquad \text{II-17}$$

$$\frac{\gamma_{f\ dyn}}{\gamma_f} = \frac{1}{\sqrt{.0034 + 1}} = 1 \qquad \text{II-18}$$

Hence $\gamma_{f\ dyn} = \gamma_f$ and

$$\gamma_{fmax} = 2\,\gamma_f = 2 \text{ Arc Sin } \left\{ - \frac{b}{I_B \omega_o} \left(\frac{I_B}{M}\right) \frac{1}{.0235} \right\} \qquad \text{II-19}$$

And $$\text{Sin } \frac{\gamma}{2}_{fmax} = - \frac{b}{I_B \omega_o} \left(\frac{I_B}{M} \right) \frac{1}{.0235} \qquad \text{II-20}$$

In connection with the use of this graph it should be noted that the constant .0235 is based on an average field strength. For an overall vehicle performance, this average is adequate. However, to prevent the magnet from deviating too far from the magnetic field, it is desirable to consider the weakest field. The constant then becomes

$$\frac{.0235}{1.58} \times 1 = .0149$$

Hence

$$\text{Sin } \frac{\gamma}{2}_{f_{max}} = - \frac{b}{I_B \omega_o} \left(\frac{I_B}{M} \right) \frac{1}{.0149} \qquad \text{II-21}$$

Rearranging

$$\frac{M}{I_B} = - \frac{b}{I_B \omega_o} \left(\frac{1}{.0149} \right) \frac{1}{\text{Sin } \frac{\gamma_{fmax}}{2}} \qquad \text{II-22}$$

This is the equation plotted in Figure 4-3

DEFINITION OF SYMBOLS FOR APPENDIX III

The symbols are as defined in Nomenclature at the front of the report, with the following exceptions -

a_W = wire spacing from center to center on mesh

$\overline{D}$ = vector to the center of the lens shape from the center of the spherical surface

$\overline{F}$ = force vector with appropriate subscripts

$J_1, J_2, ..J_7$ = constants in terms of ϕ

$\overline{L}$ = Torque vector with appropriate subscripts

m_W = Number of summation terms to be taken to find the total case uv torques

N_W = number of case uv longitude wires grouped together as identical to find the summation of the wire torques.

t_1 = thickness of the wire

$\overline{V}_L$ = torque lever arm for both the offset and the geometry of the vehicle.

ϕ' = latitude angle of an incremental surface area of the wires

$\Delta\phi'$ = change in ϕ' for consecutive longitude wires

ψ_1 = value of ψ (see Nomenclature) along the edge of the shadow line

$\Delta\psi$ = change in ψ (see Nomenclature) for consecutive latitude wires

Subscripts

a = indicates latitude wires

b = indicates longitude wires

T = indicates summation of all similar wire torques

u = used when $\theta > \phi'$ for longitude wires and $\psi < \psi_1$

uv = used for total of u and v quantities - Sun can see inside and outside of conical longitude wires

APPENDIX III

SOLAR TORQUE ON RADIAL SIDES

To the present the surfaces illuminated have been considered as parallel to the surfaces of two spherical segments. With a square cross sectioned wire mesh, this is half of the illuminated surfaces. We now consider the radial areas. The sun can see at most two surfaces of a square cross sectioned wire. Consider the wires as two types, longitudinal, that is, going around the configuration's axis of symmetry, and latitude wires, that is, arcs of circles all of which pass through the axis of symmetry. The planes of these arcs all contain the axis of symmetry.

These two wire types each have two cases. The front and back surfaces of the complete configuration each present a different geometry so each is considered. Let the subscripts "a" be on terms concerning the latitude arcs and "b" be on terms concerning the longitude circles for the surfaces closer to the sun. The respective subscripted quantities primed are the respective quantities for the back surfaces farther from the sun. Shadowing is neglected but may be added by a proportional multiplier approximation.

Latitude Surfaces Closest to Sun

Figure III-1 shows the area in the $\bar{i}\ \bar{j}\ \bar{k}$ coordinate system.

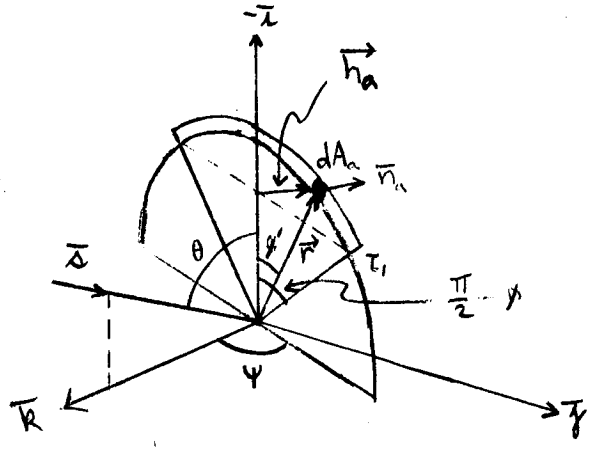

Figure III-1

The vectors in Figure III-1 are more easily seen in Figure III-2 where $\vec{x}$ measures from the geometric center of the lens. From this figure,

$$\vec{r} = \vec{D} + \vec{x} + \vec{V}_L$$

or

$$\vec{V}_L = \vec{r} - \vec{D} - \vec{x}$$

Now we let

$$\vec{r} - \vec{D} = \vec{h}$$

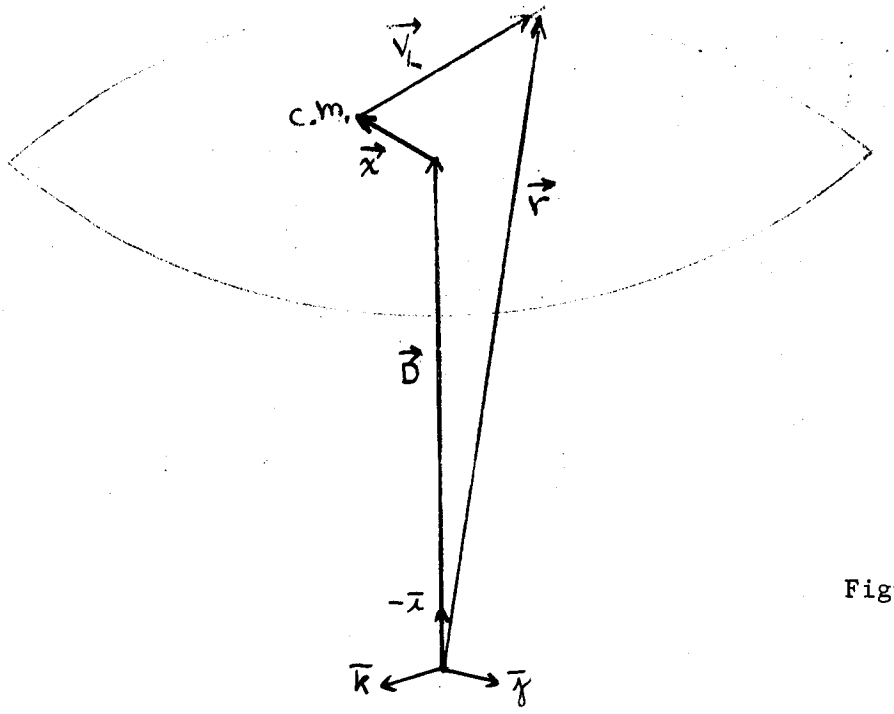

Figure III-2

The vectors $\bar{n}_a$, $\bar{s}$, and $\vec{h}_a$ are then

$$\bar{n}_a = \begin{bmatrix} 0 \\ \cos\psi \\ -\sin\psi \end{bmatrix}, \quad \bar{s} = \begin{bmatrix} \cos\theta \\ 0 \\ -\sin\theta \end{bmatrix}, \quad \vec{h}_a = r \begin{bmatrix} (\sin\phi - \cos\phi') \\ \sin\phi' \sin\psi \\ \sin\phi' \cos\psi \end{bmatrix} \qquad \text{(III-1)}$$

The offset vector (not illustrated in Figure III-1) is,

$$x = \begin{bmatrix} x_o \\ y_L \\ z_L \end{bmatrix} \qquad \text{(III-2)}$$

The incremental solar force on a differential area dA is, as explained previously,

$$\vec{dF} = P_o dA \left[\bar{s}(\bar{s}\cdot\bar{n})(1-\rho_s) + \frac{2}{3}\rho_d \bar{n}(\bar{s}\cdot\bar{n}) + 2\rho_s \bar{n}(\bar{s}\cdot\bar{n})^2 \right] \qquad \text{(III-3)}$$

and the torque about the c.m. of the balloon is

$$\vec{L} = \int \vec{V}_L \times \vec{dF} = \int \vec{h} \times \vec{hF} - \vec{x} \times \int \vec{dF} \qquad \text{(III-4)}$$

where $\vec{h}$ may be considered as the vector from the geometric center of the complete balloon to a dA.

From Figure III-1,

$$dA_a = r\,\tau_1\,d\phi' \tag{III-5}$$

$$\vec{s}\cdot\vec{n}_a = \sin\theta\,\sin\psi \tag{III-6}$$

Then

$$\vec{dF}_a = P_o r\,\tau_1\,d\phi' \begin{bmatrix} (1-\rho_s)\sin\theta\cos\theta\sin\psi \\ \qquad + \frac{2}{3}\rho_d\sin\theta\sin\psi\cos\psi + 2\rho_s\sin^2\theta\sin^2\psi\cos\psi \\ -(1-\rho_s)\sin^2\theta\sin\psi - \frac{2}{3}\rho_d\sin\theta\sin^2\psi - 2\rho_s\sin^2\theta\sin^3\psi \end{bmatrix} \tag{III-7}$$

Then the torque integrated over this one wire arc is, from Equation (III-4),

$$\vec{L}_a = \int_{-\left(\frac{\pi}{2}-\phi\right)}^{\left(\frac{\pi}{2}-\phi\right)} (\vec{h}_a - \vec{x}) \times \vec{dF}_a = \vec{L}_{ha} - \vec{L}_{xa} \tag{III-8}$$

where $$\vec{L}_{ha} = \int_{-\left(\frac{\pi}{2}-\phi\right)}^{\left(\frac{\pi}{2}-\phi\right)} \vec{h}_a \times \vec{dF}_a \tag{III-9}$$

and $$\vec{L}_{xa} = \vec{x} \times \int_{-\left(\frac{\pi}{2}-\phi\right)}^{\left(\frac{\pi}{2}-\phi\right)} \vec{dF}_a = \vec{x} \times \vec{F}_a \tag{III-10}$$

Breaking $\vec{L}_{ha}$ into components gives,

$$L_{ha_1} = \int_{-\left(\frac{\pi}{2}-\phi\right)}^{\left(\frac{\pi}{2}-\phi\right)} P_o r^2\,\tau_1 \left\{ \sin\phi'\,\sin\psi\left[-(1-\rho_s)\sin^2\theta\sin\psi - \frac{2}{3}\rho_d\sin\theta\sin^2\psi - 2\rho_s\sin^2\theta\sin^3\psi\right] \right.$$

$$\left. -\sin\phi'\cos\psi\left[\frac{2}{3}\rho_d\sin\theta\sin\psi\cos\psi + 2\rho_s\sin^2\theta\sin^2\psi\cos\psi\right]\right\} d\phi' = 0$$

$$L_{ha_1} = 0 \qquad L_{ha_1 T} = 0 \tag{III-11}$$

since all terms are odd functions of ϕ'

$$dL_{ha_2} = P_o r^2 \tau_1 \left\{ \sin\phi' \cos\psi \left[(1-\rho_s)\sin\theta\cos\theta\sin\psi \right] + (\sin\phi - \cos\phi') \left[(1-\rho_s)\sin^2\theta\sin\psi + \frac{2}{3}\rho_d \sin\theta \sin^2\psi + 2\rho_s \sin^2\theta \sin^3\psi \right] \right\} d\phi'$$

Integrating from $\phi' = -(\frac{\pi}{2} - \phi)$ to $\phi' = (\frac{\pi}{2} - \phi)$ gives,

$$L_{ha_2} = P_o r^2 \tau_1 \left[(1-\rho_s)\sin^2\theta\sin\psi + \frac{2}{3}\rho_d \sin\theta\sin^2\psi + 2\rho_s \sin^2\theta\sin^3\psi \right] \cdot \left[\sin\phi \int_{-(\frac{\pi}{2}-\phi)}^{(\frac{\pi}{2}-\phi)} d\phi' - \int_{-(\frac{\pi}{2}-\phi)}^{(\frac{\pi}{2}-\phi)} \cos\phi' \, d\phi' \right]$$

$$L_{ha_2} = P_o r^2 \tau_1 \left[(1-\rho_s)\sin^2\theta\sin\psi + \frac{2}{3}\rho_d \sin\theta\sin^2\psi + 2\rho_s \sin^2\theta\sin^3\psi \right] \cdot \left[2(\tfrac{\pi}{2} - \phi)\sin\phi - 2\cos\phi \right] \qquad \text{(III-12)}$$

The summation of each wire's torque may be approximated by an integral by solving the trapezoidal rule for the summation,

$$\sum_{i=o}^{n} y_i \doteq \frac{1}{\Delta x} \int_a^b y \, dx + \frac{y_o + y_n}{2} \; * \qquad \text{(III-13)}$$

Let $\Delta\psi$ be the change in ψ for adjacent wire centers. Then if a_w is the distance from the centers of adjacent wires, we assume this is the spacing at the periphery of the balloon.

We have

$$\Delta\psi = \frac{a_w}{r\cos\phi} \qquad \text{(III-14)}$$

Integrating (III-12) via (III-13) from $\psi = 0$ to $\psi = \pi$ and substituting (III-14) gives,

$$L_{ha_{2T}} = 2P_o r^2 \tau_1 \cdot \frac{r\cos\phi}{a_w} \left[(\tfrac{\pi}{2} - \phi)\sin\phi - \cos\phi \right] \cdot \sin\theta \left[2(1-\rho_s)\sin\theta + \frac{\pi}{3}\rho_d + \frac{8}{3}\rho_s \sin\theta \right]$$

$$L_{ha_{2T}} = 2P_o r^3 \frac{\tau_1}{a_w} \sin\theta\cos\phi \left[(\tfrac{\pi}{2} - \phi)\sin\phi - \cos\phi \right] \cdot \left[(2 + \frac{2}{3}\rho_s)\sin\theta + \frac{\pi}{3}\rho_d \right] \qquad \text{(III-15)}$$

This is the total torque second component due to all the latitude arcs closer to the sun. The first component was found to be zero for each wire in Equation (III-11), The third component is,

* This notation is used only in this one equation and has no other significance.

$$L_{ha_3} = P_o r^2 \tau_1 \int_{\left(-\frac{\pi}{2}+\phi\right)}^{\left(\frac{\pi}{2}-\phi\right)} \left\{(\sin\phi - \cos\phi')\left[\frac{2}{3}\rho_d \sin\theta \sin\psi \cos\psi + 2\rho_s \sin^2\theta \sin^2\psi \cos\psi\right] - \right.$$

$$\left. - \sin\phi' \sin\psi\left[(1-\rho_s)\sin\theta\cos\theta\sin\psi\right]\right\} d\phi'$$

$$L_{ha_3} = 2 P_o r^2 \tau_1 \left[\left(\frac{\pi}{2}-\phi\right)\sin\phi - \cos\phi\right] \cdot \left[\frac{2}{3}\rho_d \sin\theta \sin\psi\cos\psi + 2\rho_s \sin^2\theta \sin^2\psi\cos\psi\right] \quad \text{(III-16)}$$

This component is now integrated via the trapezoidal rule in reverse, Equation (III-13) from $\psi = 0$ to $\psi = \pi$, piecewise

$$L_{ha_3 T} = 2 P_o r^2 \tau_1 \frac{r\cos\phi}{a_w}\left[\left(\frac{\pi}{2}-\phi\right)\sin\phi - \cos\phi\right] \cdot \left[\frac{2}{3}\rho_d \sin\theta \int_0^{\pi} \sin\psi\cos\psi\, d\psi + \right.$$

$$\left. + 2\rho_s \sin^2\theta \int_0^{\pi} \sin^2\psi\cos\psi\, d\psi\right] = 0 \quad \text{(III-17)}$$

We see from Equations (III-8) and (III-10) the integration of the forces $\vec{F}_a$ are needed. From Equation (III-7),

$$\vec{F}_a = \int_{-\left(\frac{\pi}{2}-\phi\right)}^{\left(\frac{\pi}{2}-\phi\right)} d\vec{F}_a = 2\left(\frac{\pi}{2}-\phi\right) P_o r \tau_1 \left[\begin{array}{l} (1-\rho_s)\sin\theta\cos\theta\sin\psi \\ \qquad + \frac{2}{3}\rho_d \sin\theta\sin\psi\cos\psi + 2\rho_s \sin^2\theta\sin^2\psi\cos\psi \\ -(1-\rho_s)\sin^2\theta\sin\psi - \frac{2}{3}\rho_d \sin\theta\sin^2\psi - 2\rho_s \sin^2\theta\sin^3\psi \end{array}\right] \quad \text{(III-18)}$$

Then the torque first component is, from Equation (III-10),

$$L_{xa_1} = 2\left(\frac{\pi}{2}-\phi\right) P_o r \tau_1 \left\{y_L\left[-(1-\rho_s)\sin^2\theta\sin\psi - \frac{2}{3}\rho_d \sin\theta\sin^2\psi - 2\rho_s \sin^2\theta\sin^3\psi\right] + \right.$$

$$\left. - z_L\left[\frac{2}{3}\rho_d \sin\theta\sin\psi\cos\psi + 2\rho_s \sin^2\theta \sin^2\psi \cos\psi\right]\right\} \quad \text{(III-19)}$$

and a piecewise integration of the wires in(III-19) from $\psi = 0$ to $\psi = \pi$ using (III-13) and (III-14) gives,

$$L_{xa_1 T} = -2\left(\frac{\pi}{2}-\phi\right) P_o r \tau_1 \frac{r\cos\phi}{a_w} \cdot y_L\left[2(1-\rho_s)\sin^2\theta + \frac{\pi}{3}\rho_d \sin\theta + \frac{8}{3}\rho_s \sin^2\theta\right]$$

$$L_{xa_1 T} = -2\left(\frac{\pi}{2}-\phi\right) P_o r^2 \frac{\tau_1}{a_w} y_L \cos\phi \sin\theta\left[\left(2+\frac{2}{3}\rho_s\right)\sin\theta + \frac{\pi}{3}\rho_d\right] \quad \text{(III-20)}$$

$$L_{xa_2} = 2\left(\frac{\pi}{2}-\phi\right) P_o r \tau_1 \left\{z_L\left[(1-\rho_s)\sin\theta\cos\theta\sin\psi\right] + x_o\left[(1-\rho_s)\sin^2\theta\sin\psi + \right.\right.$$

$$\left.\left. + \frac{2}{3}\rho_d \sin\theta\sin^2\psi + 2\rho_s \sin^2\theta\sin^3\psi\right]\right\} \quad \text{(III-21)}$$

and piece wise integration of the wires in (III-21) from $\Psi = 0$ to $\psi = \pi$ using (III-13) and (III-14) gives,

$$L_{xa_2T} = 2\left(\frac{\pi}{2} - \phi\right) P_o r \tau_1 \frac{r\cos\phi}{a_w}\left\{2z_L(1-\rho_s)\sin\theta\cos\theta + \right.$$
$$\left. + x_o\left[2(1-\rho_s)\sin^2\theta + \frac{\pi}{3}\rho_d\sin\theta + \frac{8}{3}\rho_s\sin^2\theta\right]\right\}$$

$$L_{xa_2T} = 2\left(\frac{\pi}{2} - \phi\right) P_o r^2 \frac{\tau_1}{a_w}\cos\phi\sin\theta\left\{2z_L(1-\rho_s)\cos\theta + \right.$$
$$\left. + x_o\left[(2 + \frac{2}{3}\rho_s)\sin\theta + \frac{\pi}{3}\rho_d\right]\right\} \qquad \text{(III-22)}$$

$$L_{xa_3} = 2\left(\frac{\pi}{2} - \phi\right) P_o r \tau_1\left\{x_o\left[\frac{2}{3}\rho_d\sin\theta\sin\psi\cos\psi + 2\rho_s\sin^2\theta\sin^2\psi\cos\psi\right] + \right.$$
$$\left. - y_L\left[(1-\rho_s)\sin\theta\cos\theta\sin\psi\right]\right\} \qquad \text{(III-23)}$$

and piecewise integration of (III-23) by (III-13) from $\psi = 0$ to $\psi = \pi$ using (III-14) gives,

$$L_{xa_3T} = -2\left(\frac{\pi}{2} - \phi\right) P_o r \tau_1 \frac{r\cos\phi}{a_w} 2y_L(1-\rho_s)\sin\theta\cos\theta$$

$$L_{xa_3T} = -4\left(\frac{\pi}{2} - \phi\right) P_o r^2 \frac{\tau_1}{a_w}(1-\rho_s) y_L\cos\phi\sin\theta\cos\theta \qquad \text{(III-24)}$$

From Equation (III-8) $\vec{L}_{aT}$ in components is, when integrated to total the effects of all such wires,

$$\vec{L}_{aT} = \vec{L}_{haT} - \vec{L}_{xaT} \qquad \text{(III-25)}$$

The components of $\vec{L}_{haT}$ are found in Equations (III-11), (III-15), (III-17), while (III-20), (III-22) and (III-24) form $\vec{L}_{xaT}$.

$$L_{a_1T} = 2\left(\frac{\pi}{2} - \phi\right) P_o r^2 \frac{\tau_1}{a_w} y_L\cos\phi\sin\theta\left[\left(2 + \frac{2}{3}\rho_s\right)\sin\theta + \frac{\pi}{3}\rho_d\right] \qquad \text{(III-26)}$$

from Equations (III-11) and (III-20).

The second component is found from (III-15) and (III-22) substituted into (III-25)

$$L_{a_2T} = 2 P_o r^2 \frac{\tau_1}{a_w} \sin\theta \cos\phi \left\{ r\left[\left(\frac{\pi}{2} - \phi\right) \sin\phi - \cos\phi\right] \cdot \left[\left(2 + \frac{2}{3}\rho_s\right) \cdot \sin\theta + \frac{\pi}{3}\rho_d\right] - \left(\frac{\pi}{2} - \phi\right)\left[2 z_L (1 - \rho_s) \cos\theta + x_o \cdot \left\{\left(2 + \frac{2}{3}\rho_s\right) \cdot \sin\theta + \frac{\pi}{3}\rho_d\right\}\right]\right\} \quad \text{(III-27)}$$

$$L_{a_2T} = 2 P_o r^2 \frac{\tau_1}{a_w} \sin\theta \cos\phi \left\{ \sin\theta \left(2 + \frac{2}{3}\rho_s\right)\left[\left(\frac{\pi}{2} - \phi\right) (r \sin\phi - x_o) - r \cos\phi\right] - 2\left(\frac{\pi}{2} - \phi\right)(1 - \rho_s) z_L \cos\theta + \frac{\pi}{3}\rho_d \left[\left(\frac{\pi}{2} - \phi\right) (r \sin\phi - x_o) - r \cos\phi\right]\right\} \quad \text{(III-28)}$$

$$L_{a_3T} = 4\left(\frac{\pi}{2} - \phi\right) P_o r^2 \frac{\tau_1}{a_w} (1 - \rho_s) y_L \cos\phi \sin\theta \cos\theta \quad \text{(III-29)}$$

from Equations (III-17) and (III-24) in (III-25).

Latitude Surfaces Farthest From Sun

Figure III-3 shows the area in $\bar{i}\ \bar{j}\ \bar{k}$ coordinates.

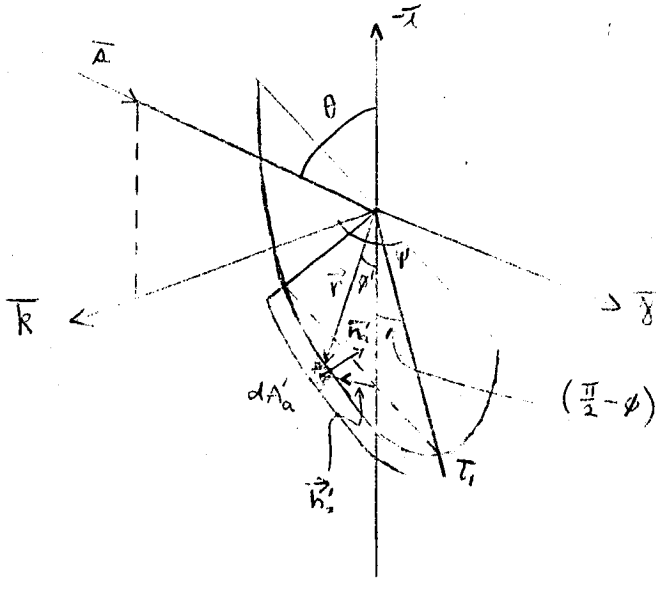

(Figure III-3)

Equations (III-1) become

$$\bar{n}'_a = \begin{bmatrix} 0 \\ \cos\psi \\ -\sin\psi \end{bmatrix} \qquad \bar{s} = \begin{bmatrix} \cos\theta \\ 0 \\ -\sin\theta \end{bmatrix} \qquad \vec{h}'_a = r \begin{bmatrix} -(\sin\phi - \cos\phi') \\ -\sin\phi' \sin\psi \\ -\sin\phi' \cos\psi \end{bmatrix} \tag{III-30}$$

The offset vector (III-2) becomes

$$\vec{x}' = \begin{bmatrix} x_o \\ y_L \\ z_L \end{bmatrix} \tag{III-31}$$

and equations (III-5) and (III-6) are still

$$dA'_a = r r_1 \, d\phi' \, d\psi \tag{III-32}$$

$$\bar{s} \cdot \bar{n}'_a = \sin\theta \sin\psi \tag{III-33}$$

A comparison of Figures III-1 and III-3 shows that $\bar{n}_a = \bar{n}'_a$ and $\vec{x} = \vec{x}'$ always and $\bar{s}$ is unchanged. Also $dA_a = dA'_a$. Therefore $d\vec{F}_a = d\vec{F}'_a$. We also see the variables ϕ' and ψ are to be integrated over the same intervals as in the previous case. But $\vec{h}_a = -\vec{h}'_a$ always. Equations (III-8) to (III-10) for this case are

$$\vec{L}'_a = \int_{-\left(\frac{\pi}{2} - \phi\right)}^{\left(\frac{\pi}{2} - \phi\right)} (\vec{h}'_a - \vec{x}') \times d\vec{F}'_a = \vec{L}'_{ha} - \vec{L}'_{xa}$$

which may be written

$$\vec{L}'_a = \int_{-\left(\frac{\pi}{2} - \phi\right)}^{\left(\frac{\pi}{2} - \phi\right)} (-\vec{h}_a - \vec{x}) \times d\vec{F}_a = -\vec{L}_{ha} - \vec{L}_{xa} \tag{III-34}$$

and piecewise integration of ψ from 0 to π gives

$$\vec{L}'_{aT} = -\vec{L}_{haT} - \vec{L}_{xaT} \tag{III-35}$$

The components of $\vec{L}_{haT}$ are given in Equations (III-11), (III-15) and (III-17). The components of $\vec{L}_{xaT}$ are given by (III-20), (III-22) and (III-24).

Then

$$L'_{a_1T} = 2\left(\frac{\pi}{2} - \phi\right) P_o r^2 \frac{\tau_1}{a_w} y_L \cos\phi \sin\theta \left[\left(2 + \frac{2}{3}\rho_s\right) \sin\theta + \frac{\pi}{3}\rho_d\right] \tag{III-36}$$

$$L'_{a_2T} = -2 P_o r^2 \frac{\tau_1}{a_w} \sin\theta \cos\phi \left\{ r\left[\left(\frac{\pi}{2} - \phi\right) \sin\phi \cos\phi\right] \cdot \left[\left(2 + \frac{2}{3}\rho_s\right) \cdot \sin\theta + \frac{\pi}{3}\rho_d\right] + \left(\frac{\pi}{2} - \phi\right)\left[2 z_L (1 - \rho_s) \cos\theta + x_o \left\{\left(2 + \frac{2}{3}\rho_s\right) \cdot \sin\theta + \frac{\pi}{3}\rho_d\right\}\right]\right. \tag{III-37}$$

$$L'_{a_2T} = -2 P_o r^2 \frac{\tau_1}{a_w} \sin\theta \cos\phi \left\{ \sin\theta \left(2 + \frac{2}{3}\rho_s\right)\left[\left(\frac{\pi}{2} - \phi\right)(r \sin\phi + x_o) - r\cos\phi\right] + 2\left(\frac{\pi}{2} - \phi\right)(1 - \rho_s) z_L \cos\theta + \frac{\pi}{3}\rho_d\left[\left(\frac{\pi}{2} - \phi\right)(r \sin\phi + x_o) - r\cos\phi\right]\right\} \tag{III-38}$$

$$L'_{a_3T} = 4\left(\frac{\pi}{2} - \phi\right) P_o r^2 \frac{\tau_1}{a_w} (1 - \rho_s) y_L \cos\phi \sin\theta \cos\theta \tag{III-39}$$

This completes the derivation of the "a" torques. These are expressed in components in Equations (III-26), (III-28), (III-29), (III-36), (III-38) and (III-39). If there is no shading

$$\vec{L}_{A'T} = \vec{L}_{aT} + \vec{L}_{a'T}$$

$$L_{A'_1T} = 4\left(\frac{\pi}{2} - \phi\right) P_o r^2 \frac{\tau_1}{a_w} y_L \cos\phi \sin\theta \left[\left(2 + \frac{2}{3}\rho_s\right) \sin\theta + \frac{\pi}{3}\rho_d\right] \tag{III-40}$$

$$L_{A'_2T} = 4 P_o r^2 \frac{\tau_1}{a_w} \sin\theta \cos\phi \left\{ \sin\theta \cdot \left(2 + \frac{2}{3}\rho_s\right)\left[-X_o\left(\frac{\pi}{2} - \phi\right)\right] + \right.$$

$$\left. - \cos\theta \cdot 2 \left(\frac{\pi}{2} - \phi\right)\left(1 - \rho_s\right) z_L + \frac{\pi}{3}\rho_d \left[-X_o\left(\frac{\pi}{2} - \phi\right)\right]\right\} \qquad \text{(III-41)}$$

$$L_{A'_3T} = 8\left(\frac{\pi}{2} - \phi\right) P_o r^2 \frac{\tau_1}{a_w} (1 - \rho_s)\, y_L \cos\phi \sin\theta \cos\theta \qquad \text{(III-42)}$$

The torque $L_{A'T}$ given by Equations (III-40) to (III-42) is a theoretical consideration in which absolutely no shadowing exists. Actually the back surfaces are shadowed by the front surfaces. This is approximated by taking only a proportionate amount of the back surface torques. The front surfaces are shadowed by themselves around the edges. This effect is neglected. The total torque on the whole lens' latitude radial surfaces is

$$\vec{L}_{AT} = \vec{L}_{aT} + K_1 \vec{L}'_{aT} \qquad \text{(III-43)}$$

where $\vec{L}_{aT}$ components are given in Equations (III-26), (III-28), and (III-29) while the components of L'_{aT} are given in Equations (III-36), (III-38) and (III-39).

Longitude Surfaces Closest to Sun When $\phi' > \theta$

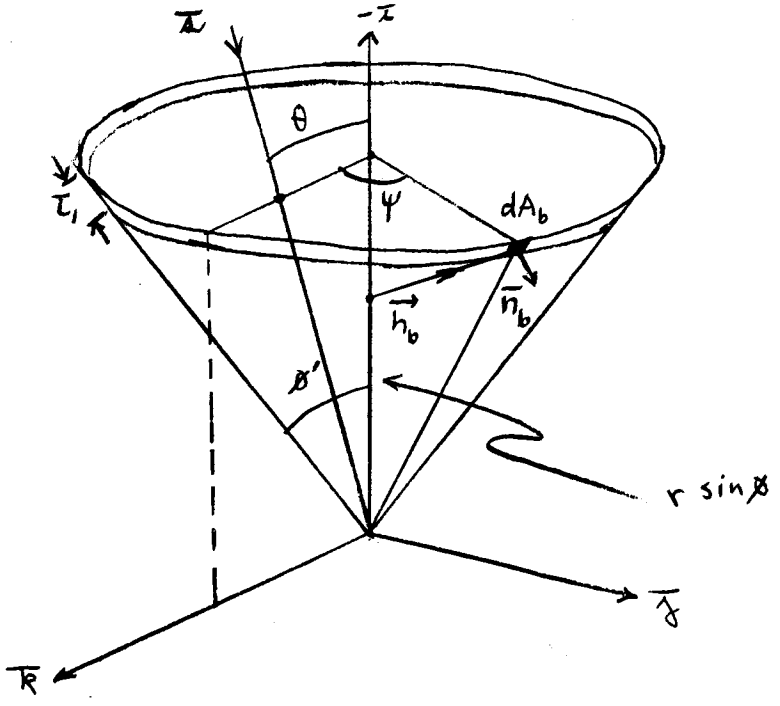

(Figure III-4)

The vectors $\bar{n}_b$, $\bar{s}$ and $\vec{h}_b$ are

$$\bar{n}_b = \begin{bmatrix} \sin\phi' \\ \cos\phi' \sin\psi \\ \cos\phi' \cos\psi \end{bmatrix} \qquad \bar{s} = \begin{bmatrix} \cos\theta \\ 0 \\ -\sin\theta \end{bmatrix} \qquad \vec{h}_b = r \begin{bmatrix} \sin\phi - \cos\phi' \\ \sin\phi' \sin\psi \\ \sin\phi' \cos\psi \end{bmatrix} \tag{III-44}$$

The offset vector (III-2) is

$$\vec{x} = \begin{bmatrix} x_o \\ y_L \\ z_L \end{bmatrix} \tag{III-45}$$

Also

$$dA_b = \tau_1 \, r \sin\phi' \, d\psi$$

$$\bar{s} \cdot \bar{n}_b = \cos\theta \sin\phi' - \sin\theta \cos\phi' \cos\psi \tag{III-46}$$

For this case, Equation (III-4) becomes

$$\vec{L}_b = \int \vec{h}_b \, X \, d\vec{F}_b - \vec{x} \, X \int d\vec{F}_b = \vec{L}_{hb} - \vec{L}_{xb} \tag{III-47}$$

where

$$\vec{L}_{hb} = \int \vec{h}_b \, X \, d\vec{F}_b \tag{III-48}$$

$$\vec{L}_{xb} = \vec{x} \, X \int d\vec{F}_b = \vec{x} \, X \, \vec{F}_b \tag{III-49}$$

If Equations (III-44) and (III-46) are substituted into (III-3), we have the force components of $d\vec{F}_b$

$$dF_{b_1} = P_o \tau_1 \, r \sin\phi' \, d\psi \Big[(1 - \rho_s)(\cos^2\theta \sin\phi' - \sin\theta \cos\theta \cos\phi' \cos\psi) +$$

$$+ \frac{2}{3} \rho_d (\cos\theta \sin^2\phi' - \sin\theta \sin\phi' \cos\phi' \cos\psi) + 2\rho_s (\cos^2\theta \sin^3\phi' -$$

$$- 2 \sin\theta \cos\theta \sin^2\phi' \cos\phi' \cos\psi + \sin^2\theta \sin\phi' \cos^2\phi' \cos^2\psi) \Big] \tag{III-50}$$

$$dF_{b_2} = P_o \tau_1 r \sin\phi' \, d\psi \left[\frac{2}{3} \rho_d (\cos\theta \sin\phi' \cos\phi' \sin\psi - \sin\theta \cos^2\phi' \sin\psi \cos\psi) + \right.$$

$$+ 2\rho_s (\cos^2\theta \sin^2\phi' \cos\phi' \sin\psi - 2 \sin\theta \cos\theta \sin\phi' \cos^2\phi' \sin\psi \cos\psi +$$

$$\left. + \sin^2\theta \cos^3\phi' \sin\psi \cos^2\psi) \right] \qquad \text{(III-51)}$$

$$dF_{b_3} = P_o \tau_1 r \sin\phi' \, d\psi \left[(1 - \rho_s) (-\sin\theta \cos\theta \sin\phi' + \sin^2\theta \cos\phi' \cos\psi) + \right.$$

$$+ \frac{2}{3} \rho_d (\cos\theta \sin\phi' \cos\phi' \cos\psi - \sin\theta \cos^2\phi' \cos^2\psi) + 2\rho_s \cdot$$

$$\cdot (\cos^2\theta \sin^2\phi' \cos\phi' \cos\psi - 2 \sin\theta \cos\theta \sin\phi' \cos^2\phi' \cos^2\psi +$$

$$\left. + \sin^2\theta \cos^3\phi' \cos^3\psi) \right] \qquad \text{(III-52)}$$

Substituting the Equations (III-44) and (III-50) through (III-52) into (III-48) has as a first component,

$$dL_{h_1 b} = P_o \tau_1 r^2 \sin\phi' \left\{ \sin\phi' \left[(1 - \rho_s) (-\sin\theta \cos\theta \sin\phi' \sin\psi + \right.\right.$$

$$+ \sin^2\theta \cos\phi' \sin\psi \cos\psi) + \frac{2}{3} \rho_d (\cos\theta \sin\phi' \cos\phi' \sin\psi \cos\psi -$$

$$- \sin\theta \cos^2\phi' \sin\psi \cos^2\psi) + 2\rho_s (\cos^2\theta \sin^2\phi' \cos\phi' \sin\psi \cos\psi -$$

$$\left. - 2 \sin\theta \cos\theta \sin\phi' \cos^2\phi' \sin\psi \cos^2\psi + \sin^2\theta \cos^3\phi' \sin\psi \cos^3\psi) \right] -$$

$$- \sin\phi' \left[\frac{2}{3} \rho_d (\cos\theta \sin\phi' \cos\phi' \sin\psi \cos\psi - \sin\theta \cos^2\phi' \sin\psi \cos^2\psi) + \right.$$

$$+ 2\rho_s (\cos^2\theta \sin^2\phi' \cos\phi' \sin\psi \cos\psi - 2 \sin\theta \cos\theta \sin\phi' \cos^2\phi' \cdot$$

$$\left.\left. \cdot \sin\psi \cos^2\psi + \sin^2\theta \cos^3\phi' \sin\psi \cos^3\psi) \right] \right\} d\psi \qquad \text{(III-53)}$$

Integration of ψ from $-\pi$ to π gives

$$L_{h_1 b} = 0 \qquad L_{h_1 bT} = 0 \qquad \text{(III-54)}$$

since all terms are odd functions of ψ.

The second term of $\vec{L}_{hb}$ is,

$$dL_{h_2b} = P_o \tau_1 r^2 \sin\phi' \Big\{ \sin\phi' \Big[(1-\rho_s)(\cos^2\theta \sin\phi' \cos\psi - \sin\theta\cos\theta\cos\phi'\cos^2\psi) + \frac{2}{3}\rho_d(\cos\theta\sin^2\phi'\cos\psi - \sin\theta\sin\phi'\cos\phi'\cos^2\psi) + 2\rho_s(\cos^2\theta\sin^3\phi'\cos\psi - 2\sin\theta\cos\theta\sin^2\phi'\cos\phi'\cos^2\psi + \sin^2\theta\sin\phi'\cos^2\phi'\cos^3\psi)\Big] - (\sin\phi - \cos\phi')\Big[(1-\rho_s)(-\sin\theta\cos\theta\sin\phi' + \sin^2\theta\cos\phi'\cos\psi) + \frac{2}{3}\rho_d(\cos\theta\sin\phi'\cos\phi'\cos\psi - \sin\theta\cos^2\phi'\cos^2\psi) + 2\rho_s \cdot (\cos^2\theta\sin^2\phi'\cos\phi'\cos\psi - 2\sin\theta\cos\theta\sin\phi'\cos^2\phi'\cos^2\psi + \sin^2\theta\cos^3\phi'\cos^3\psi)\Big]\Big\} d\psi$$

Integrating,

$$L_{h_2b} = P_o \tau_1 r^2 \sin\phi' \Big\{ (1-\rho_s)\Big[\sin\theta\cos\theta\sin\phi'(\sin\phi - \cos\phi')\int d\psi + (\cos^2\theta\sin^2\phi' - \sin^2\theta\sin\phi\cos\phi' + \sin^2\theta\cos^2\phi')\int\cos\psi\, d\psi - \sin\theta\cos\theta\sin\phi'\cos\phi'\int\cos^2\psi\, d\psi\Big] + \frac{2}{3}\rho_d(1 - \sin\phi\cos\phi')\cdot \Big[\cos\theta\sin\phi'\int\cos\psi\, d\psi - \sin\theta\cos\phi'\int\cos^2\psi\, d\psi\Big] + 2\rho_s(1 - \sin\phi\cos\phi')\Big[\cos^2\theta\sin^2\phi'\int\cos\psi\, d\psi - 2\sin\theta\cos\theta\sin\phi'\cos\phi'\int\cos^2\psi\, d\psi + \sin^2\theta\cos^2\phi'\int\cos^3\psi\, d\psi\Big]\Big\} \quad \text{(III-55)}$$

Integrating Equation (III-55) from $\psi = -\pi$ to $\psi = \pi$ gives

$$L_{h_2 b} = \pi P_o \tau_1 r^2 \sin\phi' \Big\{ (1-\rho_s) \Big[2 \sin\theta \cos\theta \sin\phi' (\sin\phi - \cos\phi') - \\ - \sin\theta \cos\theta \sin\phi' \cos\phi' \Big] + \frac{2}{3} \rho_d (1 - \sin\phi \cos\phi') \Big[- \sin\theta \cos\phi' \Big] + \\ + 2\rho_s (1 - \sin\phi \cos\phi') \Big[- 2 \sin\theta \cos\theta \sin\phi' \cos\phi' \Big]$$

$$L_{h_2 b} = \pi P_o \tau_1 r^2 \sin\theta \Big[(1-\rho_s) \cos\theta (2 \sin\phi \sin^2\phi' - 3 \sin^2\phi' \cos\phi') + \\ - \frac{2}{3} \rho_d \sin\phi' \cos\phi' (1 - \sin\phi \cos\phi') - 4\rho_s \cos\theta \sin^2\phi' \cos\phi' \cdot \\ \cdot (1 - \sin\phi\cos\phi') \Big] \qquad \text{(III-56)}$$

For piecewise integrations $\Delta\phi'$, the change in ϕ' between the centers of adjacent longitude wires is

$$\Delta\phi' = \frac{a_w}{r} \qquad \text{(III-57)}$$

assuming that the wires are spaced by a_w.

Piecewise integration of (III-56) from $\phi' = \theta$ to $\phi' = \frac{\pi}{2} - \phi$,

$$L_{h_2 bT} = \pi P_o \tau_1 r^2 \sin\theta \Big\{ (1-\rho_s) \cos\theta \Big[\frac{r}{a_w} \Big(\Big\{ J_1 - \theta + \sin\theta \cos\theta \Big\} \sin\phi - \\ - \cos^3\phi + \sin^3\theta \Big) + \frac{1}{2} (2 \sin^2\theta \sin\phi - 3 \sin^2\theta \cos\theta - \sin\phi \cos^2\phi) \Big] + \\ + \frac{2}{3} \rho_d \Big[\frac{r}{a_w} \Big(\frac{1}{2} \sin^2\theta + \frac{1}{3} \sin\phi \cos^3\theta + J_3 \Big) + \frac{1}{2} (\sin\phi \sin\theta \cos^2\theta - \\ - \sin\theta \cos\theta + J_4) \Big] + 4\rho_s \cos\theta \Big[\frac{r}{a_w} \Big(\frac{1}{8} \sin\phi \Big\{ - \theta - \sin\theta \cos\theta + \\ + 2 \sin\theta \cos^3\theta \Big\} + \frac{1}{3} \sin^3\theta + J_5 \Big) + \frac{1}{2} (- \sin^2\theta \cos\theta + \sin\phi \sin^2\theta \cdot \\ \cdot \cos^2\theta + J_6) \Big] \qquad \text{(III-58)}$$

The third component of $\vec{L}_{hb}$ is, using Equations (III-44), (III-48) and (III-50) through (III-52),

$$dL_{h_3b} = P_o \tau_1 r^2 \sin\phi' \left\{ (\sin\phi - \cos\phi') \left[\frac{2}{3} \rho_d (\cos\theta \sin\phi' \cos\phi' \sin\psi - \right.\right.$$

$$- \sin\theta \cos^2\phi' \sin\psi \cos\psi) + 2\rho_s (\cos^2\theta \sin^2\phi' \cos\phi' \sin\psi -$$

$$\left. - 2 \sin\theta \cos\theta \sin\phi' \cos^2\phi' \sin\psi \cos\psi + \sin^2\theta \cos^3\phi' \sin\psi \cos^2\psi) \right] -$$

$$- \sin\phi' \left[(1 - \rho_s) (\cos^2\theta \sin\phi' \sin\psi - \sin\theta \cos\theta \cos\phi' \sin\psi \cos\psi) + \right.$$

$$+ \frac{2}{3} \rho_d (\cos\theta \sin^2\phi' \sin\psi - \sin\theta \sin\phi' \cos\phi' \sin\psi \cos\psi) + 2\rho_s \cdot$$

$$\cdot (\cos^2\theta \sin^3\phi' \sin\psi - 2 \sin\theta \cos\theta \sin^2\phi' \cos\phi' \sin\psi \cos\psi +$$

$$\left.\left. + \sin^2\theta \sin\phi' \cos^2\phi' \sin\psi \cos^2\psi) \right] \right\} d\psi \qquad \text{(III-59)}$$

Integrating ψ from $-\pi$ to π gives

$$L_{h_3b} = 0 \qquad L_{h_3bT} = 0 \qquad \text{(III-60)}$$

since all terms are odd functions of ψ. Now $\vec{L}_{hbT}$ is complete.

From Equation (III-47) and (III-49) we need $\vec{F}_b$ so from (III-50), (III-51) and (III-52) integrated from $\psi = -\pi$ to π, we have a first component of

$$F_{b_1} = \pi P_o \tau_1 r \left[(1 - \rho_s) \cdot 2\cos^2\theta \sin^2\phi' + \frac{2}{3} \rho_d \cdot 2\cos\theta \sin^3\phi' + \right.$$

$$\left. + 2\rho_s (2\cos^2\theta \sin^4\phi' + \sin^2\theta \sin^2\phi' \cos^2\phi') \right] \qquad \text{(III-61)}$$

Integration of F_{b1} for all the circular wires via Equation (III-13) from $\phi' = \theta$ to $\phi' = \frac{\pi}{2} - \phi$ gives,

$$F_{b_1T} = \pi P_o \tau_1 r \left\{ (1 - \rho_s) \cos^2\theta \left[\frac{r}{a_w} (J_1 - \theta + \sin\theta \cos\theta) + (\sin^2\theta + \cos^2\phi) \right] + \right.$$

$$\left. + \frac{4}{3} \rho_d \cos\theta \left[\frac{r}{a_w} \cdot \frac{1}{3} (2\cos\theta + \sin^2\theta \cos\theta - J_2) + \frac{1}{2} (\sin^3\theta + \cos^3\phi) \right] + \right.$$

$$+ 2\rho_s \left[\frac{r}{a_w} \left\{ 2\cos^2\theta \left(-\frac{1}{4}\sin\phi\cos^3\phi + \frac{1}{4}\sin^3\theta\cos\theta + \frac{3}{8}\left\{ \left\{ J_1 - \theta + \sin\theta\cos\theta \right\} \right) + \sin^2\theta \cdot \frac{1}{8}\left(2\sin\theta\cos^3\theta - \sin\theta\cos\theta - \theta + J_7\right) \right\} + \right.\right.$$

$$\left.\left. + \frac{1}{2}\left\{ 2\cos^2\theta\left(\sin^4\theta + \cos^4\phi\right) + \sin^2\theta\left(\sin^2\theta\cos^2\theta + \sin^2\phi\cos^2\phi\right) \right\} \right] \right] \qquad \text{(III-62)}$$

The second component of $\vec{F}_b$, Equation (III-51), when integrated from $\psi = -\pi$ to $\psi = \pi$ is

$$F_{b2} = 0 \qquad F_{b_2T} = 0 \qquad \text{(III-63)}$$

since all terms are odd functions of ψ.

The third component of $\vec{F}_b$, Equation (III-52) when integrated from $\psi = -\pi$ to $\psi = \pi$ is,

$$F_{b_3} = -\pi P_o \tau_1 r \sin\theta \left[2(1-\rho_s)\cos\theta\sin^2\phi' + \frac{2}{3}\rho_d \sin\phi'\cos^2\phi' + \right.$$

$$\left. + 4\rho_s \cos\theta \sin^2\phi' \cos^2\phi' \right] \qquad \text{(III-64)}$$

and piecewise integration for all the longitude wires in the range $\phi' = \theta$ to $\phi' = \frac{\pi}{2} - \phi$ gives,

$$F_{b_3T} = -\pi P_o \tau_1 r \sin\theta \left\{ (1-\rho_s)\cos\theta \left[\frac{r}{a_w}\left(J_1 - \theta + \sin\theta\cos\theta\right) + \left(\sin^2\theta + \cos^2\theta\right) \right] + \right.$$

$$+ \frac{2}{3}\rho_d \left[\frac{r}{a_w} \cdot \frac{1}{3}\left(\cos^3\theta - \sin^3\phi\right) + \frac{1}{2}\left(\sin\theta\cos^2\theta + \sin^2\phi\cos\phi\right) \right] +$$

$$+ 4\rho_s \cos\theta \left[\frac{r}{a_w} \cdot \frac{1}{8}\left(-\theta - \sin\theta\cos\theta + 2\sin\theta\cos^3\theta + J_7\right) + \right.$$

$$\left. \left. + \frac{1}{2}\left(\sin^2\theta\cos^2\theta + \sin^2\phi\cos^2\phi\right) \right] \right\} \qquad \text{(III-65)}$$

The torque $\vec{L}_{xbT}$ is found by piecewise integration of Equation (III-49),

$$\vec{L}_{xbT} = \vec{x} \times \vec{F}_{bT} \qquad \text{(III-66)}$$

The Equations (III-45), (III-62), (III-63) and (III-65) substituted into (III-66) gives a first component of,

$$L_{xb_1T} = y_L F_{b_3T} \tag{III-67}$$

since $F_{b_2T} = 0$, where F_{b_3T} is given by Equation (III-65). The second component of $\vec{L}_{xbT}$ is

$$L_{xb_2T} = z_L F_{b_1T} - x_o F_{b_3T} \tag{III-68}$$

where F_{b_1T} and F_{b_3T} are found in Equations (III-62) and (III-65) and the third component of $\vec{L}_{xbT}$ is

$$L_{xb_3T} = - y_L F_{b_1T} \tag{III-69}$$

where again F_{b_1T} is found in Equation (III-62).

Piecewise integration of Equation (III-47) is

$$\vec{L}_{bT} = \vec{L}_{hbT} - \vec{L}_{xbT} \tag{III-70}$$

where the components of $\vec{L}_{hbT}$ are found in Equations (III-54), (III-58) and (III-60) while the components of $\vec{L}_{xbT}$ are found in Equations (III-67), (III-68) and (III-69). Note (III-54) and (III-60) are zero.

Longitude Surfaces Farthest from Sun $\theta < \phi'$

Figure III-5 shows the area in $\bar{i}\bar{j}\bar{k}$ coordinates.

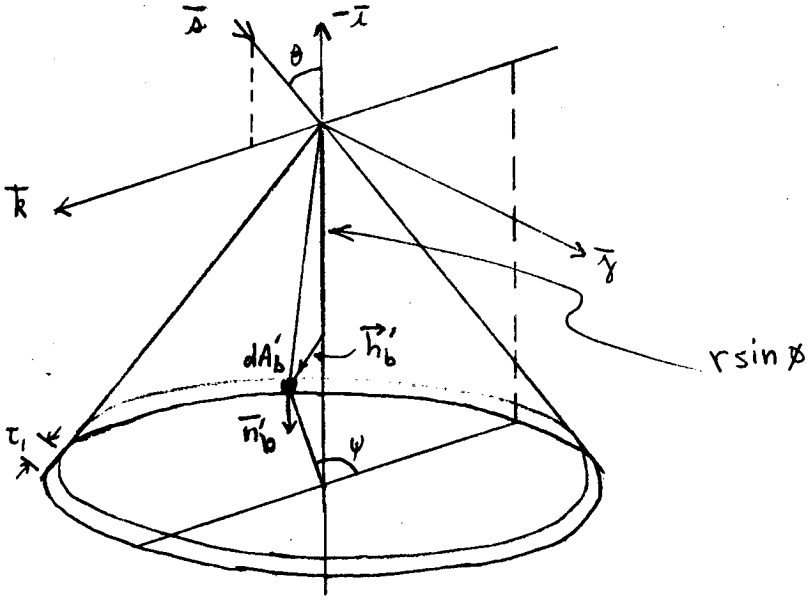

Figure III-5

The vectors $\bar{n}'_b$, $\bar{s}$ and $\vec{h}'_b$ are

$$\bar{n}'_b = \begin{bmatrix} \sin\phi' \\ \cos\phi' \sin\psi \\ \cos\phi' \cos\psi \end{bmatrix} \quad \bar{s} = \begin{bmatrix} \cos\theta \\ 0 \\ -\sin\theta \end{bmatrix} \quad \vec{h}'_b = r \begin{bmatrix} -(\sin\phi - \cos\phi') \\ -\sin\phi' \sin\psi \\ -\sin\phi' \cos\psi \end{bmatrix} \tag{III-71}$$

The offset vector is

$$\vec{x} = \begin{bmatrix} x_o \\ y_L \\ z_L \end{bmatrix} \tag{III-72}$$

And

$$dA'_b = \tau_1 \, r \sin\phi' \, d\psi$$

$$\bar{s} \cdot \bar{n}'_b = +\cos\theta \sin\phi' - \sin\theta \cos\phi' \cos\psi \tag{III-73}$$

By comparing Figures 4 and 5 we see that $\bar{s}$ and $\bar{x}$ do not change, $dA_b = dA'_b$, $\bar{n}_b = \bar{n}'_b$ at all positions and $\vec{h}_b = -\vec{h}'_b$ at all positions. Therefore $\vec{dF}_b = \vec{dF}'_b$. Also we see that integrations in this case are over the same regions as was in the case closer to the sun. We may write these torques like in Equation (III-70),

$$\vec{L}'_{bT} = \vec{L}'_{hbT} - \vec{L}'_{xbT} \tag{III-74}$$

Equation (III-48) indicates that

$$\vec{L}'_{hb} = \int \vec{h}'_b X \vec{dF}'_b = -\int \vec{h}_b X \vec{dF}_b = -\vec{L}_{hb} \tag{III-75}$$

then $$\vec{L}'_{hbT} = -\vec{L}_{hbT}$$

while from Equation (III-49)

$$\vec{L}'_{xb} = \vec{x}' X \vec{F}'_b = \vec{x} X \vec{F}_b = \vec{L}_{xb} \tag{III-76}$$

then, $$\vec{L}'_{xbT} = \vec{L}_{xbT}$$

Equations (III-75) and (III-76) substituted into (III-74) gives

$$\vec{L}'_{bT} = -\vec{L}_{hbT} - \vec{L}_{xbT} \tag{III-77}$$

where the components of $\vec{L}_{hbT}$ are respectively Equations (III-54), (III-58), (III-60) and the components of $\vec{L}_{xbT}$ are Equations (III-67), (III-68), (III-69). Again (III-54) and (III-60) are zero.

Like Equation (III-43), the back surface is shaded a factor of K_1 so (III-43) becomes for this case,

$$\vec{L}_{BT} = \vec{L}_{bT} + K_1 \vec{L}'_{bT} \tag{III-78}$$

Case when $\phi' < \theta$ on Longitude sides closest to sun

Figure (III-6) shows the area in the $\bar{i}\bar{j}\bar{k}$ coordinate system and the related vectors.

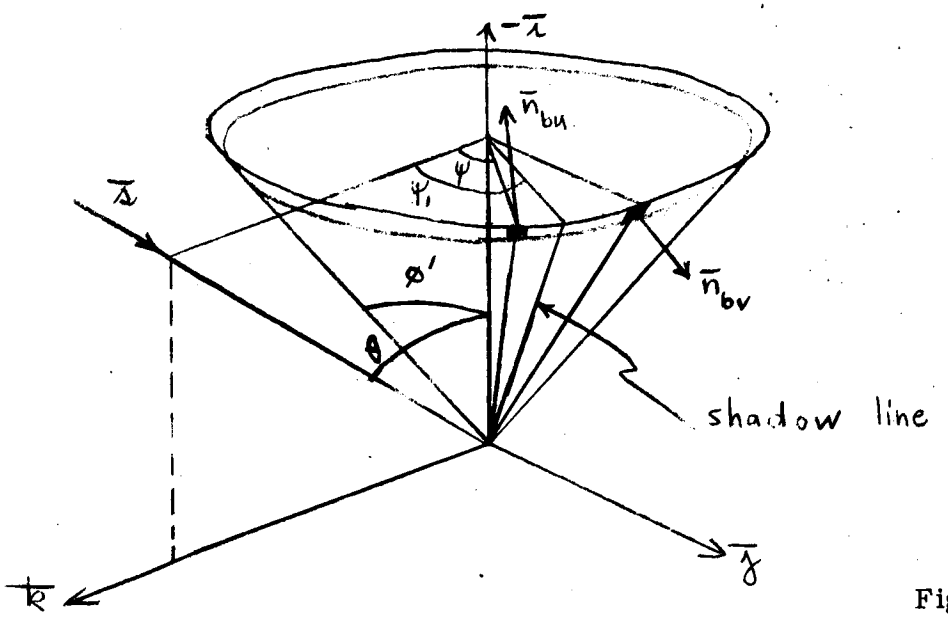

Figure III-6

With $\phi' < \theta$, $\bar{s}$ shines on the outside and the inside of the cone. The solar force equation is valid only if $\bar{n}_b \cdot \bar{s} \geq 0$ therefore let ψ_1 be ψ when $\bar{s} \cdot \bar{n}_b = 0$. Then we define $\bar{n}_b$ for $\psi < \psi_1$. Let these $\bar{n}_b$ s be respectively $\bar{n}_{b1}$ and $\bar{n}_{b2}$. Then

$$\bar{s} = \begin{bmatrix} \cos\theta \\ 0 \\ -\sin\theta \end{bmatrix} \quad \vec{h}_b = r \begin{bmatrix} (\sin\phi - \cos\phi' \\ \sin\phi' \sin\psi \\ \sin\phi' \cos\psi \end{bmatrix} \quad x = \begin{bmatrix} x_o \\ y_L \\ z_L \end{bmatrix} \tag{III-79}$$

and the normal vectors are

$$\bar{n}_{bu} = \begin{bmatrix} -\sin\phi' \\ -\cos\phi' \sin\psi \\ -\cos\phi' \cos\psi \end{bmatrix} \quad \text{where } \psi < \psi_1 \tag{III-80}$$

$$\bar{n}_{bv} = \begin{bmatrix} \sin\phi' \\ \cos\phi' \sin\psi \\ \cos\phi' \cos\psi \end{bmatrix} \quad \text{where } \psi > \psi_1 \tag{III-81}$$

We may find ψ_1 by $\bar{s} \cdot \bar{n}_{bu} = 0$.

$$\bar{s} \cdot \bar{n}_{bu} = \sin\theta \cos\phi' \cos\psi_1 - \cos\theta \sin\phi' = 0$$

Then

$$\cos\psi_1 = \frac{\tan\phi'}{\tan\theta} \tag{III-82}$$

Since $\bar{n}_{bu} = -\bar{n}_{bv}$ we may compare this case with the case when the sun $\bar{s}$ sees only the inside of the cone, Figure III-4. In this figure, $\bar{n}_b = \bar{n}_{bv} = -\bar{n}_{bu}$. Therefore if $\psi < \psi_1$, (III-50) through (III-52) become

$$dF_{b_1u} = P_o \tau_1 r \sin\phi' \, d\psi \left[(1-\rho_s)(-\cos^2\theta \sin\phi' + \sin\theta\cos\theta\cos\phi'\cos\psi) + \frac{2}{3}\rho_d (\cos\theta\sin^2\phi' - \sin\theta\sin\phi'\cos\phi'\cos\psi) + 2\rho_s (-\cos^2\theta\sin^3\phi' + 2\sin\theta\cos\theta\sin^2\phi'\cos\phi'\cos\psi - \sin^2\theta\sin\phi'\cos^2\phi'\cos^2\psi) \right] \quad \text{(III-83)}$$

$$dF_{b_2u} = P_o \tau_1 r \sin\phi' \, d\psi \left[\frac{2}{3}\rho_d (\cos\theta\sin\phi'\cos\phi'\sin\psi - \sin\theta\cos^2\phi'\sin\psi\cos\psi) + 2\rho_s (-\cos^2\theta\sin^2\phi'\cos\phi'\sin\psi + 2\sin\theta\cos\theta\sin\phi'\cos^2\phi'\sin\psi\cos\psi - \sin^2\theta\cos^3\phi'\sin\psi\cos^2\psi) \right] \quad \text{(III-84)}$$

$$dF_{b_3u} = P_o \tau_1 r \sin\phi' \, d\psi \left[(1-\rho_s)(\sin\theta\cos\theta\sin\phi' - \sin^2\theta\cos\phi'\cos\psi) + \frac{2}{3}\rho_d (\cos\theta\sin\phi'\cos\phi'\cos\psi - \sin\theta\cos^2\phi'\cos^2\psi) + 2\rho_s (-\cos^2\theta\sin^2\phi'\cos\phi'\cos\psi + 2\sin\theta\cos\theta\sin\phi'\cos^2\phi'\cos^2\psi - \sin^2\theta\cos^3\phi'\cos^3\psi) \right] \quad \text{(III-85)}$$

We may readily see that if Equation (III-53) had the specular reflection and absorption sign changes, it's integral from $-\psi_1$ to ψ_1 would still be zero, therefore

$$L_{h_1bu} = 0 \quad L_{h_1bTu} = 0 \quad \text{(III-86)}$$

Changing the sign on the specular reflection and absorption terms and integrating Equation (III-55) from $\psi = -\psi_1$ to $\psi = \psi_1$ gives

$$L_{h_2bu} = P_o \tau_1 r^2 \sin\phi' \left\{ (1-\rho_s) \left[-2\psi_1 \sin\theta\cos\theta\sin\phi'(\sin\phi - \cos\phi') - 2\sin\psi_1 (\cos^2\theta\sin^2\phi' - \sin^2\theta\sin\phi\cos\phi' + \sin^2\theta\cos^2\phi') + (\psi_1 + \sin\psi_1\cos\psi_1)\sin\theta\cos\theta\sin\phi'\cos\phi' \right] + \right.$$

$$+\frac{2}{3}\rho_d\,(1-\sin\phi\cos\phi')\left[2\sin\psi_1\cos\theta\sin\phi'-(\psi_1+\sin\psi_1\cos\psi_1)\sin\theta\cos\phi'\right]+$$

$$+2\rho_s(1-\sin\phi\cos\phi')\left[-2\sin\psi_1\cos^2\theta\sin^2\phi'+\right. \tag{III-87}$$

$$\left.+2\sin\theta\cos\theta\sin\phi'\cos\phi'(\psi_1+\sin\psi_1\cos\psi_1)-\frac{2}{3}\sin\psi_1(2+\cos^2\psi_1)\sin^2\theta\cos^2\phi'\right]$$

Integration of (59) from $\psi=-\psi_1$ to $\psi=\psi_1$ with the sign changes gives,

$$L_{h_3 bu}=0 \qquad L_{h_3 bu_T}=0 \tag{III-88}$$

To find the offset torque we need to integrate dF_{bu} from $\psi=-\psi_1$ to $\psi=\psi_1$. Thus the first component is, using (83)

$$F_{b_1 u}=P_o r_1 r\sin\phi'\left\{(1-\rho_s)\left[-2\psi_1\cos^2\theta\sin\phi'+2\sin\psi_1\sin\theta\cos\theta\cos\phi'\right]+\right.$$

$$+\frac{2}{3}\rho_d\left[2\psi_1\cos\theta\sin^2\phi'-2\sin\psi_1\sin\theta\sin\phi'\cos\phi'\right]+ \tag{III-89}$$

$$+2\rho_s\left[-2\psi_1\cos^2\theta\sin^3\phi'+4\sin\psi_1\sin\theta\cos\theta\sin^2\phi'\cos\phi'-\right.$$

$$\left.\left.-(\psi_1+\sin\psi_1\cos\psi_1)\sin^2\theta\sin\phi'\cos^2\phi'\right]\right\}$$

Integration of Equation (III-84) from $\psi=-\psi_1$ to $\psi=\psi_1$ gives

$$F_{b_2 u}=0 \qquad F_{b_2 uT}=0 \tag{III-90}$$

and integration of Equation (85) from $\psi=-\psi_1$ to $\psi=\psi_1$ gives

$$F_{b_3 u}=P_o r_1 r\sin\phi'\left\{(1-\rho_s)\left[2\psi_1\sin\theta\cos\theta\sin\phi'-2\sin\psi_1\sin^2\theta\cos\phi'\right]+\right.$$

$$+\frac{2}{3}\rho_d\left[2\sin\psi_1\cos\theta\sin\phi'\cos\phi'-(\psi_1+\sin\psi_1\cos\psi_1)\sin\theta\cos^2\phi'\right]+ \tag{III-91}$$

$$+2\rho_s\left[-2\sin\psi_1\cos^2\theta\sin^2\phi'\cos\phi'+2(\psi_1+\sin\psi_1\cos\psi_1)\sin\theta\cos\theta\sin\phi'\cos^2\phi'-\right.$$

$$\left.\left.-\frac{2}{3}\sin\psi_1(2+\cos^2\psi_1)\sin^2\theta\cos^3\phi'\right]\right\}$$

Instead of finding those u torques we duplicate this work on the v torques. Since these equations are very similar, they combine in many places.

When $\psi > \psi_1$, Equations (III-44) through (III-53) are valid. From the table of integrals for integration of ψ from ψ_1 to $2\pi - \psi_1$ in Equation (III-53) gives

$$L_{h_1bv} = 0 \qquad L_{h_1bTv} = 0 \tag{III-92}$$

Likewise Equation (III-55) fits this case. Integration of this equation from ψ_1 to $2\pi - \psi_1$ gives,

$$\begin{aligned} L_{h_2bv} = P_o \tau_1 r^2 \sin\phi' \Big\{ & (1-\rho_s) \Big[2(\pi - \psi_1)\sin\theta\cos\theta\sin\phi'(\sin\phi - \cos\phi') - 2\sin\psi_1(\cos^2\theta\sin^2\phi' - \\ & -\sin^2\theta\sin\phi\cos\phi' + \sin^2\theta\cos^2\phi') - (\pi - \psi_1 - \sin\psi_1\cos\psi_1)\sin\theta\cos\theta\sin\phi'\cos\phi' \Big] + \\ & + \frac{2}{3}\rho_d(1-\sin\phi\cos\phi') \Big[-2\sin\psi_1\cos\theta\sin\phi' - (\pi - \psi_1 - \sin\psi_1\cos\psi_1)\sin\theta\cos\phi' \Big] + \\ & + 2\rho_s(1-\sin\phi\cos\phi') \Big[-2\sin\psi_1\cos^2\theta\sin^2\phi' - 2(\pi - \psi_1 - \sin\psi_1\cos\psi_1)\sin\theta\cos\theta\sin\phi'\cos\phi' - \\ & - \frac{2}{3}\sin\psi_1 (2 + \cos^2\psi_1)\sin^2\theta\cos^2\phi' \Big] \Big\} \end{aligned} \tag{III-93}$$

The third component of $\vec{L}_{hbv}$ is found by integrating Equation (III-59) from $\psi = \psi_1$ to $\psi = 2\pi - \psi_1$

$$L_{h_3bv} = 0 \qquad L_{h_3bvT} = 0 \tag{III-94}$$

Integration of Equations (III-50), (III-51) and (III-52) from $\psi = \psi_1$ to $\psi = 2\pi - \psi_1$ gives the components of $\vec{F}_{bv}$,

$$\begin{aligned} F_{b_1v} = P_o \tau_1 r \sin\phi' \Big\{ & (1-\rho_s) \Big[2(\pi - \psi_1)\cos^2\theta\sin\phi' + 2\sin\psi_1\sin\theta\cos\theta\cos\phi' \Big] + \\ & + \frac{2}{3}\rho_d \Big[2(\pi - \psi_1)\cos\theta\sin^2\phi' + 2\sin\psi_1\sin\theta\sin\phi'\cos\phi' \Big] + \\ & + 2\rho_s \Big[2(\pi - \psi_1)\cos^2\theta\sin^3\phi' + 4\sin\psi_1\sin\theta\cos\theta\sin^2\phi'\cos\phi' + \\ & + (\pi - \psi_1 - \sin\psi_1\cos\psi_1)\sin^2\theta\sin\phi'\cos^2\phi' \Big] \Big\} \end{aligned} \tag{III-95}$$

$$F_{b_2v} = 0 \qquad F_{b_2vT} = 0 \tag{III-96}$$

$$F_{b_3v} = P_o \tau_1 r \sin\phi' \left\{ (1-\rho_s) \left[-2(\pi - \psi_1)\sin\theta\cos\theta\sin\phi' - 2\sin\psi_1 \sin^2\theta\cos\phi' \right] + \right.$$

$$+ \frac{2}{3}\rho_d \left[-2\sin\psi_1 \cos\theta\sin\phi'\cos\phi' - (\pi - \psi_1 - \sin\psi_1\cos\psi_1)\sin\theta\cos^2\phi' \right] +$$

$$+ 2\rho_s \left[-2\sin\psi_1\cos^2\theta\sin^2\phi'\cos\phi' - 2(\pi - \psi_1 - \sin\psi_1\cos\psi_1)\sin\theta\cos\theta\sin\phi'\cos^2\phi' - \right.$$

$$\left. \left. - \frac{2}{3}\sin\psi_1(2 + \cos^2\psi_1)\sin^2\theta\cos^3\phi' \right] \right\} \tag{III-97}$$

We now total the torques and forces for the u and v cases. The total of Equations (III-86) and (III-92)

$$L_{h_1buv} = L_{h_1bu} + L_{h_1bv} = 0 \tag{III-98}$$

Likewise from Equations (III-87) and (III-93)

$$L_{h_2buv} = L_{h_2bu} + L_{h_2bv} = P_o \tau_1 r^2 \sin\phi' \left\{ (1-\rho_s) \left[4(\frac{\pi}{2} - \psi_1)\sin\theta\cos\theta\sin\phi'(\sin\phi - \cos\phi') - \right. \right.$$

$$-4\sin\psi_1(\cos^2\theta\sin^2\phi' - \sin^2\theta\sin\phi\cos\phi' + \sin^2\theta\cos^2\phi') -$$

$$-2(\frac{\pi}{2} - \psi_1 - \sin\psi_1\cos\psi_1)\sin\theta\cos\theta\sin\phi'\cos\phi' - \frac{2}{3}\pi\rho_d(1 - \sin\phi\cos\phi')\sin\theta\cos\phi' +$$

$$+2\rho_s(1-\sin\phi\cos\phi') \left[-4\sin\psi_1\cos^2\theta\sin^2\phi' - 4(\frac{\pi}{2} - \psi_1 - \sin\psi_1\cos\psi_1)\sin\theta\cos\theta\sin\phi'\cos\phi' - \right.$$

$$\left. \left. - \frac{4}{3}\sin\psi_1(2+\cos^2\psi_1)\sin^2\theta\cos^2\phi' \right] \right\} \tag{III-99}$$

The third component of $\vec{L}_{hbuv}$ is found by adding Equation (III-88) to (III-94),

$$L_{h_3bu} + L_{h_3bv} = L_{h_3buv} = 0 \tag{III-100}$$

The total force is likewise found by adding $\vec{F}_{bu} + \vec{F}_{bv}$. The first component is the sum of Equations (III-89) and (III-95).

$$F_{b_1uv} = F_{b_1u} + F_{b_1v} = P_o \tau_1 r \sin\phi' \left\{ (1-\rho_s) \left[4\left(\frac{\pi}{2} - \psi_1\right) \cos^2\theta \sin\phi' + \right.\right.$$

$$\left. + 4\sin\psi_1 \sin\theta\cos\theta\cos\phi' \right] + \frac{4}{3}\pi\rho_d \cos\theta \sin^2\phi' + 2\rho_s \left[4\left(\frac{\pi}{2} - \psi_1\right)\cos^2\theta\sin^3\phi' + \right.$$

$$\left.\left. + 8\sin\psi_1 \sin\theta\cos\theta\sin^2\phi'\cos\phi' + 2\left(\frac{\pi}{2} - \psi_1 - \sin\psi_1\cos\psi_1\right)\sin^2\theta \sin\phi'\cos^2\phi' \right] \right\} \quad \text{(III-101)}$$

The total of Equations (III-90) and (III-96) gives the second component,

$$F_{b_2uv} = F_{b_2u} + F_{b_2v} = 0 \quad \text{(III-102)}$$

The total of Equations (III-91) and (III-97) gives the third component,

$$F_{b_3uv} = F_{b_3u} + F_{b_3v} = P_o \tau_1 r \sin\phi' \left\{ (1-\rho_s) \left[-4\left(\frac{\pi}{2} - \psi_1\right)\sin\theta\cos\theta\sin\phi' - 4\sin\psi_1 \sin^2\theta\cos\phi' \right] - \right.$$

$$- \frac{2}{3}\pi\rho_d \sin\theta\cos^2\phi' + 2\rho_s \left[-4\sin\psi_1\cos^2\theta\sin^2\phi'\cos\phi' - \right. \quad \text{(III-103)}$$

$$\left.\left. -4\left(\frac{\pi}{2} - \psi_1 - \sin\psi_1\cos\psi_1\right)\sin\theta\cos\theta\sin\phi'\cos^2\phi' - \frac{4}{3}\sin\psi_1(2+\cos^2\psi_1)\sin^2\theta\cos^3\phi' \right] \right\}$$

The offset torque components are found using Equation (III-49) for the uv case,

$$\vec{L}_{xbuv} = \vec{x} \times \vec{F}_{buv} \quad \text{(III-104)}$$

or in components,

$$L_{xb_1uv} = y_L F_{b_3uv} \quad \text{(III-105)}$$

$$L_{xb_2uv} = z_L F_{b_1uv} - x_o F_{b_3uv} \quad \text{(III-106)}$$

$$L_{xb_3uv} = -y_L F_{b_1uv} \quad \text{(III-107)}$$

since $F_{b_2uv} = 0$ in Equation (III-102). The other two force components are found in Equations (III-101) and (III-103).

Case When $\phi < \theta$ on Longitude Sides Fartherest from Sun

Figure III-7 shows the area in the $\bar{i}\ \bar{j}\ \bar{k}$ coordinate system and the related vectors. These are constructed like those in Figure III-5.

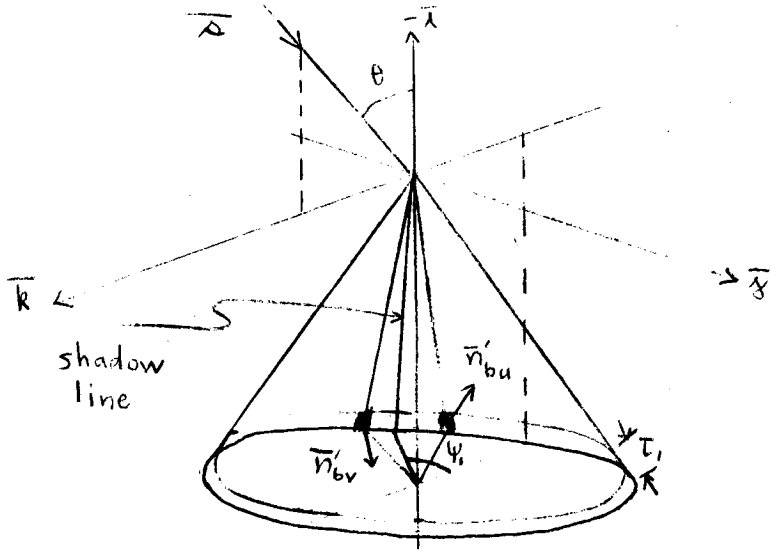

Figure III-7

Therefore we again have $\bar{s}$ and $\bar{x}$ unchanged, $dA_{bu} = dA'_{bu}$, $dA_{bv} = dA'_{bv}$, $\bar{n}_{bu} = \bar{n}'_{bu}$, $\bar{n}_{bv} = \bar{n}'_{bv}$, $\vec{h}_{bu} = -\vec{h}'_{bu}$, and $\vec{h}_{bv} = -\vec{h}'_{bv}$ for all positions. Therefore $d\vec{F}_{bu} = d\vec{F}'_{bu}$ and $d\vec{F}_{bv} = d\vec{F}'_{bv}$. Also the integrations are over the same regions as for Figure III-6.

Case uv Equations (III-47) through (III-49), not summed over all the longitude wires, become

$$\vec{L}_{buv} = \vec{L}_{bu} + \vec{L}_{bv} = \vec{L}_{hbu} + \vec{L}_{hbv} - \vec{L}_{xbu} - \vec{L}_{xbv} \qquad \text{(III-108)}$$

$$\vec{L}_{xbuv} = \vec{L}_{xbu} + \vec{L}_{xbv} = \vec{x} \times (\vec{F}_{bu} + \vec{F}_{bv}) = \vec{x} \times \vec{F}_{buv}$$

Then Equation (III-108) becomes

$$\vec{L}_{buv} = \vec{L}_{hbuv} - \vec{L}_{xbuv} \qquad \text{(III-109)}$$

Case uv' Equations (III-74) through (III-78), not summed over all the longitude wires, become

$$\vec{L}'_{buv} = \vec{L}'_{bu} + \vec{L}'_{bv} = \vec{L}'_{hbu} + \vec{L}'_{hbv} - \vec{L}'_{xbu} - \vec{L}'_{xbv} \tag{III-110}$$

$$\vec{L}'_{hbu} = \int \vec{h}'_{bu} \times d\vec{F}'_{bu} = -\int \vec{h}_{bu} \times d\vec{F}_{bu} = -\vec{L}_{hbu}$$

$$\vec{L}'_{hbv} = \int \vec{h}'_{bv} \times d\vec{F}'_{bv} = -\int \vec{h}_{bv} \times d\vec{F}_{bv} = -\vec{L}_{hbv}$$

$$\vec{L}'_{xbuv} = \vec{L}'_{xbu} + \vec{L}'_{xbv} = \vec{x} \times (\vec{F}_{bu} + \vec{F}_{bv}) = \vec{x} \times \vec{F}_{buv} = \vec{L}_{xbuv}$$

Then Equation (III-110) becomes

$$\vec{L}'_{buv} = -\vec{L}_{hbuv} - \vec{L}_{xbuv} \tag{III-111}$$

where the components of $\vec{L}_{hbuv}$ are respectively Equations (III-98), (III-99), (III-100), and the components of $\vec{x} \times \vec{F}_{buv} = \vec{L}_{xbuv}$ are given in Equations (III-105), (III-106) and (III-107).

With the back surfaces shaded by a ratio of K_1, the total uv torques, front and back are

$$\vec{L}_{BUV} = \vec{L}_{buv} + K_1 \vec{L}'_{buv} \tag{III-112}$$

Equation (III-112) is written for only one longitude wire. This equation must be piecewise integrated over ϕ' from $\phi' = 0$ to $\phi' = \theta$. This integration is rather lengthy so we may resort to numerical summation. Since there are many thousands of wires, we approximate this summation by saying N_w wires produce identical torques. Since $\vec{L}_{BUV}$ is a function only of ϕ' we write this weighted summation of every N_w wires as

$$\vec{L}_{BUVT} = \Sigma L_{BUV}(\phi') \doteq N_w \sum_{j=1}^{m_w} L_{BUV}(j N_w \Delta\phi') \tag{III-113}$$

where m_w is the number of terms of the summation. If this is a chosen constant, N_w is found by the limits of ϕ' being from 0 to θ. Then at the upper limit,

$$m_w N_w \Delta\phi' = \theta$$

then

$$N_w = \frac{\theta}{m_w \Delta\phi'} \qquad \text{(III-114)}$$

Equation (III-57), and (III-114) substituted into (III-113) gives

$$\vec{L}_{BUVT} \doteq \frac{\theta \cdot r}{m_w a_w} \sum_{j=1}^{m_w} \vec{L}_{BUV}\left(j \frac{\theta}{m_w}\right) \qquad \text{(III-115)}$$

Let the total torque due to all four cases be $\vec{L}_{TT}$, then

$$\vec{L}_{TT} = \vec{L}_{AT} + \vec{L}_{BT} + \vec{L}_{BUVT} \qquad \text{(III-116)}$$

We now have all the cases of torques. We are now interested in combining the different cases to find the total torque. To do this we define a short hand notation in terms of Equation numbers. These equation numbers are written as elements of non-transformable matrices. For example, the components of $\vec{L}_{aT}$ are found in Equations (III-26), (III-28) and (III-29) respectively. In the following equations, which contain equation numbers, the Roman numeral III is omitted. We now define the $\vec{L}_{aT}$ as the matrix,

$$\vec{L}_{aT} = \left\| \begin{matrix} 26 \\ 28 \\ 29 \end{matrix} \right\| \qquad \text{(III-117)}$$

These non-transformable matrices are all written with double bars so as not to confuse them with transformable matricies such as

$$\vec{L}_{aT} = \begin{bmatrix} L_{a_1 T} \\ L_{a_2 T} \\ L_{a_3 T} \end{bmatrix}$$

Likewise

$$\vec{L}'_{aT} = \left\| \begin{matrix} 36 \\ 38 \\ 39 \end{matrix} \right\| \tag{III-118}$$

Then from Equations (III-43), (III-117) and (III-118)

$$\vec{L}_{AT} = \vec{L}_{aT} + K_1 \vec{L}'_{aT} = \left\| \begin{matrix} 26 + K_1 \cdot 36 \\ 28 + K_1 \cdot 38 \\ 29 + K_1 \cdot 39 \end{matrix} \right\| \tag{III-119}$$

Equations (III-67), (III-68), (III-69) and (III-70) produce

$$\vec{L}_{bT} = \vec{L}_{hbT} - \vec{L}_{xbT} = \left\| \begin{matrix} 54 - y_L \cdot 65 \\ 58 - z_L \cdot 62 + x_o \cdot 65 \\ 60 + y_L \cdot 62 \end{matrix} \right\| \tag{III-120}$$

and Equation (III-77) gives

$$\vec{L}'_{bT} = -\vec{L}_{hbT} - \vec{L}_{xbT} = \left\| \begin{matrix} -54 - y_L \cdot 65 \\ -58 - z_L \cdot 62 + x_o \cdot 65 \\ -60 + y_L \cdot 62 \end{matrix} \right\| \tag{III-121}$$

Then substituting (III-120) and (III-121) into (III-78),

$$\vec{L}_{BT} = \vec{L}_{bT} + K_1 \vec{L}'_{bT} = \left\| \begin{matrix} (1-K_1) \cdot 54 - (1+K_1)\, y_L \cdot 65 \\ (1-K_1) \cdot 58 - (1+K_1)\, (z_L \cdot 62 - x_o \cdot 65) \\ (1-K_1) \cdot 60 + (1+K_1)\, y_L \cdot 62 \end{matrix} \right\| \tag{III-122}$$

Equations (III-119) and (III-122) added gives,

$$\vec{L}_{AT} + \vec{L}_{BT} = \left\| \begin{array}{l} 26 + K_1 \cdot 36 + (1-K_1) \cdot 54 - (1+K_1)\, y_L \cdot 65 \\ 28 + K_1 \cdot 38 + (1-K_1) \cdot 58 - (1+K_1)\, (z_L \cdot 62 - x_o \cdot 65) \\ 29 + K_1 \cdot 39 + (1-K_1) \cdot 60 + (1+K_1)\, y_L \cdot 62 \end{array} \right\| \quad \text{(III-123)}$$

Since the torques represented by Equations (III-54) and (III-60) are zero, (III-123) reduces to

$$\vec{L}_{AT} + \vec{L}_{BT} = \left\| \begin{array}{l} 26 + K_1 \cdot 36 \qquad\qquad - (1+K_1)\, y_L \cdot 65 \\ 28 + K_1 \cdot 38 + (1-K_1) \cdot 58 - (1+K_1)\, (z_L \cdot 62 - x_o \cdot 65) \\ 29 + K_1 \cdot 39 \qquad\qquad + (1+K_1)\, y_L \cdot 62 \end{array} \right\| \quad \text{(III-124)}$$

From Equations (III-98), (III-99) and (III-100)

$$\vec{L}_{hbuv} = \left\| \begin{array}{l} 98 \\ 99 \\ 100 \end{array} \right\| \quad \text{(III-125)}$$

and from Equations (III-101), (III-102) and (III-103)

$$\vec{F}_{buv} = \left\| \begin{array}{l} 101 \\ 102 \\ 103 \end{array} \right\| \quad \text{(III-126)}$$

Equations (III-105), (III-106) and (III-107) give

$$\vec{L}_{xbuv} = \left\| \begin{array}{l} 105 \\ 106 \\ 107 \end{array} \right\| = \left\| \begin{array}{l} y_L \cdot 103 \\ z_L \cdot 101 - x_o \cdot 103 \\ -y_L \cdot 101 \end{array} \right\| \quad \text{(III-127)}$$

Then from Equations (III-109), (III-125) and (III-127)

$$\vec{L}_{buv} = \vec{L}_{hbuv} - \vec{L}_{xbuv} = \left\| \begin{array}{l} 98 - y_L \cdot 103 \\ 99 - (z_L \cdot 101 - x_o \cdot 103 \\ 100 + y_L \cdot 101 \end{array} \right\|$$

This equation reduces to

$$\vec{L}_{buv} = \left\| \begin{array}{c} -y_L \cdot 103 \\ 99 - z_L \cdot 101 + x_o \cdot 103 \\ +y_L \cdot 101 \end{array} \right\| \qquad \text{(III-128)}$$

since the torques in Equations (III-98) and (III-100) are zero. Likewise Equation (III-111) gives

$$\vec{L}'_{buv} = -\vec{L}_{hbuv} - \vec{L}_{xbuv} = \left\| \begin{array}{c} -y_L \cdot 103 \\ -99 - z_L \cdot 101 + x_o \cdot 103 \\ +y_L \cdot 101 \end{array} \right\| \qquad \text{(III-129)}$$

and Equation (III-112) with (III-128) and (III-129) becomes

$$\vec{L}_{BUV} = \vec{L}_{buv} + K_1 \vec{L}'_{buv} \left\| \begin{array}{c} -(1+K_1)\, y_L \cdot 103 \\ (1-K_1) \cdot 99 - (1+K_1)\, z_L \cdot 101 + (1+K_1)\, x_o \cdot 103 \\ +(1+K_1)\, y_L \cdot 101 \end{array} \right\| \qquad \text{(III-130)}$$

Equations (III-99), (III-101) and (III-103) are in terms of ϕ' and ψ_1. Equation (III-82),

$$\cos \psi_1 = \frac{\tan \phi'}{\tan \theta}$$

gives ψ_1 in terms of ϕ'. These three equations are now summed according to Equation (III-115). Let this summation be symbolized in the non-transformable matrices as a Σ sigma preceding the equation number to be summed. For example,

$$\Sigma 99 \equiv \frac{\theta r}{m_w a_w} \sum_{j=1}^{m_w} L_{h_2 buv}(\phi')$$

where each ψ_1 is replaced by $\psi_1 = \cos^{-1} \frac{\tan \phi'}{\tan \theta}$* and each ϕ' is then replaced by $\phi' = j \frac{\theta}{m_w}$.

*Note $0 < \psi_1 < \pi$

Then from Equation (III-130)

$$\vec{L}_{BUVT} = \left\| \begin{array}{c} -(1+K_1)\, y_L \cdot \Sigma 103 \\ (1-K_1)\cdot \Sigma 99 - (1+K_1)(z_L \cdot \Sigma 101 - x_o \cdot \Sigma 103) \\ +(1+K_1)\, y_L \cdot \Sigma 101 \end{array} \right\| \qquad \text{(III-131)}$$

and substituting (III-124) and (III-131) into (III-116) gives

$$\vec{L}_{TT} = \left\| \begin{array}{ccc} 26+K_1 \cdot 36 & -(1+K_1)\, y_L \cdot 65 & -(1+K_1)\, y_L \cdot \Sigma 103 \\ 28+K_1 \cdot 38+(1-K_1)\cdot 58 & -(1+K_1)(z_L \cdot 62 - x_o \cdot 65)+(1-K_1)\cdot \Sigma 99 & -(1+K_1)(z_L \cdot \Sigma 101 - x_o \cdot \Sigma 103) \\ 29+K_1 \cdot 39 & +(1+K_1)\, y_L \cdot 62 & +(1+K_1)\, y_L \cdot \Sigma 101 \end{array} \right\|$$

(III-132)

The torque represented by Equation (III-132) is due to the wire surfaces that are radial. This torque must be added to the torques on the spherical surfaces found previously.

Constants of ϕ

$$J_1 = \frac{\pi}{2} - \phi - \sin\phi \cos\phi$$

$$J_2 = \sin\phi\,(2 + \cos^2\phi)$$

$$J_3 = -\frac{1}{2}\cos^2\phi - \frac{1}{3}\sin^4\phi$$

$$J_4 = -\sin\phi\cos\phi + \sin^3\phi\cos\phi$$

$$J_5 = +\frac{1}{8}\sin\phi\,(\frac{\pi}{2} - \phi + \sin\phi\cos\phi - 2\sin^3\phi\cos\phi) - \frac{1}{3}\cos^3\phi$$

$$J_6 = -\sin\phi\cos^2\phi + \sin^3\phi\cos^2\phi$$

$$J_7 = \frac{\pi}{2} - \phi + \sin\phi\cos\phi - 2\sin^3\phi\cos\phi$$